STATE OF CALIFORNIA • DEPARTMENT OF TRANSPORTATION

TECHNICAL REPORT DOCUMENTATION PAGE

TR0003 (REV 10/98)

ADA Notice

For individuals with sensory disabilities, this document is available in alternate formats. For alternate format information, contact the Forms Management Unit at (916) 445-1233, TTY 711, or write to Records and Forms Management, 1120 N Street, MS-89, Sacramento, CA 95814.

1. REPORT NUMBER	2. GOVERNMENT ASSOCIATION NUMBER	3. RECIPIENT'S CATALOG NUMBER
CA16-2563		

4. TITLE AND SUBTITLE	5. REPORT DATE
A706 Grade 80 Reinforcement for Seismic Applications	August 2015
	6. PERFORMING ORGANIZATION CODE

7. AUTHOR	8. PERFORMING ORGANIZATION REPORT NO.
David Overby, Mervyn Kowalsky, Rudi Seracino	

9. PERFORMING ORGANIZATION NAME AND ADDRESS	10. WORK UNIT NUMBER
North Carolina State University, Department of Civil Construction and Environmental Engineering, Mann Hall, 208 Stinson Drive, Raleigh, NC 27695	

12. SPONSORING AGENCY AND ADDRESS	11. CONTRACT OR GRANT NUMBER
California Department of Transportation Division of Engineering Services 1801 30th Street, MS #9-2/5i Sacramento, CA 95816	65A0525
	13. TYPE OF REPORT AND PERIOD COVERED Final
California Department of Transportation Division of Research, Innovation, and System Information P.O. Box 942873 Sacramento, CA 94273-0001	14. SPONSORING AGENCY CODE

15. SUPPLEMENTARY NOTES

16. ABSTRACT

In the seismic design of reinforced concrete structures, the overstrength of the steel reinforcement plays a critical role in the structure's ability to dissipate energy inelastically as unaccounted for strength could lead to sudden, non-ductile modes of failure. Thus, knowledge of the expected mechanical properties of the rebar being used is extremely important. The current availability of ASTM A706 Grade 80 rebar material test results is practically non-existent in regards to both strength and, in particular, the associated strains. In response to this issue, a research program was developed to determine the expected monotonic stress-strain profile of ASTM A706 Grade 80 high strength steel reinforcement.

In total, 788 tensile tests of A706 Grade 80 rebar were conducted. Tests were performed on all bar sizes No. 4 through No. 18 in the as-rolled condition. Steel was provided by multiple producing mills and multiple heats were tested from each mill. A non-contact 3D position measurement system was used to simultaneously evaluating strains over multiple gage lengths for the full duration of each test, including fracture of the bar.

Results generated by the tests were used to develop recommendations for the yield strength, yield strain, strain at onset of strain hardening, tensile strength, and ultimate tensile strain based on the mean values obtained across all bar sizes. Further statistical analysis was used to identify the distributions of the material properties and evaluate variability in the data. Additional recommendations related to future member-level tests are proposed.

17. KEY WORDS	18. DISTRIBUTION STATEMENT
reinforcing steel, seismic, bridges, grade 80	No Restrictions. This document is available to the public through the National Technical Information Service, Springfield, VA 22161

19. SECURITY CLASSIFICATION *(of this report)*	20. NUMBER OF PAGES	21. COST OF REPORT CHARGED
Unclassified	114	

DISCLAIMER STATEMENT

This document is disseminated in the interest of information exchange. The contents of this report reflect the views of the authors who are responsible for the facts and accuracy of the data presented herein. The contents do not necessarily reflect the official views or policies of the State of California or the Federal Highway Administration. This publication does not constitute a standard, specification or regulation. This report does not constitute an endorsement by the Department of any product described herein.

For individuals with sensory disabilities, this document is available in alternate formats. For information, call (916) 654-8899, TTY 711, or write to California Department of Transportation, Division of Research, Innovation and System Information, MS-83, P.O. Box 942873, Sacramento, CA 94273-0001.

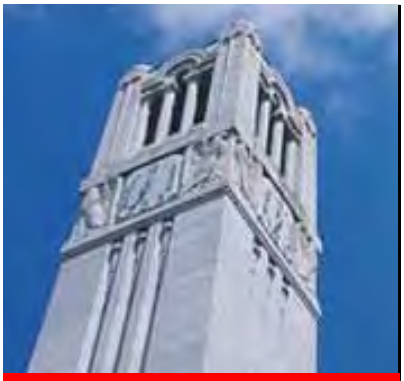

NC STATE UNIVERSITY

Constructed Facilities Laboratory

Department of Civil, Construction, and Environmental Engineering

Research Report

No. RD-15-15

A706 GRADE 80 REINFORCEMENT FOR SEISMIC APPLICATIONS

Prepared by:

David Overby, *Graduate Research Assistant*
Dr. Mervyn Kowalsky, *Principle Investigator*
Dr. Rudolf Seracino, *Co-Principle Investigator*

Prepared for:

California Department of Transportation
Sacramento, California

Constructed Facilities Laboratory
NC STATE UNIVERSITY

August 2015

Constructed Facilities Laboratory
2414 Campus Shore Drive
North Carolina State University
Raleigh, NC 27695-7533
Tel: (919) 513-1733
Fax: (919) 513-1765
Email: cfl@ncsu.edu
Web Site: www.cfl.ncsu.edu

A706 GRADE 80 REINFORCEMENT FOR SEISMIC APPLICATIONS

Final Report

November 2, 2015

The research described in this report is supported by the California Department of Transportation under agreement #65A0525. Their support is gratefully acknowledged. The conclusions are those of the authors alone and should not be construed as to imply endorsement by Caltrans.

Disclaimer

This document is disseminated in the interest of information exchange. The contents of this report reflect the views of the authors who are responsible for the facts and accuracy of the data presented herein. The contents do not necessarily reflect the official views or policies of the State of California or the Federal Highway Administration. This publication does not constitute a standard, specification or regulation. This report does not constitute an endorsement by the Department of any product described herein.

For individuals with sensory disabilities, this document is available in Braille, large print, audiocassette, or compact disk. To obtain a copy of this document in one of the alternate formats, please contact: the Division of Research and Innovation MS-83, California Department of Transportation, P.O. Box 942873, Sacramento, CA 94273-0001.

Acknowledgments

Funding for this research which was provided by the California Department of Transportation under Agreement #65A0525 is gratefully acknowledged. Additionally, the authors would like to thank the three producing mills for their generous donation of the reinforcing steel used in the project. Lastly, the assistance of the entire staff of the Constructed Facilities Laboratory is greatly appreciated.

Abstract

In the seismic design of reinforced concrete structures, the overstrength of the steel reinforcement plays a critical role in the structure's ability to dissipate energy inelastically as unaccounted for strength could lead to sudden, non-ductile modes of failure. Thus, knowledge of the expected mechanical properties of the rebar being used is extremely important. The current availability of ASTM A706 Grade 80 rebar material test results is practically non-existent in regards to both strength and, in particular, the associated strains. In response to this issue, a research program was developed to determine the expected monotonic stress-strain profile of ASTM A706 Grade 80 high strength steel reinforcement.

In total, 788 tensile tests of A706 Grade 80 rebar were conducted. Tests were performed on all bar sizes No. 4 through No. 18 in the as-rolled condition. Steel was provided by multiple producing mills and multiple heats were tested from each mill. A non-contact 3D position measurement system was used to simultaneously evaluating strains over multiple gage lengths for the full duration of each test, including fracture of the bar.

Results generated by the tests were used to develop recommendations for the yield strength, yield strain, strain at onset of strain hardening, tensile strength, and ultimate tensile strain based on the mean values obtained across all bar sizes. Further statistical analysis was used to identify the distributions of the material properties and evaluate variability in the data. Additional recommendations related to future member-level tests are proposed.

Notation and Definitions

A_g	area of gross section
A_{st}	longitudinal steel area
C_1	parameter for curvature of strain hardening curve used in Raynor rebar model
D	section diameter
E_s	modulus of elasticity
E_y	parameter for slope of the yield plateau used in the Raynor rebar model
$\varepsilon c_{yield}^{spiral}$	longitudinal compressive strain at spiral yield
$\varepsilon s_{buckling}^{bar}$	longitudinal tensile strain at bar buckling
ε_{sh}	strain at the onset of strain hardening for an individual bar test
ε_{sh}	expected or mean strain at the onset of strain hardening
$\varepsilon_{sh\ (mean)}$	same as ε_{sh}
ε_u	ultimate tensile strain of an individual bar test
ε_{su}	expected or mean ultimate tensile strain
ε_{su}^R	reduced ultimate tensile strain (Caltrans SDC notation)
$\varepsilon_{su\ off\text{-}bar}$	expected or mean ultimate tensile strain of No. 11-18 bars resulting from the off-bar load cell
$\varepsilon_{su\ (mean)}$	same as ε_{su}
$\varepsilon_{su\ (5\%)}$	5th percentile ultimate tensile strain
ε_y	nominal yield strain; equal to $f_y \div 29000$ (Caltrans SDC notation)
ε_{ye}	expected or mean yield strain
$\varepsilon_{ye\ (mean)}$	same as ε_{ye}
$\varepsilon_{y\ ADM}$	Autographic Diagram Method yield strain; corresponding to top-of-the-knee
$\varepsilon_{y\ EUL}$	Extension Under Load yield strain (0.0035)
$\varepsilon_{y\ OM}$	0.2% Offset Method yield strain; corresponding to intersection of 0.2% offset line with the stress-strain curve
f_{sh}	stress at onset of strain hardening for an individual bar test
f_u	specified minimum tensile strength (Caltrans SDC notation)
f_u	tensile strength of an individual bar test
f_{ue}	expected or mean tensile strength
$f_{ue\ off\text{-}bar}$	expected or mean tensile strength of No. 11-18 bars resulting from the off-bar load cell
$f_{ue\ (mean)}$	same as f_{ue}
$f_{ue\ (95\%)}$	95th percentile tensile strength
$f_{u\ min}$	ASTM minimum allowable tensile strength; same as f_u
f_y	specified minimum yield strength (Caltrans SDC notation)
f_{ye}	expected or mean yield strength

$f_{ye\ off\text{-}bar}$	expected or mean yield strength of No. 11-18 bars resulting from the off-bar load cell
$f_{ye\ (mean)}$	same as f_{ye}
f_{yhe}	Expected yield strength of transverse steel
$f_{y\ ADM}$	Autographic Diagram Method yield strength; corresponding to top-of-the-knee
$f_{y\ EUL}$	Extension Under Load yield strength; stress at a strain of 0.0035
$f_{y\ max}$	ASTM maximum allowable yield strength
$f_{y\ min}$	ASTM minimum allowable yield strength; same as f_y
$f_{y\ OM}$	0.2% Offset Method yield strength; corresponding to intersection of 0.2% offset line with the stress-strain curve
f'_{ce}	expected concrete strength
L_c	cantilever length
Lpr_c	plastic hinge length in compression
Lpr_t	plastic hinge length in tension
P	axial load
ρ_s	volumetric steel ratio

TABLE OF CONTENTS

LIST OF FIGURES

LIST OF TABLES

1. CHAPTER 1 - INTRODUCTION

This report summarizes the results of a research program aimed at assessing the monotonic stress-strain behavior of ASTM A706 Grade 80 rebar. Specific subjects included determination of the expected mechanical properties and nature of the stress-strain curve.

1.1. Problem Statement

The need for such an investigation arises from the limited presence of tensile test results from A706 Grade 80 rebar found in the literature. A review of the existing literature conducted at the onset of this project identified two papers containing expected material properties for A706 Grade 80 rebar. Two additional papers provided stress-strain curves with no accompanying numerical data. The literature data was further limited in that it only considered a few bar sizes and often lacked strain values for the provided stress values.

1.2. Research Relevance

In the capacity design of structures, locations of damage are chosen and then detailed to dissipate energy in a ductile manner while ensuring that surrounding members remain elastic while resisting the input demands from the plastic hinges. Rebar being used in seismic applications must, therefore, possess large inelastic strain capacity (ductility) as well as sufficient strain hardening to ensure the spread of plasticity over the plastic hinge and reduce the maximum strains occurring at a given point.

Reinforcing steel is manufactured to provide a specified, minimum level of strength; however, as this requirement is a lower limit, it follows that producing mills would want to maintain an average strength that is safely above the minimum. As a result, actual reinforcing steel strengths are typically higher than their specified values. Failure to account for this in seismic design could lead to failure of capacity protected members due to unexpectedly high moment demands arising from the increased strength of the adjoining member provided by the steel reinforcement. Material overstrength factors may be used to account for this behavior where actual (expected) material properties are unavailable.

The Caltrans Seismic Design Criteria (Caltrans, 2013) currently specifies both nominal and expected material properties for A706 Grade 60 reinforcing steel. It is Caltrans' desire to include recommendations for A706 Grade 80 rebar in a future version of the SDC; however, due to the limited presence of available material test results, a database of expected material properties must first be developed.

1.3. Research Objectives

Several key points are needed to define the monotonic stress-strain curve of a low-carbon steel exhibiting a well-defined yield plateau: the yield point, the onset of strain hardening, and ultimate tensile point or peak of the strain hardening curve. In the case of a non-well-defined

yield plateau or “roundhouse” stress-strain curve, other methods such as the 0.2% Offset Method may be used to establish the yield point. The primary objective of the current research program was to determine the expected values of stress and strain at these key points. A secondary objective was to identify the nature of the stress-strain curve on which these points lie and evaluate whether or not existing stress-strain models can be used to characterize this region or if a new model needed to be developed.

1.4. Research Methods

The program followed a three-step process in order to accomplish the above-stated objectives. The initial step was a review of the literature for existing test data. This served as an opportunity to gauge the extent to which existing test data was unavailable and to identify trends that might serve as a reference point during the experimental phase of the project. The second step was a comprehensive tensile testing program to generate new data. In total, 788 tensile tests of as-rolled or “deformed” A706 Grade 80 rebar including bar sizes No. 4 through No. 18 were conducted as part of this phase. Reinforcing steel was provided by three producing mills, each supplying three heats per bar size. The third step was a statistical evaluation of the generated data to define recommended values of stress and strain at specific key points and establish the nature of the associated stress-strain curve. Additional analyses were performed to identify trends in the data and explain unexpected results.

1.5. Overview of Report Contents

Chapter 2 presents the findings of the literature review and briefly discusses how these findings relate to the experimental data acquired during the second phase of the project. The chapter is divided into two main parts: reports providing actual test data and reports solely providing stress-strain curves. Additional distinction is made between tensile test results originating from producing mills and those originating from a research laboratory.

Chapter 3 presents the details of the experimental phase of the project in which 788 tensile tests of A706 Grade 80 rebar were conducted on deformed reinforcing bars ranging in size from No. 4 to No. 18. Included in this chapter is a discussion of the material that was tested, instrumentation and major equipment used, and how the key parameters needed to characterize the stress-strain curve were determined.

Chapter 4 opens with a description of the statistical methods used in analyzing the experimental results. Following this is a discussion of the results of the statistical analysis on a parameter-by-parameter basis. Also included are the results of an investigation into a concern that arose with the No. 11, 14, and 18 bar data, the problem that was discovered, how it was resolved, and the impact this had on the final recommendations. A short section is dedicated to re-examining three of the affected parameters. The chapter concludes by evaluating the shape of the strain hardening curve and highlighting additional uses of the dataset beyond providing the recommended values for the key parameters.

Chapter 5 summarizes the research findings relative to the stated objectives and presents the recommendations in the form of expected numerical values for the yield strength, yield strain, onset of strain hardening, tensile strength, and ultimate tensile strain of ASTM A706 Grade 80 rebar. Included in this are recommendations for two new parameters arising from the statistical analysis: the 95^{th} percentile tensile strength and the 5^{th} percentile ultimate tensile strain. Also included in the chapter are recommendations for future tensile testing programs as well as future research related to member level testing.

Chapter 6 presents a look at how the proposed recommendations would be implemented into a future version of the Caltrans Seismic Design Criteria. Effort is made to ensure that the new A706 Grade 80 material properties section would closely parallel the format of the existing A706 Grade 60 material properties section. Also proposed is a new A706 Grade 80 stress-strain profile based on the recommendations provided in Chapter 5 to accompany the existing profile for A706 Grade 60 rebar.

2. CHAPTER 2 – LITERATURE REVIEW

2.1. Chapter Summary

This chapter presents the results of a search of the available literature for experimental data on ASTM A706 Grade 80 reinforcing steel. While numerous articles and papers have been published on the properties of other types of high-strength steel reinforcement and their use in concrete structures, the availability of test data for A706 Grade 80 steel continues to be scarce. At the time of the writing of this report, five reports (Rautenberg et al., 2013; WJE, 2013; NIST, 2014; Trejo et al., 2014; and Barbosa et al., 2015) were found to either directly reference or include material test results associated with A706 Grade 80 rebar.

Two of these reports (Trejo et al., 2014; Barbosa et al., 2015) originated from the same source and thus referenced the same data. Similarly, two of the remaining reports (Rautenberg et al., 2013; WJE, 2013) referenced a single different dataset, one providing numerical data and the other only the associated stress-strain curves. Consequently, the available published A706 Grade 80 stress-strain data arising as part of an original research effort is limited to two datasets consisting of twelve total tensile tests and the accompanying stress-strain curves. Beyond this, two of the reports (NIST, 2014; Trejo et al., 2014) additionally included some mill test results, in one case numeric and in the other only graphical.

Distinction is made between results obtained in a research laboratory and those provided by producing mills as stress-strain data originating from producing mills is limited to only including values for yield strength, tensile strength, and percent elongation at fracture. Additionally, it appears to be the case that producing mill tests indicate higher strength and lower ductility than research lab results of the same steel. In addition to the five literature reports mentioned above, the research project was also given access to the CRSI mill database – a substantial collection of mill test results across the full range of bar sizes and grades that have been submitted to CRSI.

2.2. Overview of A706 Grade 80

ASTM A706 reinforcing steel emerged in the early 1970s in an effort to provide the engineering community with a weldable rebar that could be used in seismic applications (Gustafson, 2010). A706 rebar posed an advantage over other reinforcing steels available at the time due to its more tightly controlled chemical and tensile material properties. When designing plastic hinges, reliability of specified materials to behave as anticipated is extremely important. Rebar being used in seismic applications must possess large inelastic strain capacity (ductility) as well as sufficient strain hardening to ensure the spread of plasticity over the plastic hinge and reduce the maximum strains occurring at a given point.

Currently, the two most common designations for reinforcing steel in the US are ASTM A615 and ASTM A706. However, the less tightly controlled material properties of A615 reinforcement make it an undesirable choice in the context of seismic design. A706 reinforcement must adhere to specific requirements regarding not only minimum, but also maximum yield stress as well as

sustain larger elongations and meet specific chemical composition requirements. As a consequence, ASTM A706 steel is routinely specified, at the minimum, for members expected to form plastic hinges.

Two grades of steel are permitted in the current version of ASTM A706/A706M "Standard Specification for Low-Allow Steel Deformed and Plain Bars for Concrete Reinforcement": Grade 60 and Grade 80. The grade denotes the minimum permissible yield strength in units of ksi. A comparison of the ASTM A615 and A706 specifications according to grade of steel is presented in Table 2.1. It is quickly apparent that A706 steels are required to provide a much higher percent elongation at fracture (over an 8-inch gage length) than A615 steels. Less apparent from the table is the requirement that A706 reinforcement have a tensile stress capacity at least 1.25 times greater than the yield stress.

Table 2.1. Comparison of ASTM A615 and A706 Specifications

	A615-40	**A615-60**	**A706-60**	**A615-75**	**A615-80**	**A706-80**
$f_{y\,min}$ **[ksi]**	40	60	60	75	80	80
$f_{y\,max}$ **[ksi]**	N/A	N/A	78	N/A	N/A	98
$f_{u\,min}$ **[ksi]**	60	90	80	100	105	100
Minimum elongation (%) as a function of bar size for each grade indicated below.						
#3	11	9	14	7	7	12
#4, #5	12	9	14	7	7	12
#6	12	9	14	7	7	12
#7, #8	N/A	8	12	7	7	12
#9, #10, #11	N/A	7	12	6	6	12
#14, #18	N/A	7	10	6	6	10

Grade 80 was not introduced into the ASTM A706 specification until December 2009, thus making its presence relatively recent. While there is an overall lack of available material test data on A706 Grade 80 rebar in the current literature, and thus a hesitancy for design codes and engineers to specify its use, its potential as a valuable alternative to A706 Grade 60 rebar seems quite high. As an example, the use of higher strength steel in capacity protected members would result in reduced congestion into footing and cap-beam joints as columns could have a smaller number of bars of the same size when compared to Grade 60 steel.

2.3. Expected Parameter Values

The primary effort of this research project is to establish the expected values of stress and strain at specific key points on the monotonic stress-strain curve for A706 Grade 80 rebar. As described in the chapter summary, only two datasets (Rautenberg et al., 2013; Trejo et al., 2014) were found to contain expected values of stress and strain for A706 Grade 80 rebar acquired as part of an original research effort. The remainder of the existing tensile test data available to the project consisted of mill test results either published in one of the five reports or provided in the

CRSI mill database. This section summarizes the available numerical test data, first from research findings and then from mill test reports.

2.3.1. Research Data

Rautenberg et al. (2013) presented the findings of a study on the applicability of high-strength reinforcement in reinforced concrete columns resisting lateral earthquake loads. The primary goal of the research, which was based on testing conducted as part of Rautenberg's PhD dissertation at Purdue in 2011 (Rautenberg, 2011), was to evaluate the 60 ksi limit imposed by ACI on the yield strength of rebar used in regions expected to form plastic hinges. A total of 8 columns consisting of either ASTM A706 Grade 60, A706 Grade 80, or A1035 Grade 120 longitudinal reinforcement were considered in the analysis. Material testing was conducted for the purpose of calibrating numerical models of full-scale buildings subjected to strong ground motions. Of particular interest are the tensile tests that were performed on three A706 Grade 80 No. 7 bars. The test specimens all originated from the same heat and were tested in a Baldwin 120-kip capacity universal testing machine upgraded with Instron control and data acquisition equipment. An Instron extensometer having two inch gauge length was used to acquire the strains. Tests were performed in compliance with ASTM A370 (2009). Data from the tests, which is publicly available on the NEES website (NEES, 2009), is presented in Table 2.2.

Table 2.2. Tensile test data from Rautenberg et al. (2013)

Specimen Number	Yield Strength		Tensile Strength		Elong. % in 8 inch
	Stress, ksi	Strain, in/in	Stress, ksi	Stress, ksi	
7a	83	---	119	---	11.7
7b	83	---	117	---	15.6
7c	84	---	118	---	14.8

The yield and tensile strengths and percent elongation essentially follow what might be expected with the exception of specimen number 7a just falling below the minimum percent elongation of 12% required by ASTM A706/A706M. The ratio of tensile to yield strengths is about 1.4 which is safely above the minimum allowable for A706 rebar. The report did not explicitly provide any strain data from the tests; however, it was made available through the NEES website. Note, though, that the strain data available on the website stopped increasing with force after reaching a value of 0.08 for all three of the tests despite values being provided for the percent elongation at fracture. Such unusual behavior is likely the result of an equipment malfunction or transcription error in sharing the data.

Trejo et al. (2014) presented the results of a study on the seismic performance of 24-inch diameter circular reinforced concrete bridge columns constructed with A706 Grade 80

reinforcement. A total of six of these half-scale columns were constructed and tested using either No. 5 or No. 6 longitudinal reinforcement, No. 3 transverse reinforcement, and either A706 Grade 60 or A706 Grade 80 steel. The study concluded that, among other things, Grade 80 columns exhibited equal or greater maximum drift ratio compared to Grade 60 columns, both grades resulted in similar column lateral displacement and ductility, and that Grade 60 columns showed higher total energy dissipation as a result of their higher area of steel. Column failure mode (bar fracture due to buckling of longitudinal bars) was consistent across both grades of steel. The tensile test data presented in the report and reproduced below (Table 2.3) is the most detailed summary of the mechanical characteristics of A706 Grade 80 reinforcing bars found in any of the other reports. This same data appears in a more recent paper by the same authors (Barbosa et al., 2015).

Table 2.3. Material test results for A706 Grade 80 rebar (Trejo et al., 2014)

Bar Size	Yield Point (0.2% offset)		Yield Point (0.0035 EUL)		Tensile Strength		Onset of Strain Harding		Ultimate Strain		Elong. % in 8 inch
	Stress, ksi	Strain, in/in	Stress, ksi	Strain, in/in	Stress, ksi	Strain, in/in	Stress, ksi	Strain, in/in	Stress, ksi	Strain, in/in	
#3	85.6	0.0055	73.3	0.0035	120.5	0.0947	N/A	N/A	85.2	0.1378	13
#5	86.2	0.0051	85.4	0.0035	114.3	0.1066	85.9	0.0084	86.8	0.1555	14
#6	86.1	0.0048	84.3	0.0035	114.0	0.1225	85.5	0.0098	93.9	0.1893	15

The tabulated stresses and strains presented in Table 2.3 are the average of 3 tests for each bar size. The No. 3 bars originated as coils, and the No. 5 and No. 6 bars were both produced from the same heat in 20 ft. straight lengths. Strain data up to necking was retrieved with a two inch gauge length extensometer. The onset of strain hardening was taken to be the point where the stress-strain curve begins to have a positive slope after the initial yield point. The ultimate stress and strain are the values obtained just before fracture.

2.3.2. CRSI and Mill Data

The Concrete Reinforcing Steel Institute (CRSI) maintains an unpublished database of certified mill test report data that is made available upon special request for research purposes. CRSI provided the current research project with access to over 253,000 tensile test results taken between 2011 and 2013. Data on yield strength, tensile strength, and percent elongation at fracture of all included types and grades of reinforcing steel is available in the database; however, the data is limited in that it does not include the associated strains. ASTM A706 Grade 80 steel accounts for just 148 of the 253,000 plus tensile tests results and ASTM Dual A615/A706 Grade 80 accounts for 76 of the tensile test results. Pertinent statistical data from the databases is summarized below (Table 2.4).

A surprising observation about the distribution of bar sizes in the databases is that a large quantity (61%) of the A706 Grade 80 bars are for sizes No. 11 through No. 18 (Fig. 2.1). Figure

2.2 illustrates the obvious increase in production of A706 Grade 80 and Dual A615/A706 Grade 80 reinforcing steel between 2011 and 2013. The normalized distributions provided in Figures 2.3 and 2.4 show a tendency of Dual A615/A706 Grade 80 coiled reinforcement to have a lower mean yield strength and higher mean tensile strength than straight reinforcement. Note that the normalized distributions are for the percent of total A706 Grade 80 and Dual A615/A706 Grade 80 not the entire 253,000 plus-entry database. As summarized in Table 2.4, the average yield strength of all of the A706 Grade 80 bars is 86.9 ksi, and the average tensile strength is 114.5 ksi. Similarly, the average yield strength of all of the Dual A615/A706 Grade 80 bars is 85.3 ksi, and the average tensile strength is 116.1 ksi.

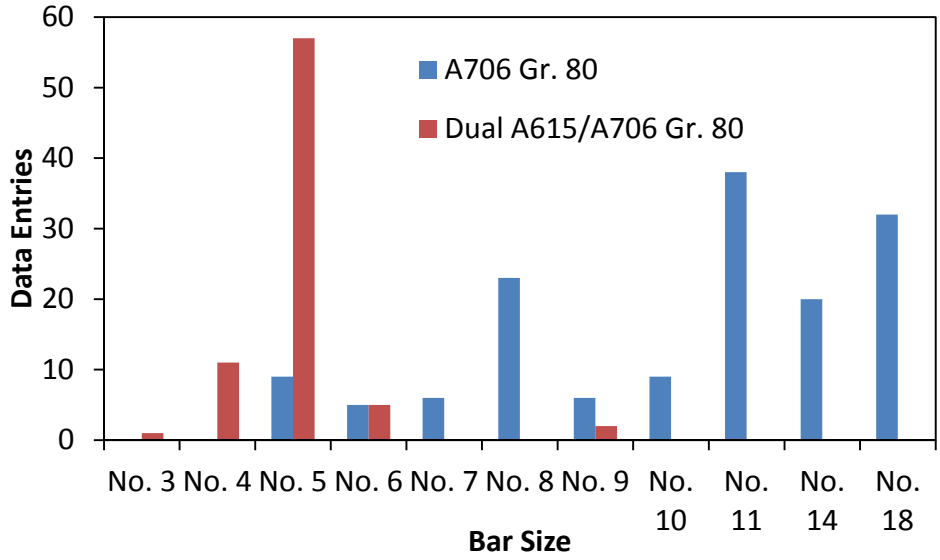

Figure 2.1. Distribution of all A706 Gr. 80 and Dual A615/A706 Gr. 80 by bar size (CRSI, 2013)

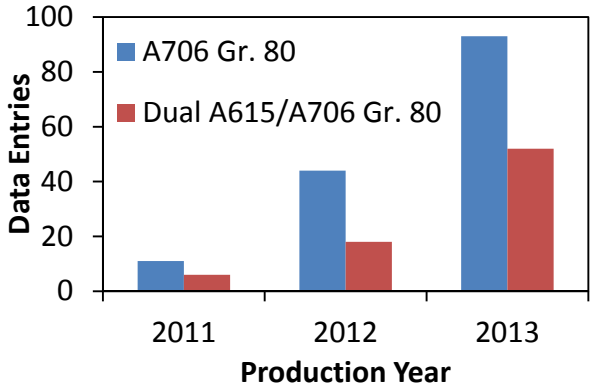

Figure 2.2. Distribution of all A706 Gr. 80 and Dual A615/A706 Gr. 80 by production year (CRSI, 2013)

Table 2.4. Statistical summary of stress data for all A706 Gr. 80 and Dual A615/A706 Gr. 80 rebar (CRSI, 2013)

A706 Grade 80		**Dual A615/A706 Grade 80**	
Entries	148	Entries	76
Max, ksi		**Max, ksi**	
Yield	95.8	Yield	97.5
Tensile	126.6	Tensile	124.5
Min, ksi		**Min, ksi**	
Yield	80.4	Yield	80.8
Tensile	107.7	Tensile	110.1
Mean, ksi		**Mean, ksi**	
Yield	86.9	Yield	85.3
Tensile	114.5	Tensile	116.1
St. Dev., ksi		**St. Dev., ksi**	
Yield	3.17	Yield	3.49
Tensile	3.72	Tensile	2.81

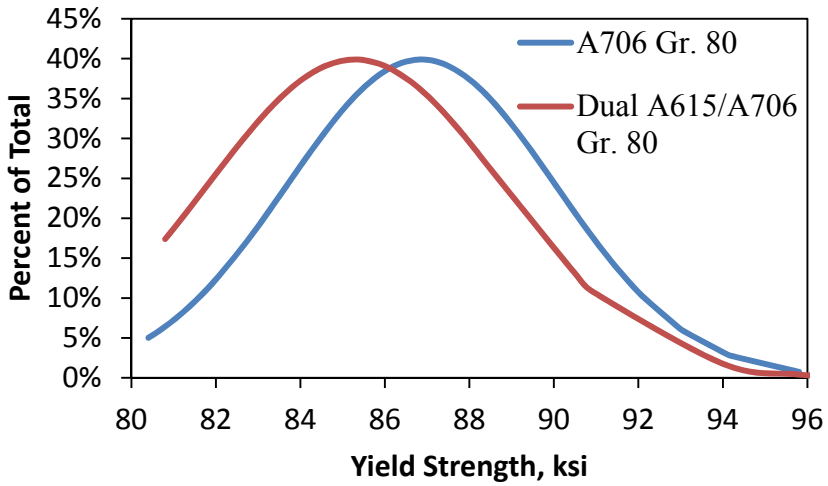

Figure 2.3. Yield strength normal distribution for all A706 Gr. 80 and Dual A615/A706 Gr. 80 rebar (CRSI, 2013)

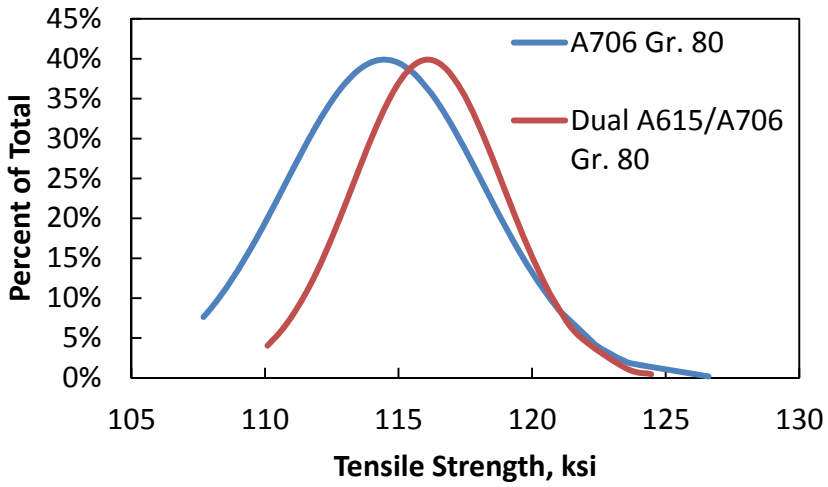

Figure 2.4. Tensile strength normal distribution for all A706 Gr. 80 and Dual A615/A706 Gr. 80 rebar (CRSI, 2013)

In addition to the mill data provided in the CRSI database, the report by Trejo et al. (2014) also included mill test results provided with the steel received as part of that research project. The data from that producing mill is provided in Table 2.5. Besides representing additional data points, these results offer insight into the way mill test results compare against laboratory test results. A comparison of Tables 2.3 and 2.5 illustrates the trend for mill-measured strength values to be higher and percent elongation at fracture values to be lower than research laboratory test results. As will be seen in Chapter 4, this trend also held true for the results obtained as part of the current research project. Note that the method by which the producing mill obtained the yield strength data was not clarified in the report.

Table 2.5. Producing mill data referenced in Trejo et al. (2014)

Bar Size	Yield Strength		Tensile Strength		Elong. % in 8 inch
	Stress, ksi	Strain, in/in	Stress, ksi	Strain, in/in	
#3	96.5	---	124.0	---	23
#5	87.5	---	114.0	---	13
#6	88.0	---	115.0	---	14

2.4. Shape of the Curve

The second objective of this research project is to assess the shape of the A706 Grade 80 stress-strain curve. Particular characteristics of interest are the transition from elastic to inelastic behavior and the shape of the strain hardening region. The literature results presented in this section served as a first look at the shape of the A706 Grade 80 stress-strain curve. A comparison

of these stress-strain curves with the stress-strain curves obtained during the experimental phase of the project is presented in section 4.6.6.

A report submitted to the Charles Pankow Foundation in late 2013 by Wiss, Janney, Elstner and Associates, Inc. (WJE, 2013) seeking to determine if it would be appropriate for ACI 318 to change the required method for measuring the yield strength of nonprestressed reinforcement without a well-defined yield point from the extension under load (EUL) method at a strain of 0.35 percent to the offset method (OM) at an offset strain of 0.2 percent, presented a number of monotonic stress-strain curves for A706 Grade 80 rebar. While tabulated values of stress and strain were not provided as part of the report, the general shape of the curves can be insightful. Data used to define the curves originated from the 2012 and 2013 CRSI Mill Databases, the archives of the WJE laboratory, and testing at a university research laboratory. Because the CRSI Mill Databases are composed of data provided by producing mills, they only contain data on yield strength, tensile strength, and percent elongation at fracture. The question of how WJE could have used this data to produce curves without the necessary strains is answered by noting that CRSI coordinated the collection of industry-recorded stress-strain curves specifically for their project.

Several of the stress-strain curves presented in the WJE (2013) report exhibit distinct yield plateaus (Fig. 2.5) while others have a more “roundhouse” distribution (Figures 2.6-2.7). It should be noted that while Figure 2.5 includes curves for A615 grades 60 and 80 and A706 grades 60 and 80 bars, the report did not distinguish between specifications for either of the grades. Similarly, Figure 2.6 presents curves for both A615 and A706 grade 80 bars but does not clarify which are A615 and which are A706. According to the report, 98% of the straight bar curves had a well-defined or sharp yield point while all of the coiled bar curves had the “roundhouse” distribution. Additionally, the coiled reinforcing bar curves had distinctly lower elastic moduli – on the order of 21,000-22,000 ksi. Black dashed lines are actual tests while red solid lines represent “normalized” stress-strain relations generated to have ideal properties.

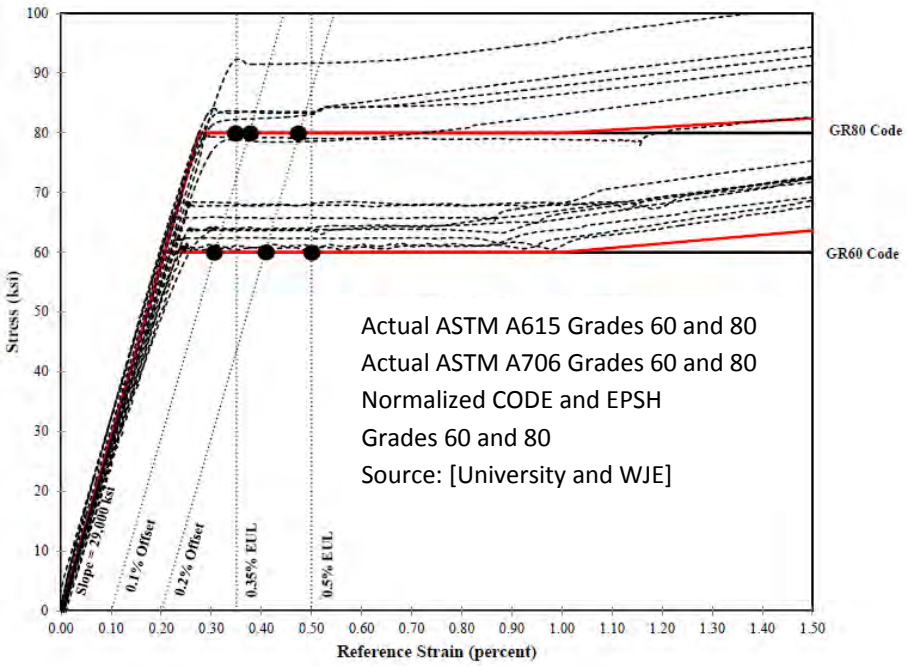

Figure 2.5. Grades 60 and 80 stress-strain curves for ASTM A615 and A706 reinforcing steel from WJE (2013) report having distinct yield plateaus

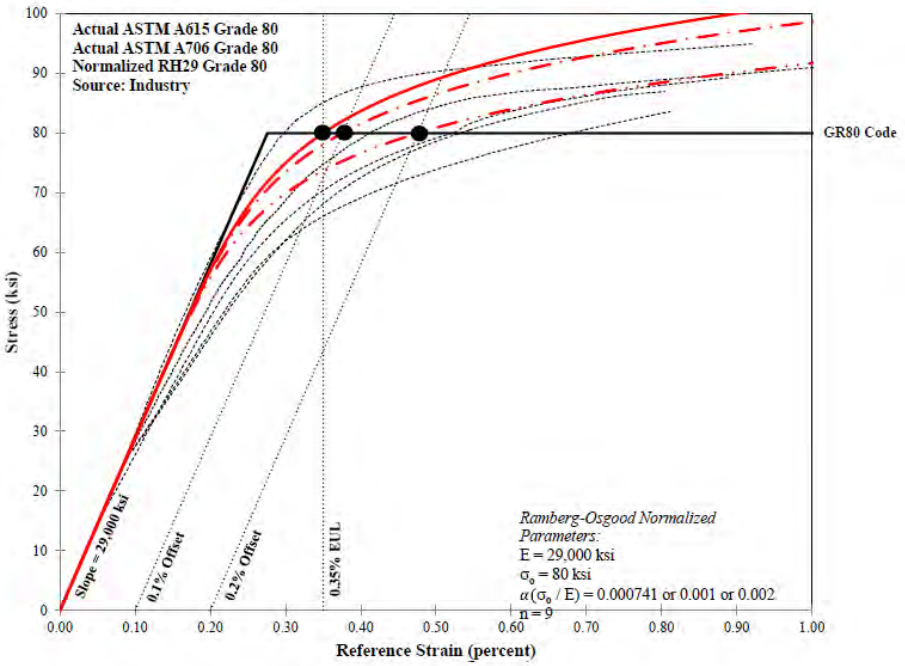

Figure 2.6. A615 and A706 Grade 80 stress-strain curves from WJE (2013) report exhibiting a "roundhouse" curve

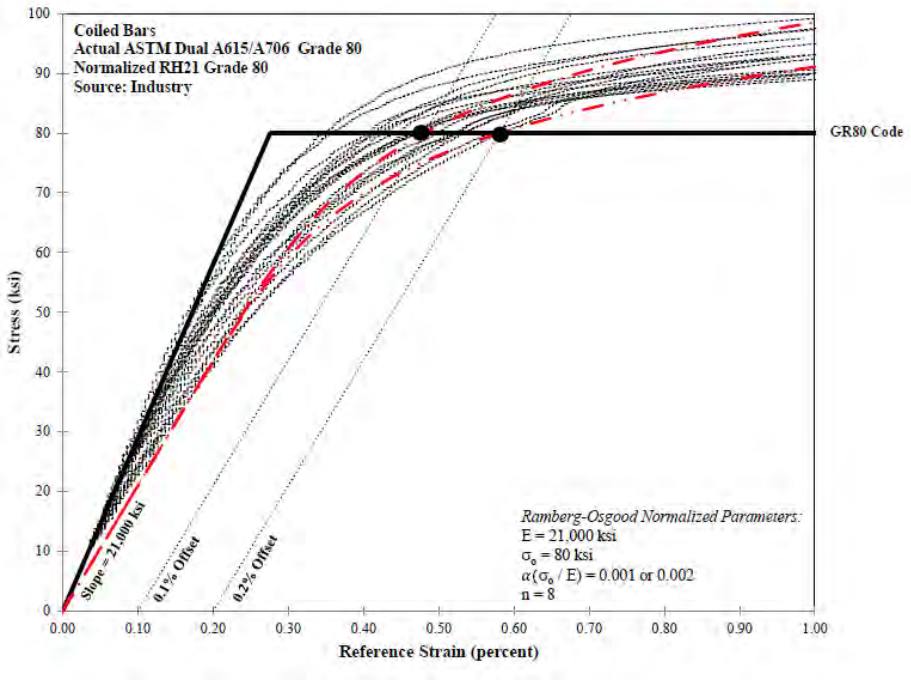

Figure 2.7. Dual A615/A706 Grade 80 coiled rebar stress-strain curve from WJE (2013) report exhibiting a "roundhouse" curve

Figure 2.8 presents the stress-strain curves associated with the Rautenberg et al. (2013) paper. A comparison of Figures 2.5 and 2.8 reveals that these were three of the curves presented in the WJE report to which Rautenberg was a contributor and therefore do not represent new data. The stress-strain curve for specimen number 7a has a very short yield plateau with no drop in stress before the onset of strain hardening. Specimens 7b and 7c have similar, longer yield plateaus.

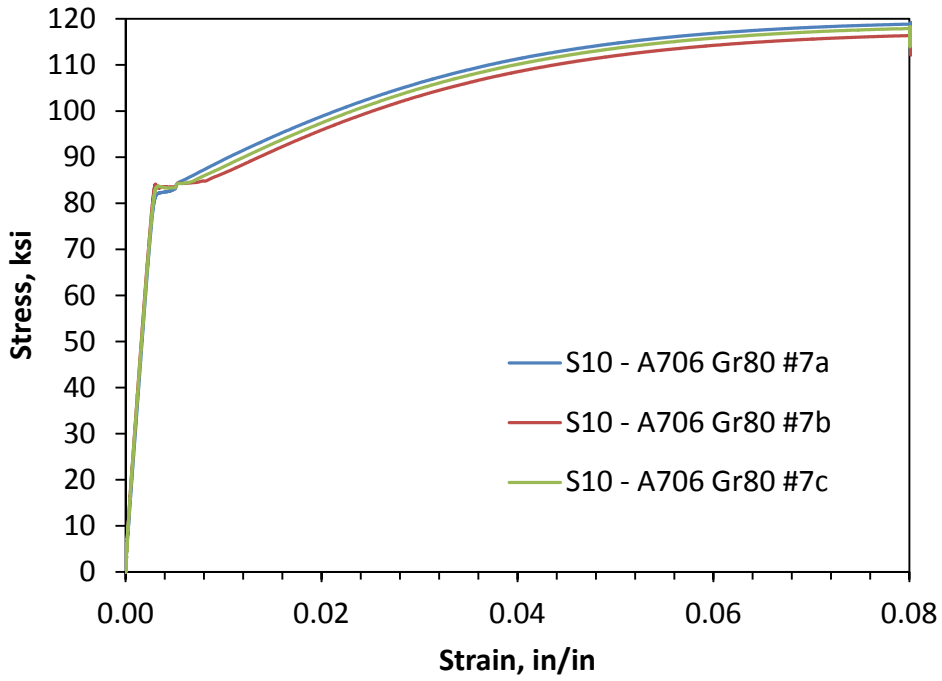

Figure 2.8. Stress-strain curves for 3 No. 7 bars from Rautenberg et al. (2013)

A detailed report produced by the National Earthquake Hazards Reduction Program (NEHRP) Consultants Joint Venture (GCR, 2014) in March 2014 focused on the use of high-strength reinforcement (f_y greater than 60 ksi) in special moment frames and special structural walls. ACI 318-14 (ACI, 2014) currently restricts the use of any reinforcement having yield strength greater than 60 ksi in seismic applications in the US. A parametric study of four building models reinforced with Grades 60, 80, and 100 longitudinal reinforcement subjected to actual recorded ground motions revealed that the different grades offered comparable performance in the considered earthquakes. Results from the study were used to validate a proposal to ACI recommending A706 Grade 80 reinforcement be allowed in special moment frames and structural walls. Reinforcing steel data was provided by Nucor Steel Seattle, Inc. and the 2011 and 2012 CRSI Mill Databases.

While no numerical stress-strain data was provided in the report, the stress-strain curve of a No. 8 and a No. 18 bar was provided courtesy of the steel mill (Fig. 2.9). Based on the graph, the No. 18 bar barely meets the minimum allowable yield strength of 80 ksi when a 2% offset line is used to define the yield point. Past research has indicated a possibility for larger diameter bars to have lower strengths, presumably due to factors associated with the manufacturing process such as reduced grain refinement and different cooling rates and times (Lim, 1991); however, other research suggests that this is not the case (Mirza and MacGregor, 1979; Nowak and Szerszen, 2003). It is unclear whether such factors influenced the results of the present research. Nonetheless, the nature of the curves offers an interesting point of comparison with test results obtained during the experimental phase of the current project (section 4.6.6). Despite their

differences in yield and tensile strength, both bars seemingly surpass the minimum tensile to yield ratio of 1.25. The strain at peak stress was approximately 10% for both bar sizes.

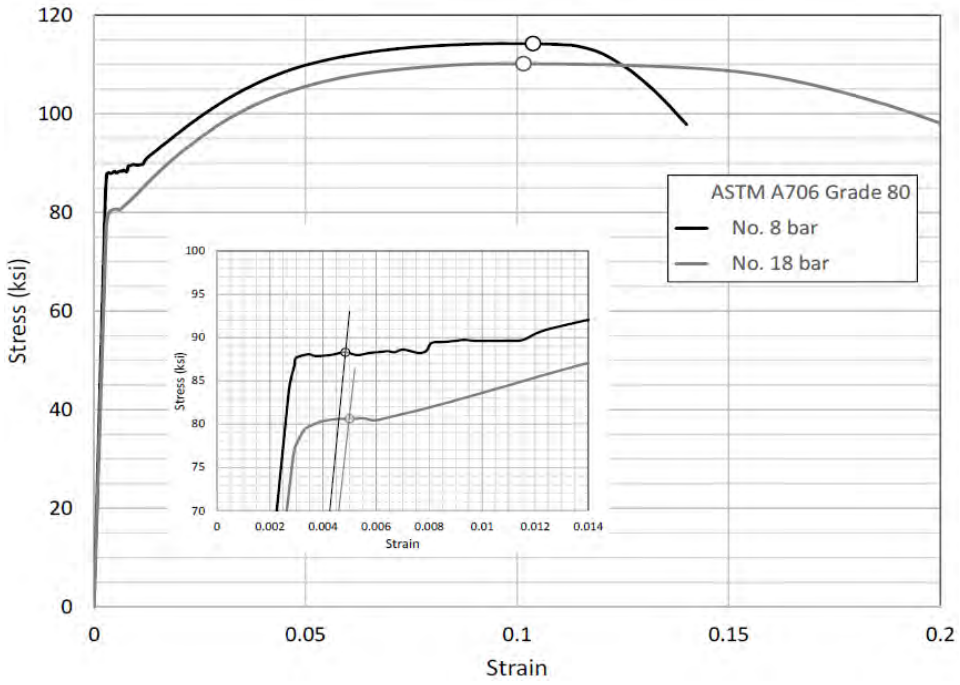

Figure 2.9. Stress-strain curves of a No. 8 and a No. 18 bar referenced in NIST GCR Report (2014). Original source: Nucor Steel Seattle, Inc.

The stress-strain curves of three No. 3 bar tests, three No. 5 bar tests, and three No. 6 bar tests were included in the report by Trejo et al. (2014). These curves have been reproduced in Figures 2.10-2.12. The "roundhouse" nature of the No. 3 bar curves follows what is typically seen in coiled reinforcing bars which undergo cold working as a result of the coiling and uncoiling process. The No. 5 and No. 6 bars both exhibited sharp-kneed yield points followed by a yield plateau. The strain at maximum stress averaged about 11.4 percent and the strain at the onset of strain hardening averaged about 0.9 percent.

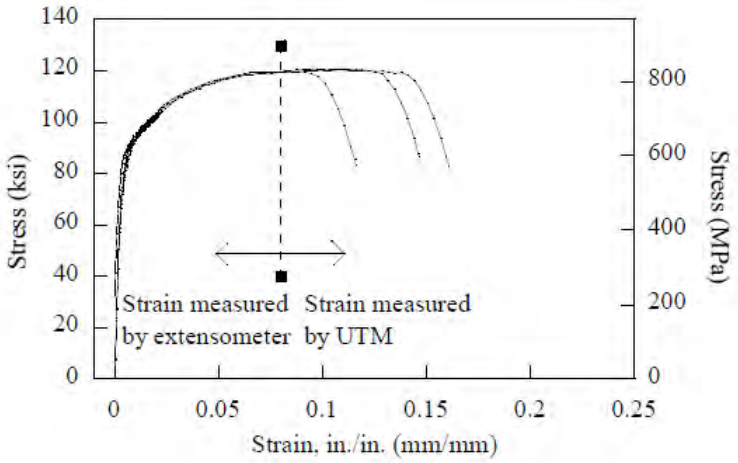

Figure 2.10. Stress-strain curves of No. 3 bars (Trejo et al., 2014)

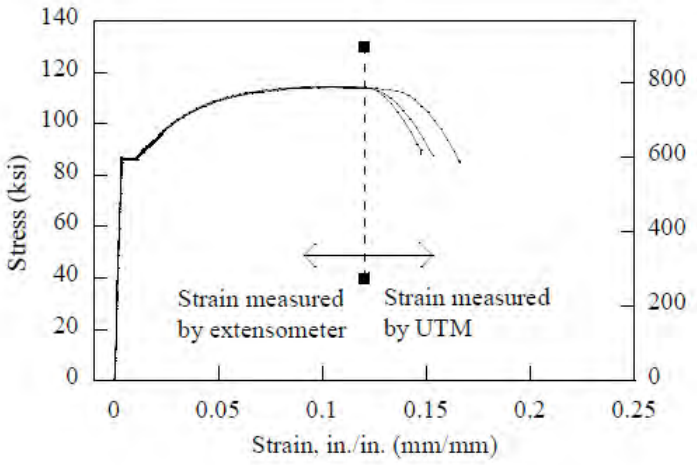

Figure 2.11. Stress-strain curves of No. 5 bars (Trejo et al., 2014)

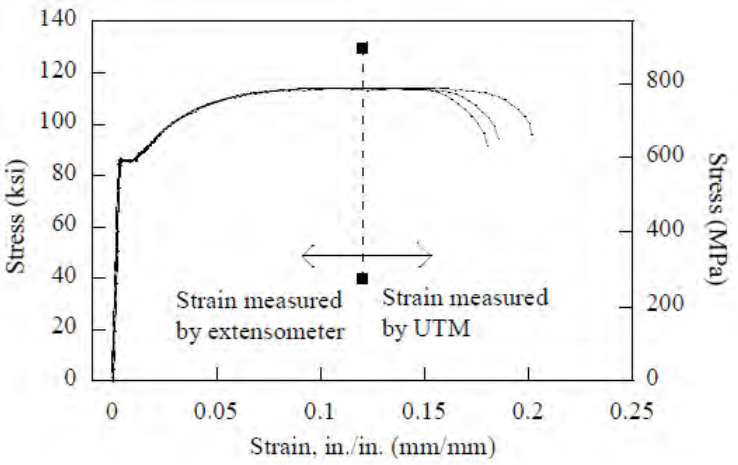

Figure 2.12. Stress-strain curves of No. 6 bars (Trejo et al., 2014)

2.5. Discussion of Literature Findings

Just five reports were found to include material test results on A706 Grade 80 steel either in tabulated or graphical form. Of the five reports, only two unique datasets could be confirmed: one consisting of three No. 7 bar tests (Rautenberg et al., 2013) and one consisting of three No. 3, three No. 5, and three No. 6 bar tests (Trejo et al., 2014). The earliest of the five reports was completed in 2013, two were completed in March of 2014, and the most recent paper was published in June of 2015. This is not surprising considering the relatively recent introduction of Grade 80 rebar into the ASTM A706/A706M specification in 2009. The available experimental data is further limited in that only a few bar sizes have been considered and that strains have generally not been provided to accompany the included yield and tensile strength data. This is

particularly true with data provided by the producing mills as they generally lack the necessary equipment required to capture strains. It should also be considered that because data obtained from producing mills does not necessarily stem from ideal laboratory conditions using appropriate, carefully calibrated measurement equipment and trained personnel, it should not be used for design purposes. This limitation extends to the CRSI Mill Databases which, while offering insight into the increased use and testing of A706 Grade 80 rebar between 2011 and 2013, are composed of submitted mill test results.

By consequence of the extremely limited amount of data found in the available literature, what does exist is not sufficient to generate recommendations on the material properties of A706 Grade 80 rebar. Rather, these findings simply served as reference points to validate trends and identify anomalies arising during the testing phase of the project. A graphical comparison of the literature-based stress-strain curves with the experimental curves generated through this project is presented in section 4.6.6.

3. CHAPTER 3 - EXPERIMENTAL PROGRAM

3.1. Chapter Summary

Presented in this chapter is a detailed explanation of the experimental work that was done to arrive at the recommended stress-strain parameters and values presented in Chapter 5. Included are a summary of the material that was tested, the nature of the testing, details related to the instrumentation and equipment that was used, and clarification on how the raw experimental data was processed.

3.2. Materials

Reinforcing steel for the project was provided by three different producing mills. Each mill provided reinforcing bars from all sizes No. 4 through No. 18. Additionally, each mill provided steel such that three different heats were represented for each of the ten bar sizes. That is not to say that each mill only provided three different heats of steel. A summary of the different bar sizes and heats for each mill can be found in Appendix A. Furthermore, each mill provided, at minimum, three twenty-foot lengths of straight rebar for each combination of heat and bar size. In some cases, additional twenty-foot bars were provided for a given heat and bar size.

Accompanying the shipments, each mill provided a certificate of compliance with the ASTM A706/A706M mechanical and chemical composition requirements. Included in these certificates were representative values of yield strength, tensile strength, and percent elongation at fracture for each heat of steel provided. Also provided with the steel were the results of a chemical analysis on each of the heats that listed the alloying elements included and their respective percentages. **According to these mill-supplied chemical compositions, each heat of steel being provided met the A706 requirements**. **Similarly, each heat qualified as A706 Grade 80 on the basis of the mechanical properties provided in the mill certificates**.

Due to constraints in cost and time associated with changing out the rollers at the steel mills, only a portion of the bars provided to the research project were actually stamped A706 Grade 80, despite meeting the required mechanical and chemical compositions as per the mill certificates. Table 3.1 provides a summary of the different markings on the bars according to mill and bar size. As will be discussed later in this chapter, special care was taken to ensure that each rebar test specimen could be traced back to the exact twenty-foot bar from which it originated. This included a record of each bar's grade stamp and associated heat number and predicted mechanical and chemical properties.

Table 3.1. As-stamped type and grade of steel by producing mill and bar size

Bar Size	Mill 1		Mill 2		Mill 3	
	Type	Grade	Type	Grade	Type	Grade
#4	A615	60	A615	60	A615	60
#5	A615	60	A615	60	A615	60 and 80
#6	A615	60	A615	60	A615	60
#7	A706	80	A615	60	A615	60
#8	A706	80	A615	60	A615	75
#9	A706	80	A615	60	A615	60 and 75
#10	A706	80	A615	60	A615	75
#11	A706	80	A615	75	A615	75
#14	A706	80	A615	75	A615	75
#18	A706	80	A615	75	A615	75

All heats met ASTM A706 Grade 80 chemical and mechanical requirements according to the mill certificates provided with the steel

3.3. Instrumentation

An Epsilon Class B1 2 inch gage length extensometer was used to record strains for all No. 4 through No. 10 bar tests. In addition to the extensometer, an Optotrak system was used to calculate strains on all tests. Final recommendations related to strains have been based on the Optotrak system measurements.

The Optotrak system is a 3D noncontact position measurement system capable of simultaneously tracking the location of up to 512 target LEDs or "markers" with an RMS accuracy of up to 0.1 mm and a resolution of 0.01 mm. The entire system operates in the infrared spectrum in which markers flash IR light at a predefined frequency of up to 4600 Hz and, depending on the number of markers used, can be recorded at a frame rate as high as 2000 Hz. The outputs from the Optotrak are the x-y-z coordinates of each marker relative to a pre-defined origin at each frame record.

The distance between any two markers at a given instant in time can be calculated using the 3D Pythagorean Theorem. Strains are then calculated by taking the change in distance between any two markers divided by the initial distance between them. Because the Optotrak is capable of tracking multiple markers simultaneously, therefore allowing multiple gage lengths to be established on a single test specimen, it is possible to assess the distribution of strain over the entire instrumented region of the specimen at each reading of the data. Furthermore, it is possible to develop a stress-strain curve for each gage length as the strains within a given gage length are necessarily unique to that gage length. The application of this additional data is discussed in further detail in Chapter 4.

Another key advantage of the Optotrak is the ability to keep the markers in place through fracture which becomes increasingly detrimental to the extensometer as bar size increases. As a result, it is possible to record the strain at the instant of fracture. Furthermore, when compared to strain gages, the ability to measure large strains is significantly enhanced.

3.4. Preparation of Test Specimens

Individual test specimens were cut from the twenty-foot bars provided by the mills. Three specimens were cut from each of the three twenty-foot bars for each combination of mill, heat, and bar size. All specimens were left in the as-rolled condition. The total number of test specimens and the complete breakdown by size, mill, heat, and bar number are provided in Table 3.2 below.

Table 3.2. Test matrix

Size	Mills	Heats	20' bars	Specimens	Tests
#4	3	3	3	3	81
#5	3	3	3	3	81
#6	3	3	3	3	81
#7	3	3	3	3	81
#8	3	3	3	3	81
#9	3	3	3	3	81
#10	3	3	3	3	81
#11	3	3	3	3	81
#14	3	3	3	3	81
#18	3	3	3	3	81
Total Possible Number of Tests					810

Each test specimen was labelled with a unique identification number to denote its exact place in the testing matrix and to ensure that test results could later be organized on the basis of mill, heat, or even single twenty-foot bar. Figure 3.1 illustrates the numbering scheme. The first number in the sequence represents the producing mill. As there were three mills providing steel, this number is always a 1, 2, or 3. The second number indicates from which of that mill's heats the bar originated. As stated previously, there were more than three heats of steel per mill, however, only three of these could be represented by a given bar size. This number ranges from1 to 9 depending on the mill. The middle number denotes the bar size and therefore ranges from 4 to 18 to correspond to one of the ten bar sizes considered. The fourth number indicates from which of the three twenty-foot bars in a particular heat the specimen was cut and varies from 1 to 3 accordingly. The final number identifies the specific test specimen and also varies from 1 to 3. Mathematically, there are 3 x 3 x 10 x 3 x 3 = 810 combinations, or, in other words, 810 possible tensile tests.

The above-described numbering scheme proved beneficial in that it offered a concise way of representing mill names and lengthy heat ID's as a single number. This additionally served to

maintain the confidentiality of the three mills; however, the specific details of what each number represents have been provided in a separate document. The numbering scheme also provided unique file names for each test that could easily be referenced either manually or by computer program.

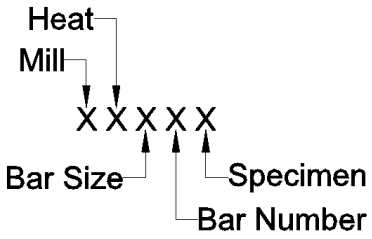

Figure 3.1. Numbering scheme used to uniquely identify each test specimen

Individual test specimen lengths were determined according to ASTM A370 which specifies a required minimum distance of two bar diameters between the grip-bar interface and the nearest gage mark. Thus, the minimum length of a test specimen is a function of its diameter and the desired number and size of the gage lengths. All specimens were cut to allow for six 2" gage lengths.

A spacing of 2" was chosen for the Optotrak markers in order to be consistent with the 2" gage length of the extensometer. Including six of these 2" gage lengths inherently offered a way of measuring strains over three overlapping 8" gage lengths (Fig. 3.2) as strains can be calculated between any two markers regardless of whether or not they are adjacent. Including three 8" gage lengths increased the likelihood that fracture could be captured in an instrumented region of the test specimen. Additionally, the ability to provide strain data in terms of an 8" gage length offered compatibility with existing test data also in terms of an 8" gage length. As will be discussed later in the report, little difference existed between 2" and 8" gage length measurements. Final recommendations related to strains have, therefore, been based on the 2" gage length data.

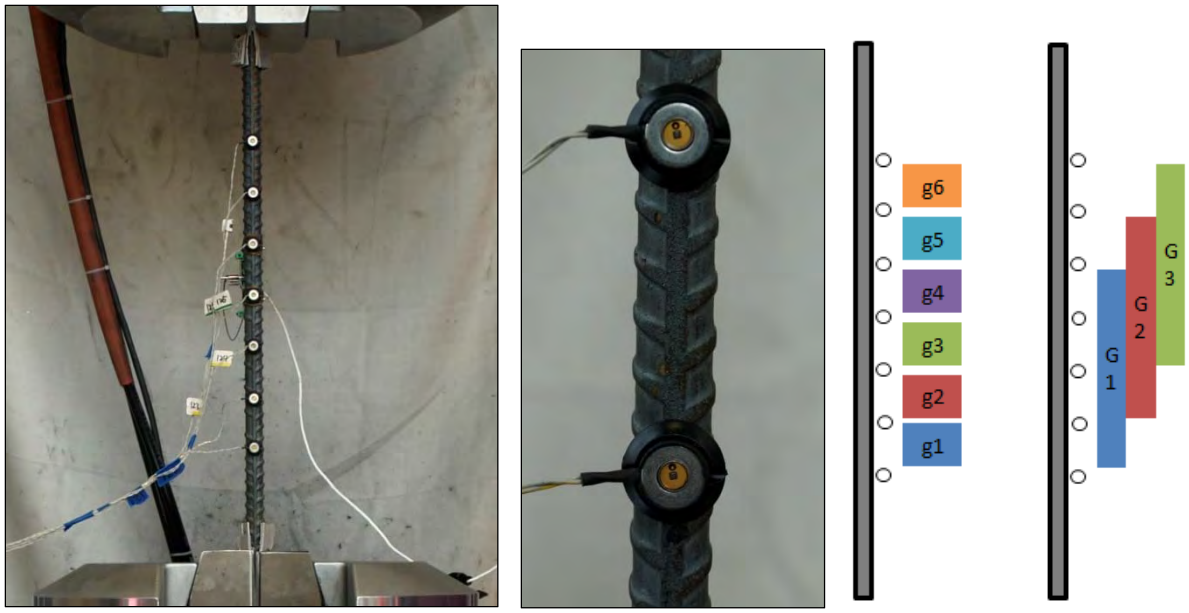

Figure 3.2. Location and spacing of Optotrak markers on a No. 4 bar and illustration of 2" and overlapping 8" gage lengths

A single specimen length of 30 inches was used for all bar sizes No. 4 through No. 10, while a longer specimen length of 48 inches was used for the No. 11 through No. 18 bars to accommodate the custom testing rig which will be described in the next section. In all cases, the chosen lengths exceeded the minimum allowable lengths for the number of gage lengths used.

3.5. Testing Equipment and Protocol

In total, 788 of the possible 810 tests were conducted. The 22 remaining tests were not performed due to incompatibility of the testing grips with the horizontal ribs on a subset of the No. 18 bars (all from the same mill) which inevitably resulted in cracking and fracture of the wedge grips in the direction of the teeth after one to two tests (Fig. 3.3). Nonetheless, of the 27 Mill 1 No. 18 bar specimens that posed this problem, five representative samples were able to be tested.

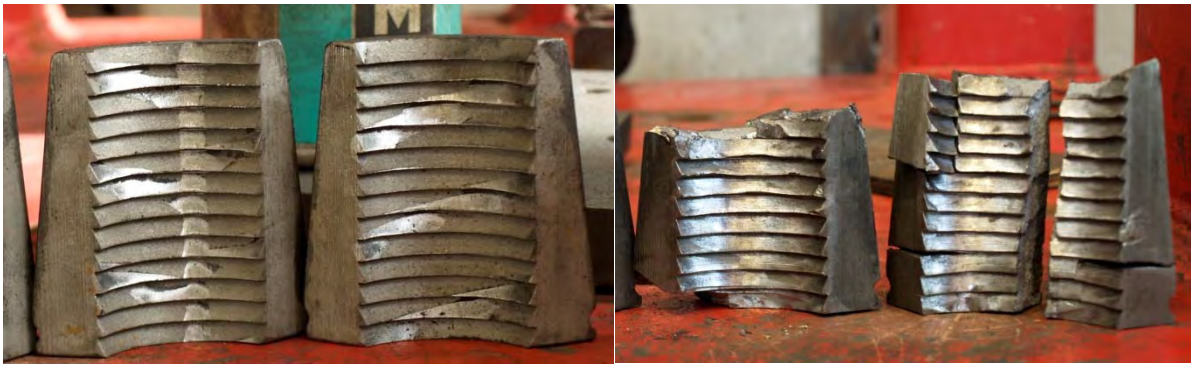

Figure 3.3. No. 18 bar wedges undamaged (left) and after testing Mill 1 bars (right)

Two different test setups were used to test the bars. A commercially available MTS universal testing machine was used to test all No. 4 through No. 10 bars while a custom-built testing rig (Fig. 3.4) was used to test the No. 11 through No. 18 bars. The MTS universal testing machine was limited by a capacity of 200 kip which precluded the testing of No. 14 and No. 18 bars. Furthermore, the maximum grip size available prevented the testing of anything greater in diameter than a No. 10 bar, thus the need for the additional test setup for the larger bars.

The MTS machine was operated at a displacement rate of 1 in/min in order to satisfy the testing speed requirements of ASTM specification A370 which specifies an upper and lower pre-yield and post-yield testing speed as a function of the free length of the bar. As stated previously, a single specimen length of 30 inches was used for all No. 4 through No. 10 tests. This corresponded to a bar free length of approximately 20 inches. Rather than select a single pre-yield speed and a different post-yield speed, which causes a momentary fluctuation in the force-displacement response at the change in load rate and necessarily adds a level of subjectivity to the test, the constant displacement rate of 1 in/min was applied for the full duration of each test. Initially, all tests were taken until fracture of the bar; however, tests conducted later in the testing program were stopped prior to fracture if necking occurred outside of the instrumented region. This prevented unnecessary wear on the testing equipment as no further useable data would have been acquired in these cases. A compilation of fractured and necked bar photos is included in Appendix F.

The custom testing rig used to test the No. 11 through No. 18 bars consisted of three 200-kip double-acting hydraulic jacks which provided a total capacity in excess of 600 kips. The jacks were operated by an electric hydraulic pump. Jacks reacted against a 5” thick hexagonal steel plate at either end and were placed radially about a 3” diameter hole at the centroid of the plates. The entire system was operated in an upright manner such that the bars were tensioned vertically. The bars were anchored at the top and bottom of the setup using a wedge-chuck system (Figs. 3.5-3.6) in which the chucks reacted on the opposite faces of the plates as the jacks. The primary motivation for using the three-jack two-plate system was that it left the entire middle length of the test specimen exposed to accommodate the Optotrak markers used to determine strains.

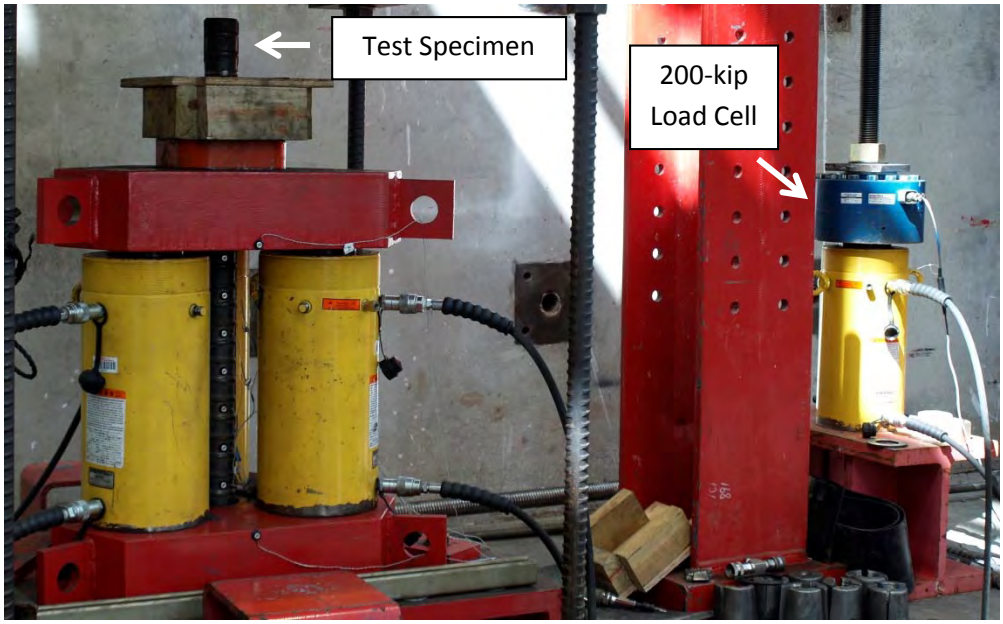

Figure 3.4. Custom testing rig used to test No. 11, 14, and 18 bars (No. 18 bar shown)

Figure 3.5 Wedge-chuck system used to anchor No. 11, 14, and 18 bars (No. 18 bar shown)

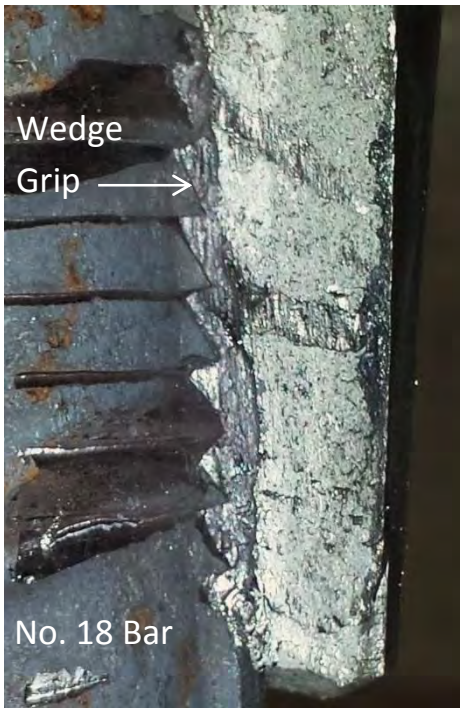

Figure 3.6. Interface between bar and wedge grips

The custom-built testing rig operated at a displacement rate proportional to the flowrate of the electric hydraulic pump. The testing rig's lack of a servomechanism to auto-regulate the displacement rate meant that this value could not be specified at the beginning of the test as with the MTS machine, but that it had to be measured during the test and then calculated afterwards.

Performing this calculation for a number of tests revealed a consistent displacement rate between the hexagonal plates of 0.3 in/min; however, due to seating of the wedge grips, this did not directly translate into a specimen displacement rate of 0.3 in/min.

Wedge seating describes the process by which the toothed wedge grips used to anchor the test specimens on either end of the 5" reaction plates progressively bite deeper into the bar (Fig. 3.6) and are consequently allowed to slide farther down into the chuck over the course of the test. Because initially the resistance of the bar to elongating is very high (slope of the elastic force-displacement curve), the majority of the wedge seating (biting and sliding) occurs prior to yielding (Fig. 3.7); however, following yielding, the stiffness of the bar essentially drops to zero (the yield plateau) and the wedges do not displace while the bar does so under nearly constant force. This explains the blip in the wedge seating and bar elongation curves immediately after yielding as seen in Figure 3.7. Note that the "wedge seating" curve was obtained by taking the difference between the displacement rate of the plates and the elongation rate of the bar. Following the onset of strain hardening, the bar again has resistance to elongation, albeit at a reduced, nonlinear rate corresponding to the shape of the strain hardening curve. As a consequence, little additional wedge seating occurs and the bar elongates at nearly the same rate as the plates displace. Thus, initially, the displacement rate of the bar is slower than that of the plates, but following yielding they are essentially the same at about 0.3 in/min.

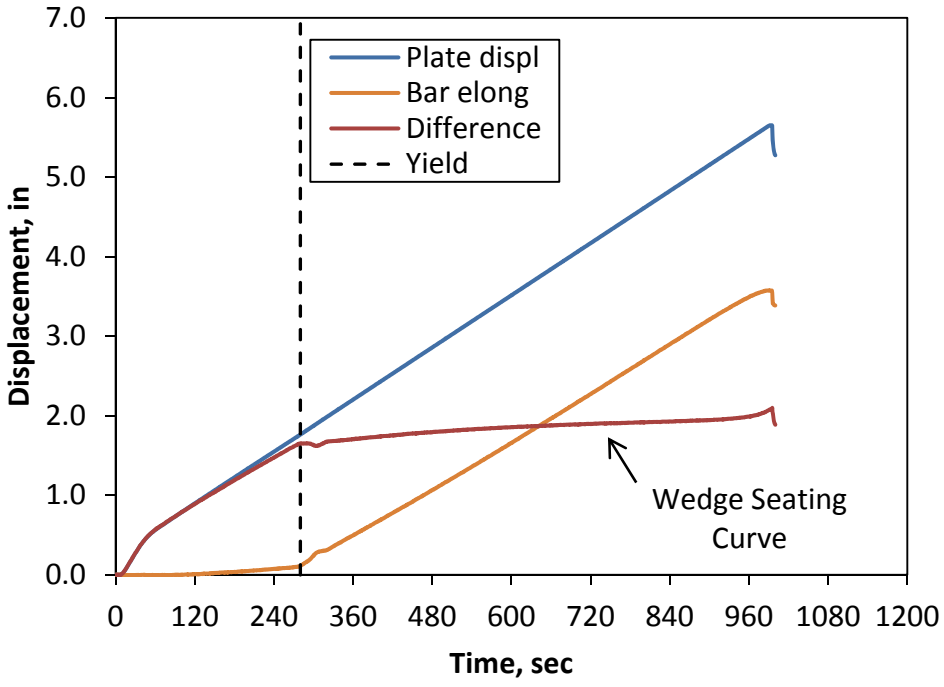

Figure 3.7. Wedge-seating phenomenon observed in No. 11-No. 18 bar tests

As a result of the wedge seating phenomenon and the associated bilinear load rate, bars tested in the custom testing rig inherently experienced a bilinear strain rate. The dimensions of the custom

testing rig dictated that each specimen have a free length of 33” between the wedge grips. This distance provided adequate length to accommodate the six 2” gage lengths and satisfy the requirements of ASTM specification A370. As stated previously, each of the No. 11, 14, and 18 bar specimens was 48” in length.

Due to the more violent nature of fracture of the larger bars and the nature of the wedge-chuck system, very few of the No. 11, 14, and 18 bars were tested completely to fracture. Instead, tests were stopped once the force readings showed a steady drop indicating that the ultimate tensile point had been reached and the bar had begun necking.

In all cases, stresses were determined by dividing the recorded forces on the test specimen by the nominal cross-sectional area in accordance with ASTM A370. The No. 4 through No. 10 bar forces were obtained from the MTS machine’s built-in load cell. The No. 11 through No. 18 bar forces were recorded using a 200-kip load cell as illustrated in Figure 3.4.

The configuration shown in Figure 3.4 resulted from the need to record forces in excess of 480 kips using a single 200-kip load cell. Due to the high forces, the load cell could not be placed directly in-line with the bar, but had to be placed on one of the hydraulic jacks where it would feel one third of the force on the bar. Rather than place the load cell on one of the three jacks surrounding the bar, which would require equal-height spacers on the other two jacks, it was placed on a fourth jack physically separated from the setup but still connected to the hydraulic pump. This fourth jack reacted against a high-strength threaded rod sized to take the full capacity of the jack. Theoretically, the fourth jack would produce the same force as the other three jacks since they were the same size and connected to the same hydraulic source; however, complicating issues of frictional losses caused this theory to break down. As will be discussed in the next chapter of the report, forces recorded using this configuration were consistently five to six percent higher than forces recorded at the location of the test specimen during the same test using a second load cell. Also to be discussed in the next chapter was the impact this had on the ultimate tensile strain values which were on average overpredicted by about 6.5 percent using the setup shown in Figure 3.4.

3.6. Determination of Stress-Strain Parameters

Each test generated two raw data files: one text file containing force data and one CSV file containing the Optotrak marker x-y-z coordinate data. Data was collected at a frequency of 8 Hz for the No. 4 through No. 10 bar tests and 2 Hz for the No. 11 through No. 18 bar tests. A slower recording rate was chosen for the large bar tests to account for the slower displacement rate produced by the electric hydraulic pump.

The two raw data files were compiled and processed in a single macro-enabled Excel workbook unique to each test in which forces were converted to stresses based on the nominal cross-sectional area of the bar and Optotrak marker coordinate data was converted to strain data using the procedure described in section 3.3. A combination of VBA programs and Excel worksheet

functions was used in these compiled individual test files to identify the values of key parameters along the stress-strain profiles corresponding to each gage length for each test. Table 3.3 provides a list of all the parameters for which values were determined for each test. Parameters highlighted in bold were used to define the recommendations for the A706 Grade 80 stress-strain curve presented in chapter 5. The remainder of this section describes each of the parameters and how they were determined.

It is important to note here the method by which the stress data was paired with the strain data. By recording both force and Optotrak coordinate data at a common frequency and starting both recordings simultaneously, it was possible to merge the resulting two data files on the basis of the record counts. While this approach worked for the No. 4-10 bar tests, it caused the No. 11-18 bar ultimate tensile strains to be overpredicted by about 6.5 percent as will be discussed in further detail in the next chapter.

Table 3.3. Complete list of parameters determined for each test

Modulus of Elasticity	Yield						Onset of Strain Hardening		Ultimate Tensile	
	ADM		EUL		0.2% OM					
E_s	$\boldsymbol{f_{y\ ADM}}$	$\boldsymbol{\varepsilon_{y\ ADM}}$	$f_{y\ EUL}$	$\varepsilon_{y\ EUL}$	$f_{y\ OM}$	$\varepsilon_{y\ OM}$	f_{sh}	$\boldsymbol{\varepsilon_{sh}}$	$\boldsymbol{f_u}$	$\boldsymbol{\varepsilon_u}$

3.6.1. Modulus of Elasticity

The modulus of elasticity, E_s, was taken as the slope of the line passing between 0.2 times the top-of-the-knee yield strength and 0.8 times the top-of-the-knee yield strength. This was to ensure that the value obtained was an accurate representation of the actual linear portion of the stress-strain curve and not biased by any non-linearity in the curve at the start of the test or just before the top-of-the-knee yield point. A graphical illustration of this process has been provided in Appendix B.

3.6.2. Yield Strength

Three methods of determining the yield strength were evaluated: the Autographic Diagram Method or "top-of-the-knee" ($f_{y\ ADM}$), the Extension Under Load Method ($f_{y\ EUL}$), and the Offset Method ($f_{y\ OM}$). The Extension Under Load yield strength was taken as the value of stress corresponding to a strain of 0.0035. The Offset yield strength was taken as the value of stress corresponding to the intersection of the stress-stain curve with a 0.2% offset line running parallel to the linear elastic region of the curve. All three methods are permitted by ASTM A370. A graphical illustration of each has been provided in Appendix B.

3.6.3. Yield Strain

Three individual yield strains were identified for each test, one corresponding to each of the three determined yield strengths: the Autographic Diagram Method yield strain ($\varepsilon_{y\ ADM}$), the Extension Under Load yield strain ($\varepsilon_{y\ EUL}$), and the Offset Method yield strain ($\varepsilon_{y\ OM}$). The ADM yield strain was taken as the strain corresponding to the top-of-the-knee yield strength ($f_{y\ ADM}$). The

EUL yield strain simply equaled 0.0035 by definition. The OM yield strain was identified as the value of strain corresponding to the intersection of the stress-strain curve with a 0.2% offset line running parallel to the linear elastic region of the curve.

3.6.4. Onset of Strain Hardening

The strain at the onset of strain hardening, ε_{sh}, was determined as the point at which a horizontal line passing through the 0.2% offset stress intersected a line tangent to the initial portion of the strain hardening curve. Specifically, the tangent line to the strain hardening curve was defined as the line passing between 1.02 times the 0.2% offset yield strength and 1.05 times the 0.2% offset yield strength. In specimens exhibiting well-defined yield plateaus, the 0.2% offset line consistently intersected the yield plateau thus making the horizontal line passing through this point analogous to the slope of the yield plateau. While not specifically required by Caltrans, the stress at the onset of strain hardening was taken as the point on the actual stress-stain curve corresponding to the strain at the onset of strain hardening using interpolation as necessary. This approach was designed to reduce subjectivity in determining when the yield plateau ceased and when the strain hardening curve commenced as well as to speed up the processing of the data. A graphical illustration of this process has been provided in Appendix B.

3.6.5. Tensile Strength and Ultimate Tensile Strain

The tensile strength, f_u, was identified as the maximum value of stress or the point at which strain hardening ceased and necking initiated. The ultimate tensile strain, ε_u, was identified as the value of strain corresponding to the point of maximum stress. This is not to be confused with the value of strain at fracture.

4. CHAPTER 4 - RESULTS

4.1. Chapter Summary

The third stage of the research program focused on five of the recorded parameters: $f_{y\,ADM}$, $\varepsilon_{y\,ADM}$, ε_{sh}, f_u, and ε_u. In order to be consistent with the notation currently used in the Seismic Design Criteria (SDC), these five key parameters are hereafter referred to as f_{ye}, ε_{ye}, ε_{sh}, f_{ue}, and ε_{su}. The values corresponding to each of these parameters for all of the tests were compiled in order to generate statistical distributions termed cumulative distribution functions (CDFs) and to identify summary statistics such as mean, standard deviation, and coefficient of variation. The compiled data was additionally used to make comparisons across the different bar sizes, mills, and heats within a mill to identify trends and detect anomalies.

Presented in this chapter is an explanation of the statistical methods used in the analysis of the compiled data and a summary of the as-measured results for each of the five key parameters. Following this is an explanation of the impact that the method of force measurement used with the custom testing rig had on the No. 11, 14, and 18 bar data and what adjustments were made to account for this in the final dataset. A short section is dedicated to re-examining three of the five key parameters in light of these adjustments. The remainder of the chapter focuses on assessment and applications of the final dataset.

4.2. Statistical Methods

Two primary approaches were taken to interpreting the body of data generated during the experimental phase of the project. The first approach was an evaluation of the distribution of the test results according to each of the five key parameters in terms of cumulative distribution curves. This approach provided a graphical way of understanding the spread of the data and additionally provided the percentiles of the data for each parameter. The second approach was to describe the results for each parameter in terms of its summary statistics, specifically: mean, standard deviation, and coefficient of variation. This section provides further clarification on the first of these two approaches.

Quantitatively, a cumulative distribution function can be used to identify the percentage of data in a dataset that exists at or below a given value. Qualitatively, it serves as a graphical way to illustrate the distribution of the data in a dataset about its median. CDFs that are short and steep imply less variability in the data while CDFs that are long and sweeping imply higher variability in the data. Note that this interpretation can be biased by the scale used in generating the graph. An added advantage of the CDF curve is that it offers a quick way to identify trends or anomalies in a dataset when plotted against other CDF curves from the same or different datasets.

Numerous types of cumulative distribution functions exist; however, only the normal CDF and the empirical CDF have been considered in the analysis of the experimental data. Past research has demonstrated that a normal distribution function is adequate to describe the distribution of yield and tensile strength in mill test results for A706 Grade 60 and other grades of rebar

(Bournonville et al., 2004; Mirza and MacGregor, 1979; Nowak and Szerszen, 2003). While the normal CDF does not describe the actual distribution of the data (unless the data is normally distributed), it does offer visual insight into how close the data is to being normally distributed. The actual distribution of the data is defined by the empirical CDF which when compared with the normal CDF illustrates graphically the level of deviation from normality in the dataset.

More comprehensive methods of identifying the level of normality of a dataset or identifying the type of distribution that best models that dataset are available; however, this level of analysis was not undertaken by the current project. Knowledge of the underlying distribution of a dataset is beneficial in that it permits the dataset to be defined by a mathematical function that can be used to approximate values from the global dataset (all A706 Grade 80 bars in existence) which is typically impossible to completely test. For the purposes of this research, the empirical distribution is sufficient to illustrate the spread of the values for each parameter with enough precision to identify trends and highlight potential anomalies. Furthermore, the recommended values of the five key stress-strain parameters have been based on the empirical (actual) data as opposed to a normal fit to the data. A potential future use of the dataset could include distribution fitting.

4.3. As-Measured Stress-Strain Data

As stated previously, the No. 11 through No. 18 bar yield strength, tensile strength, and ultimate tensile strain values were artificially inflated as a result of recording forces with a load cell not directly in line with the bar. The values and associated graphs presented in this subsection are based on the as-measured data and, in the case of the three affected parameters, do not represent final values but are, nonetheless, presented for completeness and comparison purposes. The recommendations for these three parameters are presented in section 4.5. An explanation of the recommendations for the remaining parameters has been included at the end of the subsection devoted to each of these parameters in the current section.

As previously stated, each test specimen was outfitted with six 2” gage lengths for recording strains. As a result of the nature of the instrumentation used, this additionally allowed strains to be calculated over any of three overlapping 8” gage lengths (section 3.4). Due in part to variability in recording the data and in part to the fact that strains are not perfectly uniform throughout the entire length of bar (refer section 4.6.1), there is some variability between gage lengths at a given strain recording as illustrated in Figure 4.1. As a result, six unique 2” gage length strains and three unique 8” gage length strains can be identified for every one recording of force. This translates into as many as nine values for the yield strain, onset of strain hardening, and ultimate tensile strain parameters for each test.

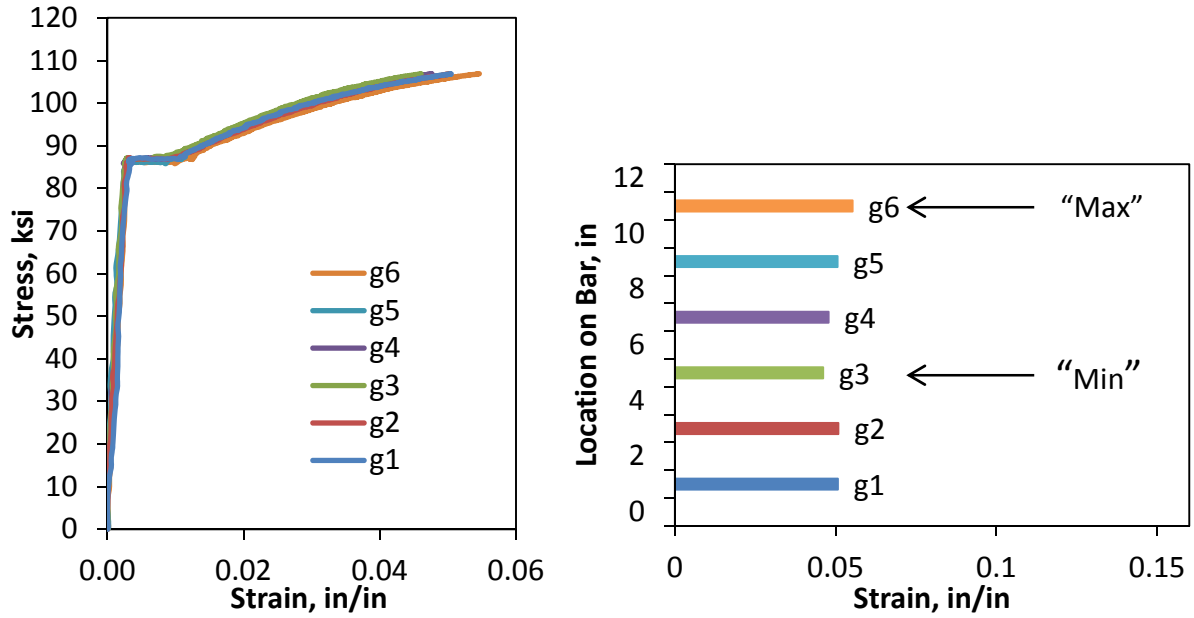

Figure 4.1. Partially plotted stress-strain curve (left) and distribution of strain over instrumented region at that instant (right)

Noting from section 3.4 that little difference existed between 2" and 8" gage length measurements, this can be reduced to six values per parameter for each test by considering only the 2" gage length results. However, in order to plot the CDF curves for the strain-based parameters, it is desirable that each test be represented by only one data point.

As a result, four CDF curves have been plotted for parameters obtained from Optotrak strain data. One of the curves is composed entirely of the minimums of the six values from each test. Similarly, one of the curves is composed entirely of the maximums of the six values from each test. A third curve is obtained by taking the mean of the six values from each test, and a fourth CDF curve is obtained by taking all six values from each test. Necessarily, this fourth curve includes on the order of six times as many data points as any of the other three curves. As will be seen, the recommended values were ultimately taken form the CDF curves of the means and the min, max, and total CDF curves left for illustrative purposes only.

4.3.1. Expected Yield Strength, f_{ye}

The expected yield strength was identified as the value of stress corresponding to the top of the knee of the stress-strain curve at the onset of yielding (formerly denoted as $f_{y\,ADM}$). Test specimens that did not exhibit well-defined yield plateaus (98 of 788 tests) were not included in this dataset. A summary of the different categories of yield behavior and percentages on how many tests fell in each category are provided in Appendix C. Additionally, a comparison of the 0.2% Offset Method yield strengths and the Autographic Diagram Method or top-of-the-knee yield strengths is provided in Appendix E. Note that the values provided in Appendix E are based on the adjusted No. 11 through No. 18 bar data which is described in section 4.4.

The normal and empirical CDF curves for the as-measured, expected yield strength considering all bar sizes are presented in Figure 4.2. The mean value of the empirical data is 86.2 ksi. The standard deviation and coefficient of variation are 2.5 ksi and 2.9% respectively. Also included in the graph are the ASTM minimum and maximum allowable yield strengths of 80 ksi and 98 ksi respectively. Because this parameter is determined based on load cell readings as opposed to Optotrak readings, there is only one normal and one empirical distribution.

Figure 4.3 illustrates the breakdown of the as-measured empirical yield strength data according to bar size. The as-measured mean values ranged from 84.2 ksi to 88.0 ksi with the No. 10 bars having the lowest mean value and the No. 11 bars having the highest. Figure 4.4 presents the normal distributions for the as-measured yield strength data. The trend from the empirical CDF is that except for the 11, 14, and 18 bars there is a decrease in median as-measured yield strength with increasing bar size; however, following the adjustments to the No. 11, 14, and 18 bar yield strengths described in section 4.4, this trend no longer held true. As will be discussed in section 4.4, the as-measured yield strength data was first adjusted before defining the recommendations presented in Chapter 5.

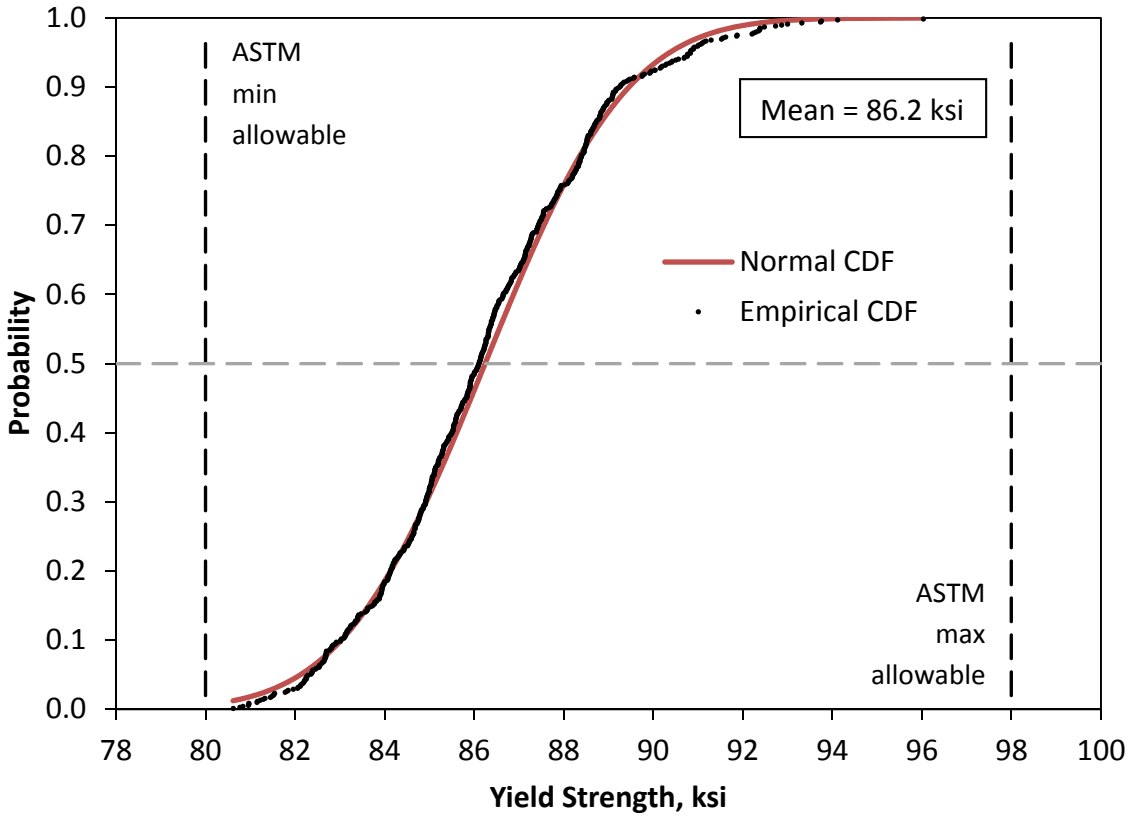

Figure 4.2. As-measured yield strength normal and empirical CDFs including all bar sizes

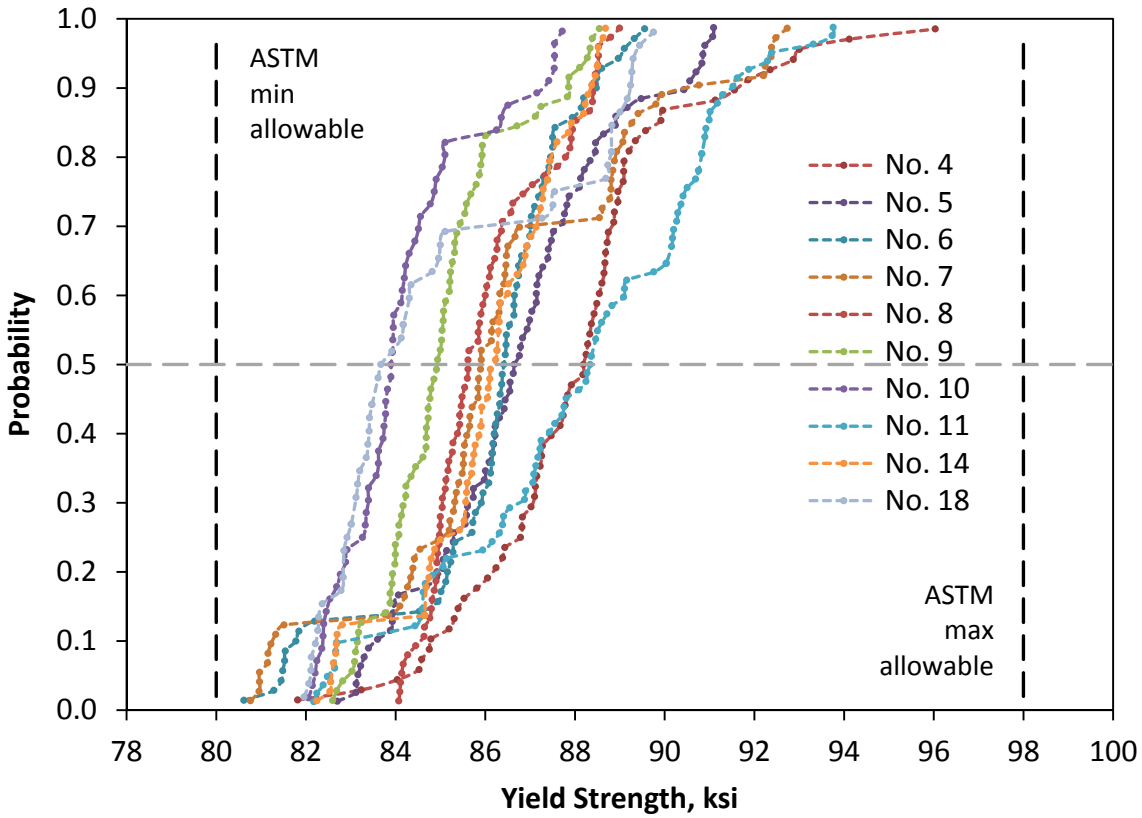

Figure 4.3. As-measured yield strength empirical CDFs for individual bar sizes

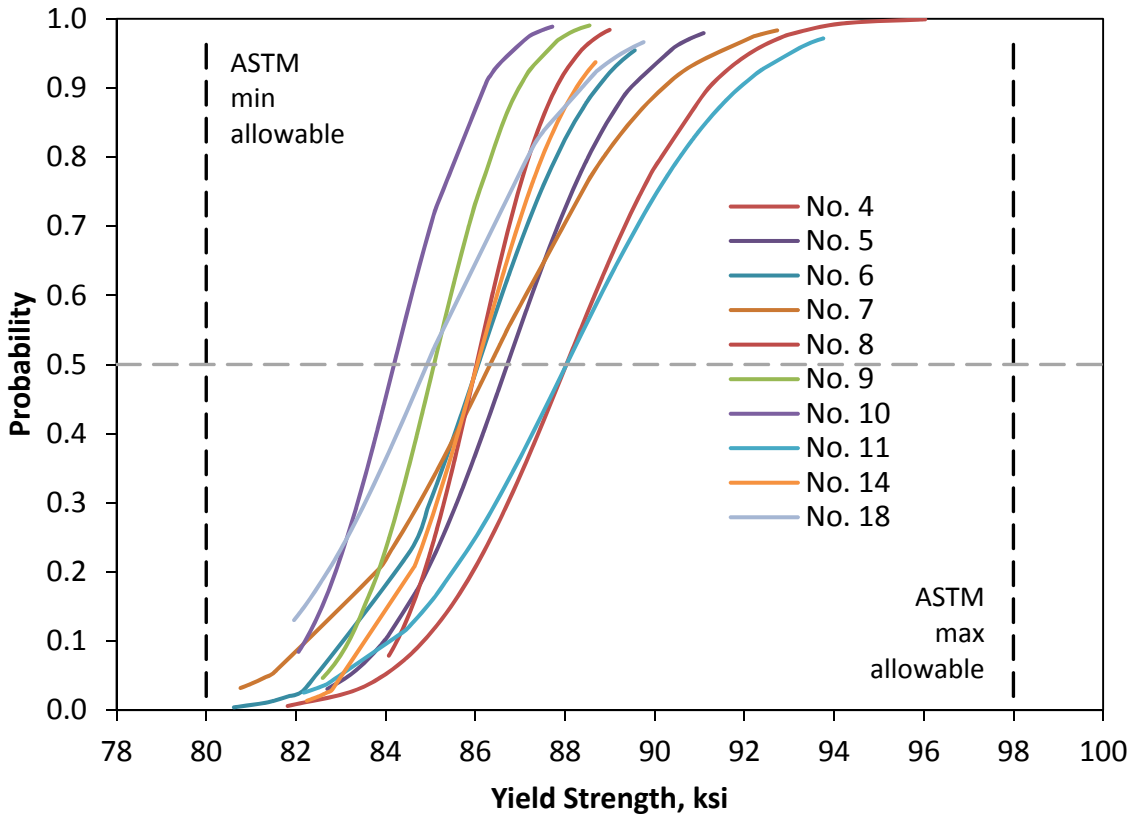

Figure 4.4. As-measured yield strength normal CDFs for individual bar sizes

4.3.2. Expected Yield Strain, ε_{ye}

The expected yield strain was identified as the value of strain corresponding to the stress at the top of the knee of the stress-strain curve at the onset of yielding (formerly denoted as $\varepsilon_{y\,ADM}$). This method of determining yield strain was chosen rather than the strain corresponding to the intersection of the 0.2% offset line ($\varepsilon_{y\,OM}$) which always either passed through a point on the yield plateau or intersected the strain hardening curve when specimens exhibited short or nonexistent yield plateaus. In either case, the intersection met the stress-strain curve well after the steel had ceased to be linear elastic. Test specimens that did not exhibit well-defined yield plateaus (98 of 788 tests) were not included in this dataset. A summary of the different categories of yield behavior and percentages on how many tests fell in each category is provided in Appendix C. Additionally, a comparison of the 2" vs 8" gage length results for the expected yield strain, onset of strain hardening, and the ultimate tensile strain is presented in Appendix D. This parameter was not affected by the configuration of the load cell used in the custom testing rig.

The normal and empirical CDF curves for the expected yield strain are presented in Figure 4.5. Because this parameter is determined based on Optotrak readings, there are four normal and four empirical distributions as described in the intro to section 4.3. The mean value of the mean

empirical data, based on a 2” gage length, is 0.0033 in/in. The corresponding standard deviation and coefficient of variation are 0.0003 in/in and 9% respectively.

Figure 4.6 illustrates the breakdown of the as-measured yield strain data according to the mean CDFs for each bar size. The mean values ranged from 0.0031 to 0.0034 with the No. 10 bars having the lowest mean value and the No. 14 bars having the highest. There is no indication that the yield strain was influenced by bar size. Figure 4.7 presents the normal distributions for the as-measured yield strain data.

The A706 Grade 60 section of the SDC currently provides a nominal yield strain and an expected yield strain. The nominal yield strain is defined as the specified yield strength divided by a modulus of elasticity of 29000 ksi. A similar calculation for A706 Grade 80 rebar results in a nominal yield strain of 0.0028. The recommended expected yield strain for A706 Grade 80 is defined as the mean value of the mean empirical data or 0.0033. A complete summary of all recommended values is presented in section 5.2.

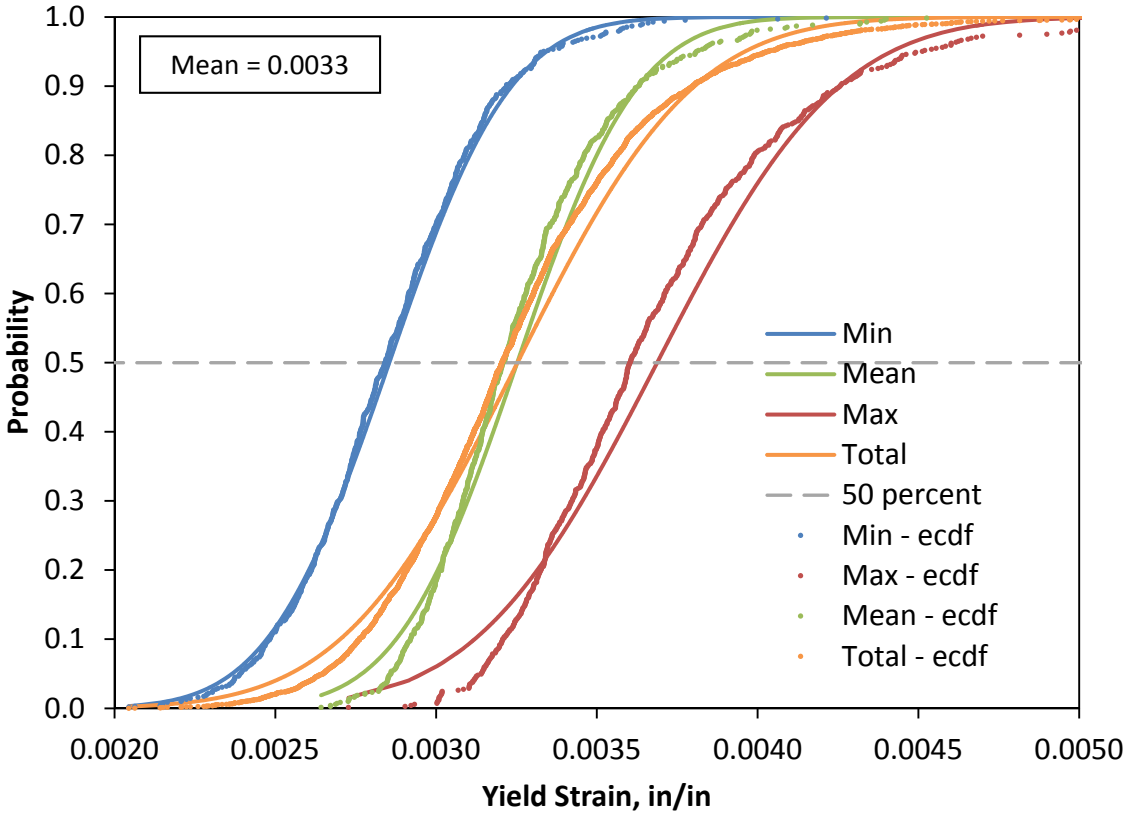

Figure 4.5. As-measured yield strain normal and empirical CDFs including all bar sizes

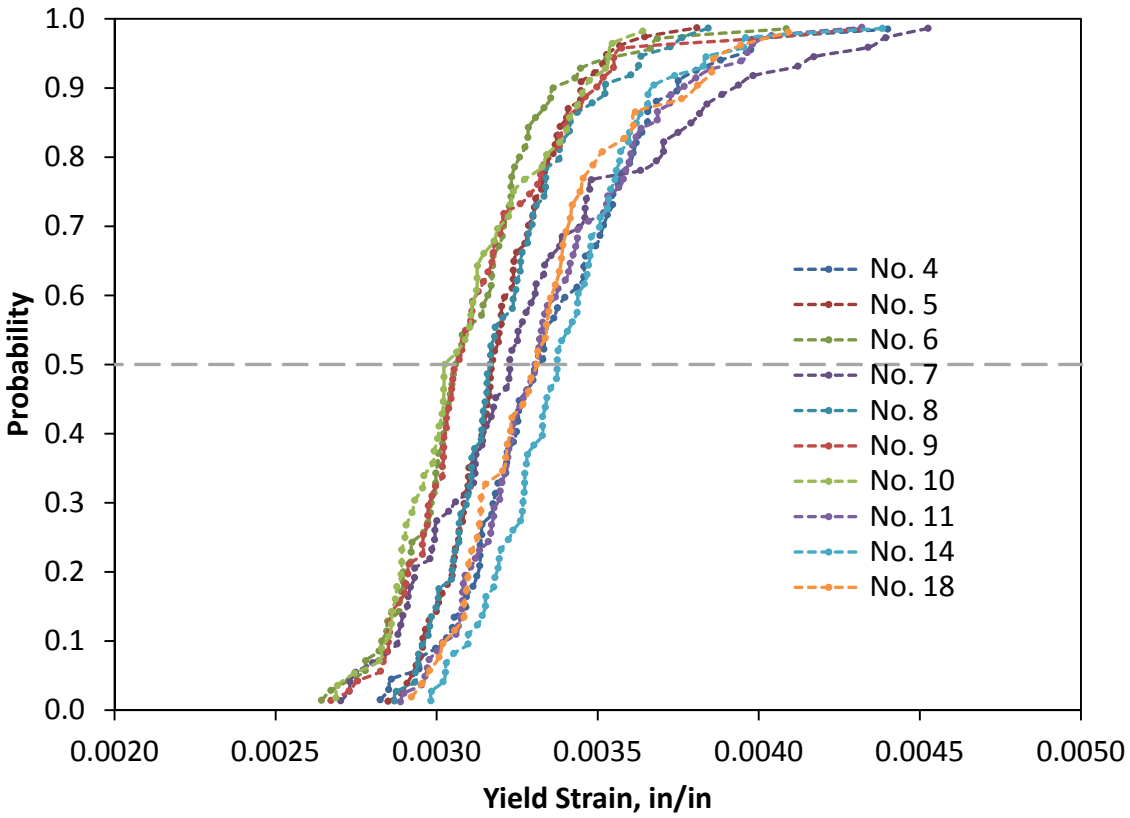

Figure 4.6. As-measured yield strain empirical CDFs for individual bar sizes

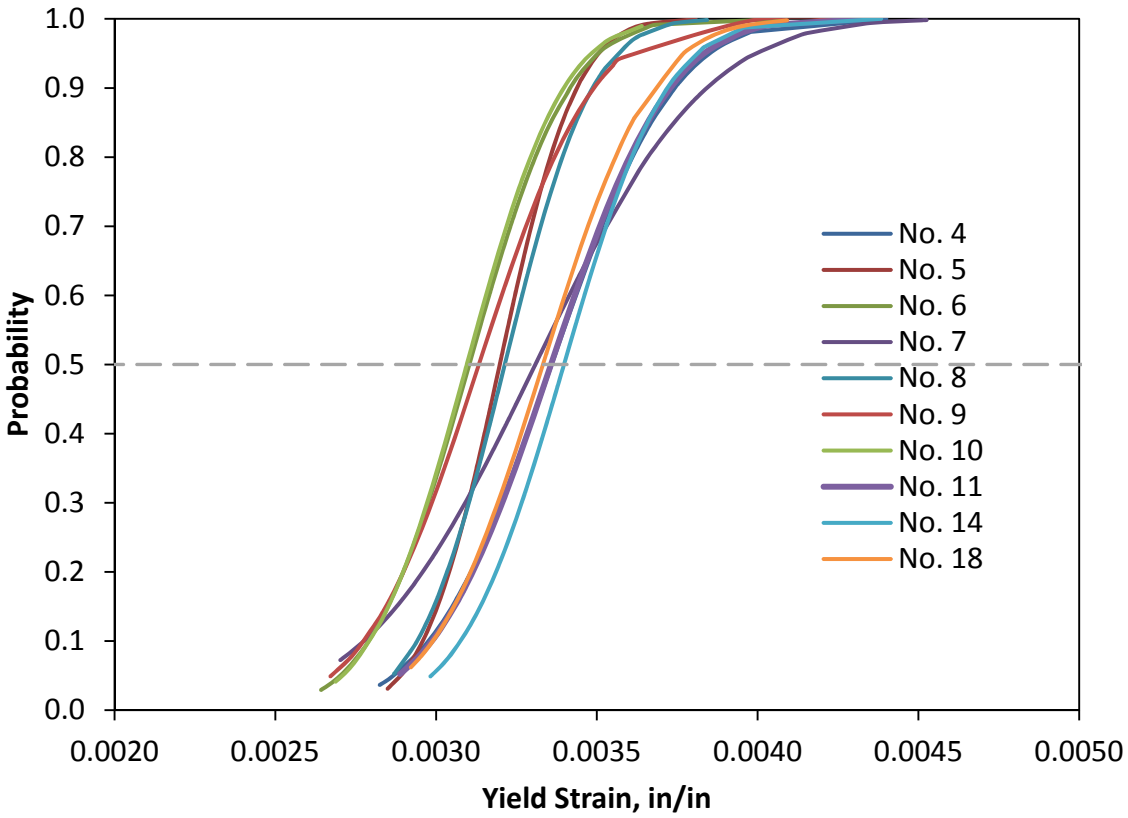

Figure 4.7. As-measured yield strain normal CDFs for individual bar sizes

4.3.3. Onset of Strain Hardening, ε_{sh}

The onset of strain hardening was identified as the value of strain corresponding to the intersection of a horizontal line passing through the 0.2% Offset Method yield strength and the slope of the initial portion of the stain hardening curve. Test specimens that did not exhibit well-defined yield plateaus are included in this dataset because they still exhibited strain hardening. In these cases, the onset of strain hardening generally coincided with the intersection of the 0.2% offset line with the stress-strain curve. This parameter was not affected by the configuration of the load cell used in the custom testing rig.

The normal and empirical CDF curves for the onset of strain hardening are presented in Figure 4.8. Because this parameter is determined based on Optotrak readings, there are four normal and four empirical distributions as described in the intro to section 4.3. The mean value of the mean empirical data is 0.0074 in/in. The corresponding standard deviation and coefficient of variation are 0.0019 in/in and 26% respectively.

Figure 4.9 illustrates the breakdown of the as-measured onset of strain hardening data according to the mean CDFs for each bar size. The mean values ranged from 0.0056 to 0.0085 with the No. 10 bars having the lowest mean value and the No. 6 bars having the highest. There is no

indication that the onset of strain hardening was influenced by bar size. Figure 4.10 presents the normal distributions for the as-measured onset of strain hardening data.

The A706 Grade 60 section of the SDC currently provides a range of values for the onset of strain hardening that varies according to bar size. The implied trend is that as bar size increases the onset of strain hardening occurs at lower values of strain. Figure 4.9 indicates that this trend did not hold true for the 788 A706 Grade 80 bars tested as part of this research. Additionally, the range in bar size mean values for A706 Grade 80 is much narrower than the provided range for A706 Grade 60 bars. The recommended onset of strain hardening for A706 Grade 80 is therefore defined for all bar sizes as the mean value of the mean empirical data or 0.0074. A complete summary of all recommended values is presented in section 5.2.

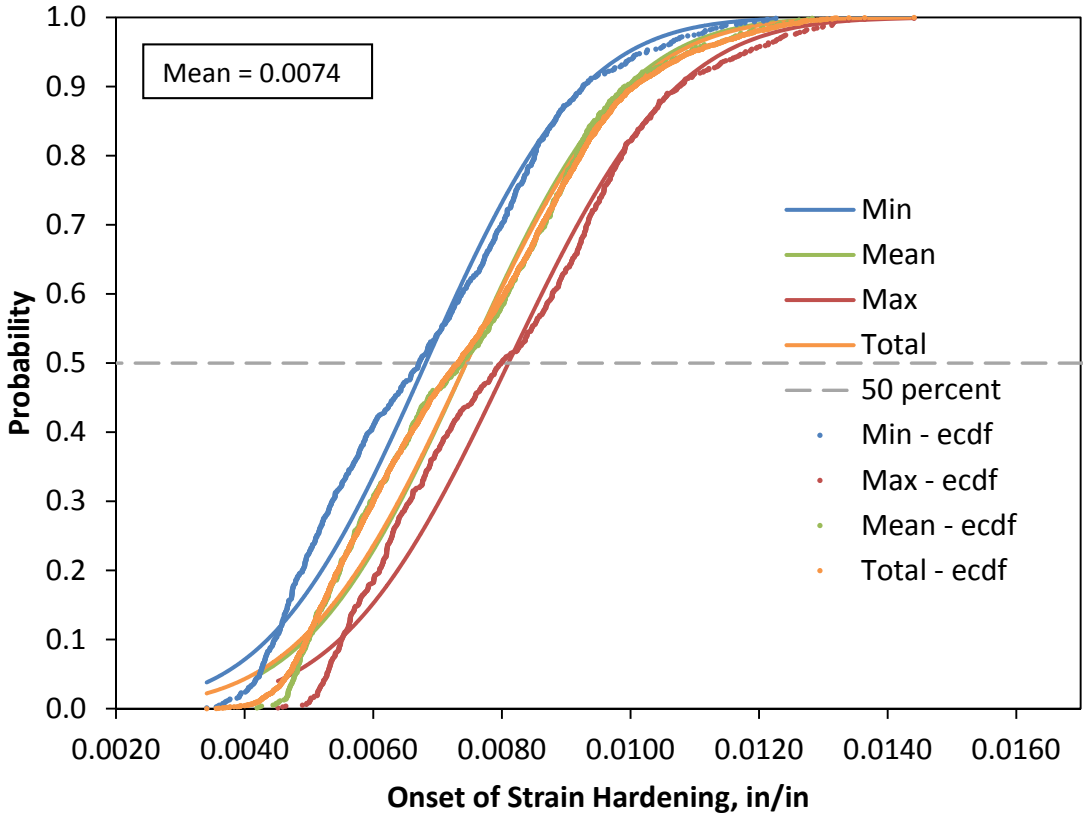

Figure 4.8. As-measured onset of strain hardening normal and empirical CDFs including all bar sizes

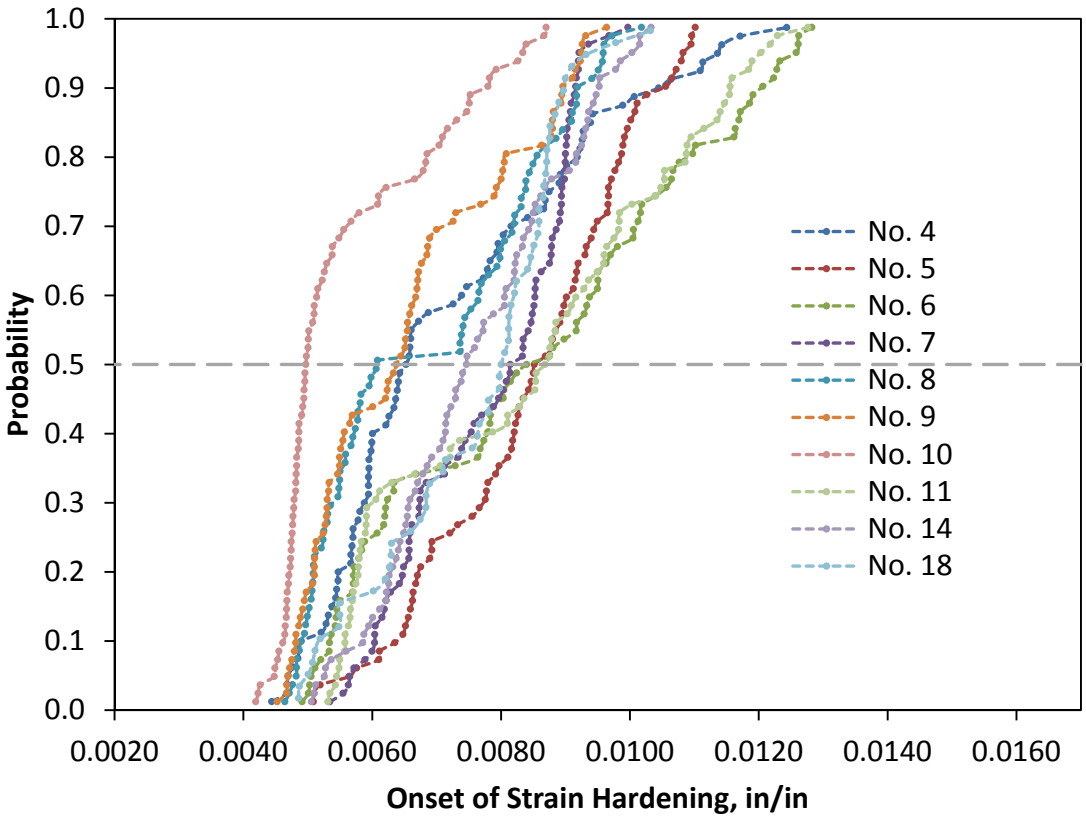

Figure 4.9. As-measured onset of strain hardening empirical CDFs for individual bar sizes

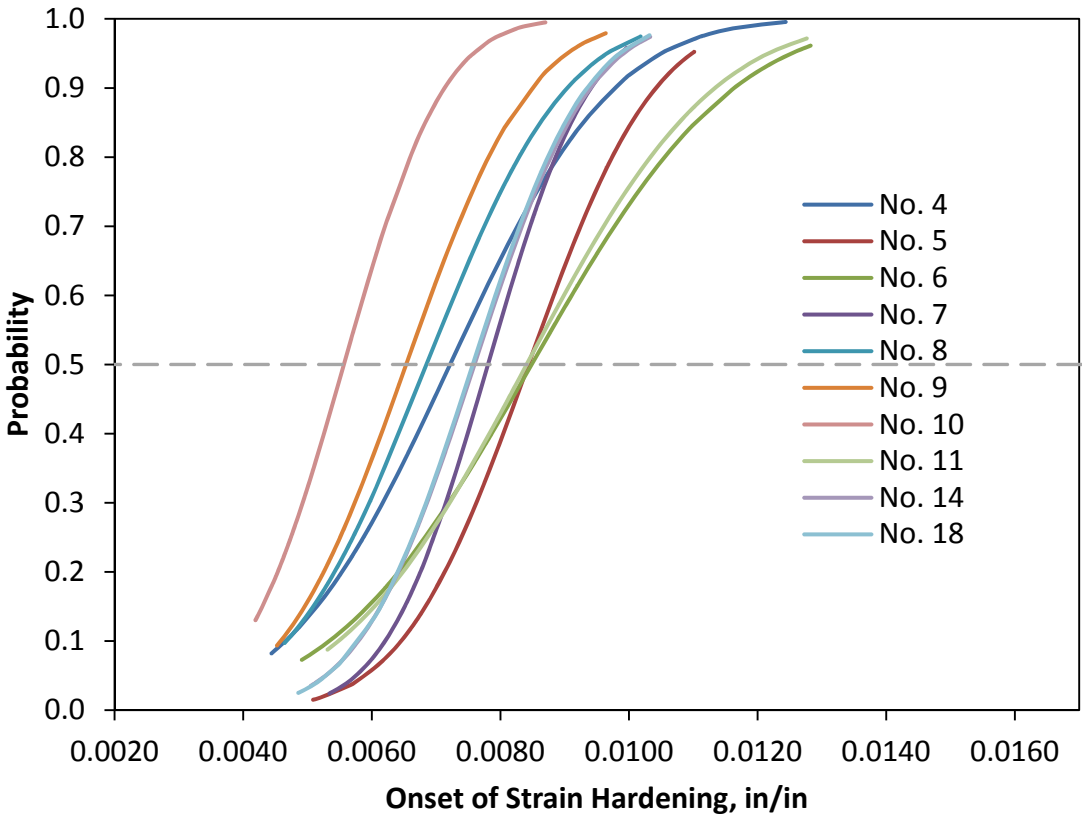

Figure 4.10. As-measured onset of strain hardening normal CDFs for individual bar sizes

4.3.4. Expected Tensile Strength, f_{ue}

The expected tensile strength was identified as the maximum value of stress recorded during the test. This represents the point at which strain hardening transitions to strain softening or necking.

The normal and empirical CDF curves for the as-measured, expected tensile strength are presented in Figure 4.11. The mean value of the empirical data is 114.3 ksi. The standard deviation and coefficient of variation are 3.2 ksi and 2.8% respectively. The value corresponding to the 95th percentile of the empirical data is 120.5 ksi. Also included in the graph is the ASTM minimum allowable tensile strength of 100 ksi. Because this parameter is determined based on load cell readings as opposed to Optotrak readings, there is only one normal and one empirical distribution.

Figure 4.12 illustrates the breakdown of the as-measured tensile strength data according to bar size. The as-measured mean values ranged from 112.1 ksi to 117.2 ksi with the No. 5 bars having the lowest mean value and the No. 11 bars having the highest. Figure 4.13 presents the normal distributions for the as-measured tensile strength data. From the figures it appears that the largest diameter bars had the highest tensile strengths; however, this did not hold true once the No. 11, 14, and 18 bar tensile strength data was adjusted as described in section 4.4 and alluded to at the

beginning of this chapter. As will be discussed in section 4.4, the as-measured tensile strength data was first adjusted before defining the recommendations presented in Chapter 5.

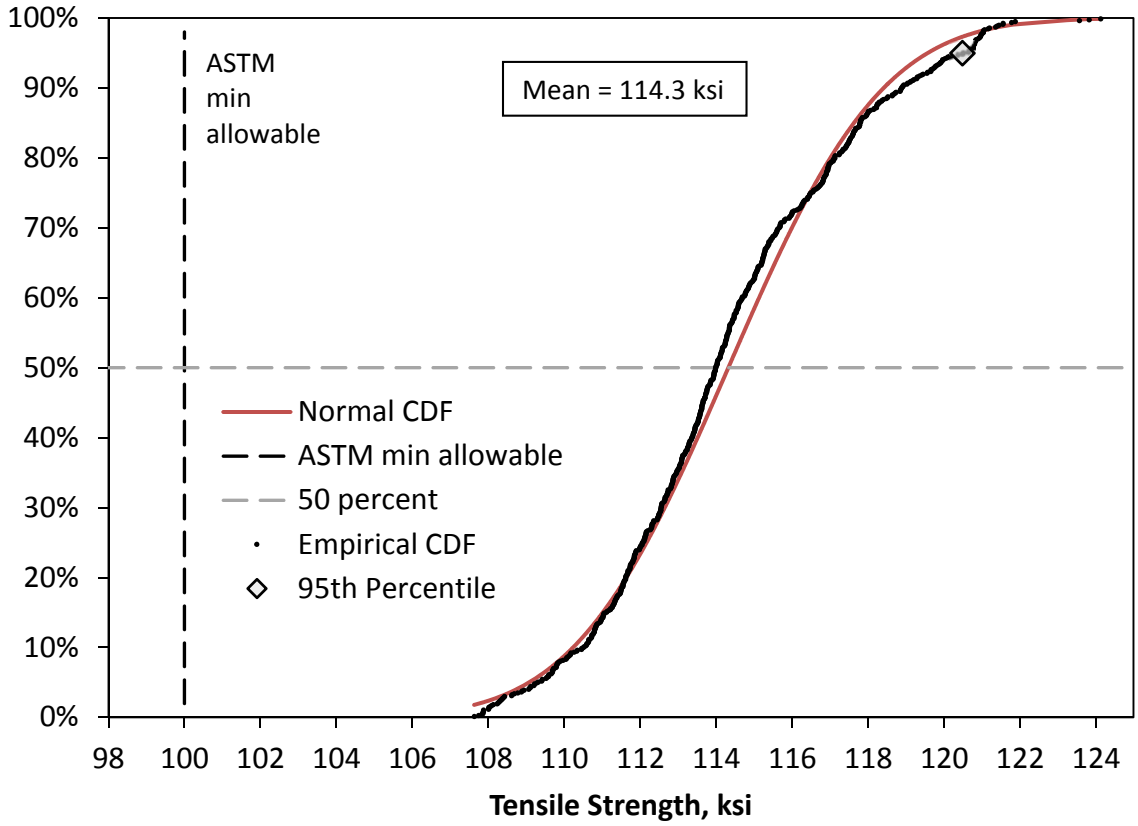

Figure 4.11. As-measured tensile strength normal and empirical CDFs including all bar sizes

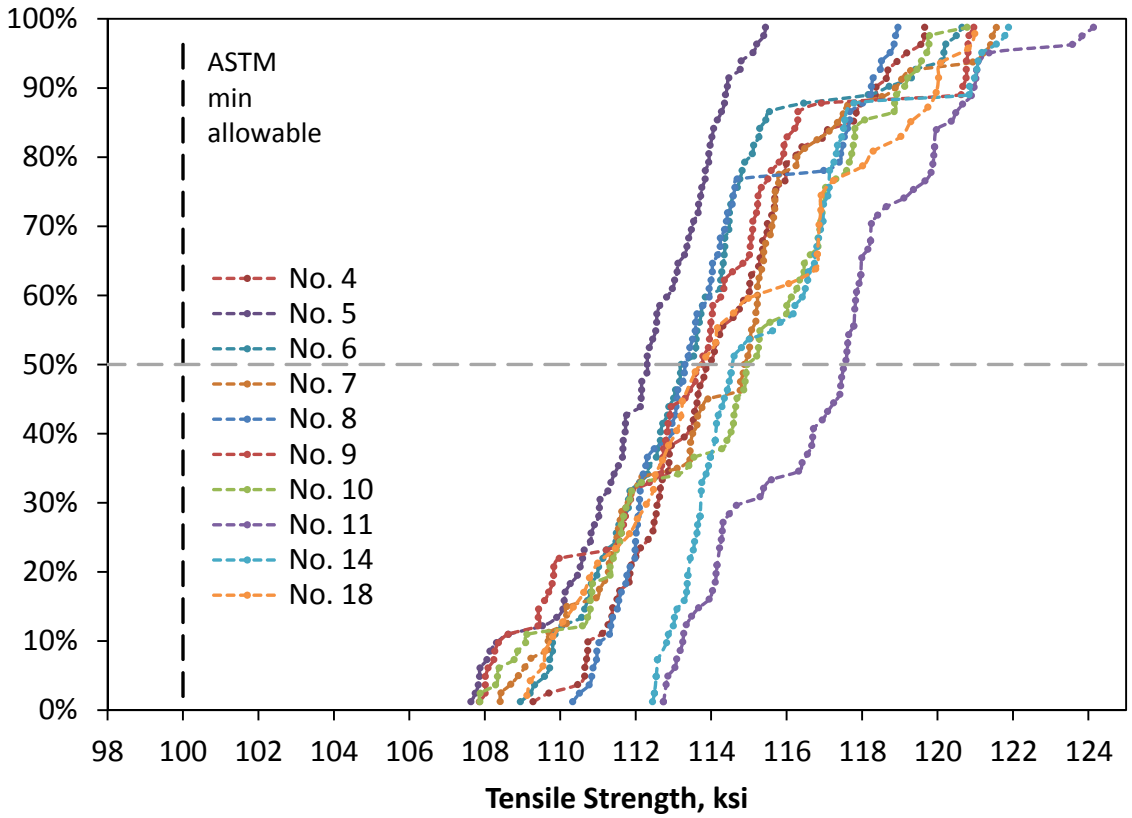

Figure 4.12. As-measured tensile strength empirical CDFs for individual bar sizes

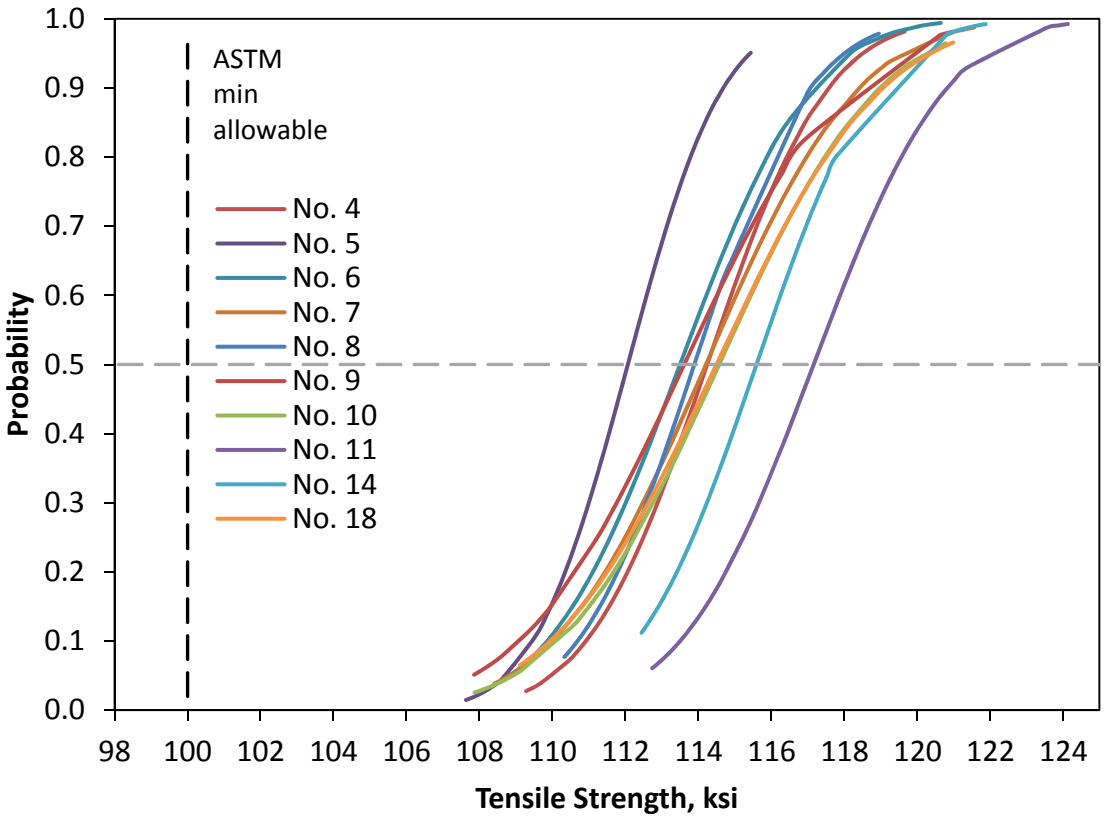

Figure 4.13. As-measured tensile strength normal CDFs for individual bar sizes

4.3.5. Ultimate Tensile Strain, ε_{su}

The ultimate tensile strain was identified as the value of strain corresponding to the maximum value of stress recorded during the test. As stated previously, this is not to be confused with the value of strain corresponding to rupture of the test specimen.

The normal and empirical CDF curves for the ultimate tensile strain are presented in Figure 4.14. Because this parameter is determined based on Optotrak readings, there are four normal and four empirical distributions as described in the intro to section 4.3. The mean value of the mean empirical data is 0.0972 in/in. The corresponding standard deviation and coefficient of variation are 0.0065 and 6.7% respectively. The value corresponding to the 5th percentile of the empirical data is 0.0852 in/in.

Figure 4.15 illustrates the breakdown of the as-measured ultimate tensile strain data according to the mean CDFs for each bar size. The mean values ranged from 0.0922 to 0.1038 with the No. 4 bars having the lowest mean value and the No. 14 bars having the highest. Figure 4.16 presents the normal distributions for the as-measured ultimate tensile strain data. From the figures it appears that the largest diameter bars had the highest ultimate tensile strains; however, this did not hold true once the No. 11, 14, and 18 bar ultimate tensile strain data was adjusted as

described in section 4.4 and alluded to at the beginning of this chapter. As will be discussed in section 4.4, the as-measured ultimate tensile strain data was first adjusted before defining the recommendations presented in Chapter 5.

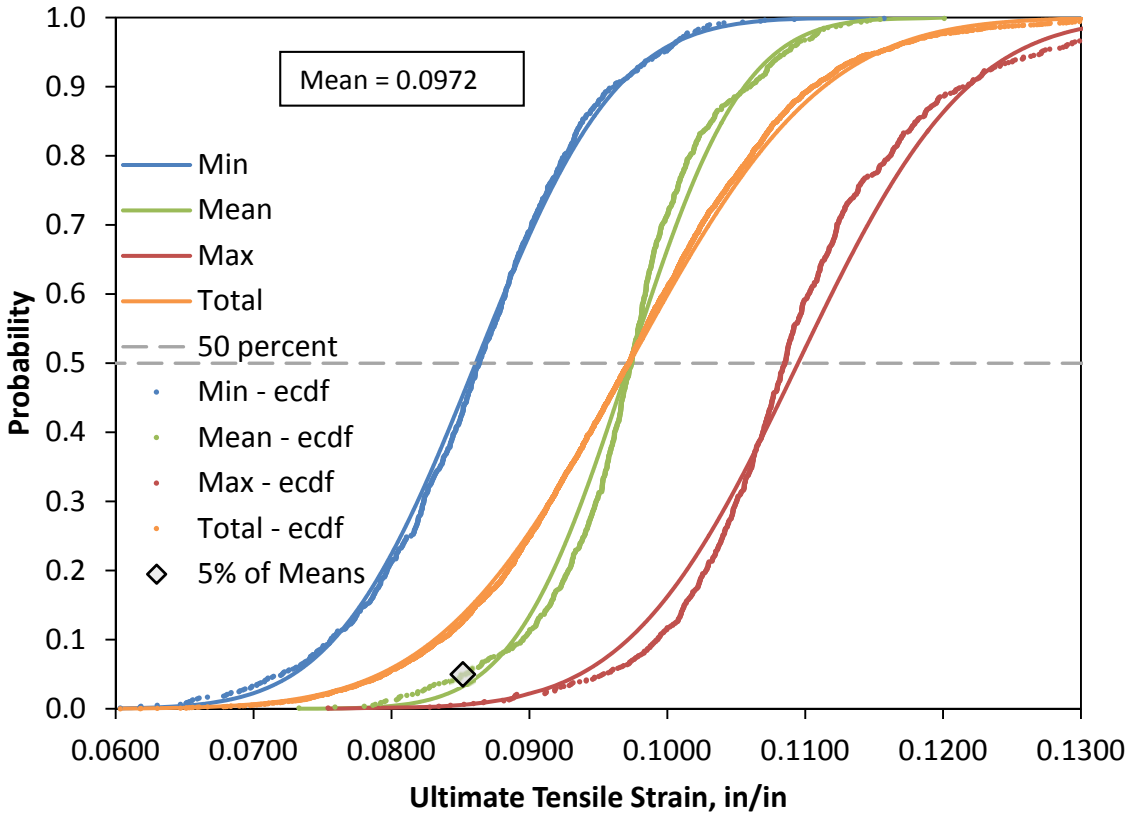

Figure 4.14. As-measured ultimate tensile strain normal and empirical CDFs including all bar sizes

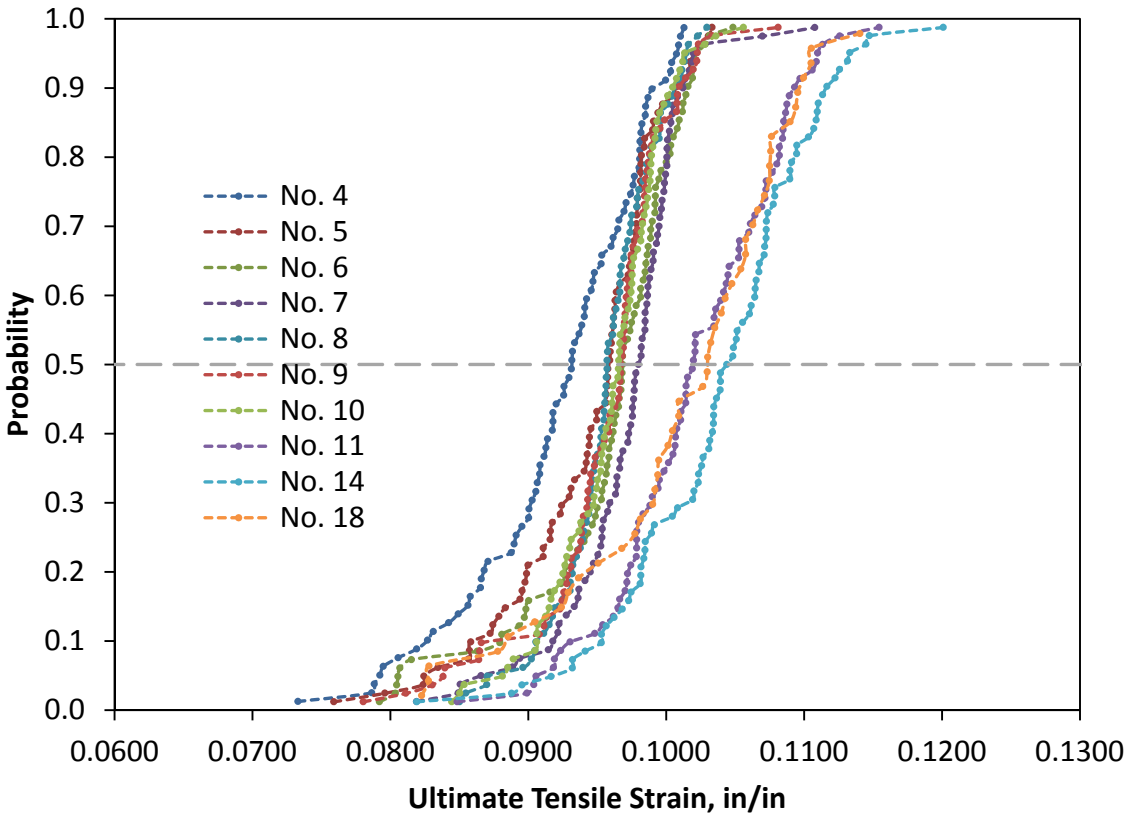

Figure 4.15. As-measured ultimate tensile strain empirical CDFs for individual bar sizes

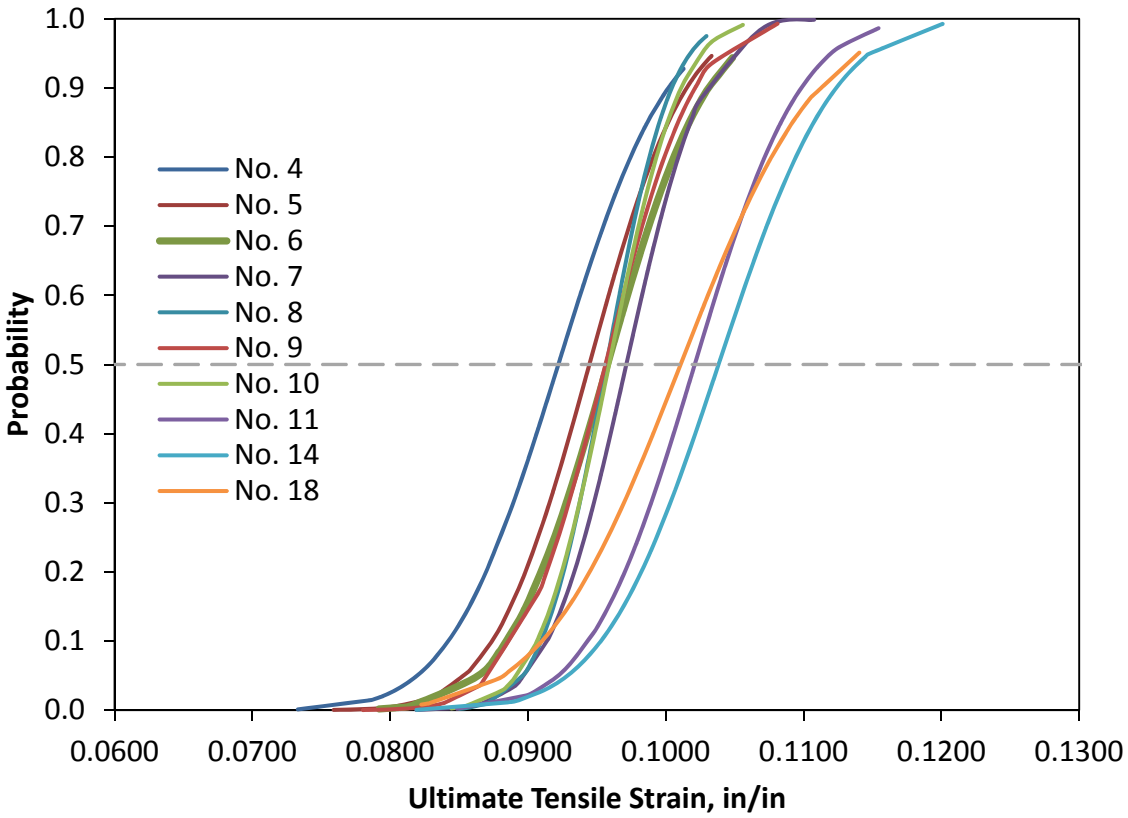

Figure 4.16. As-measured ultimate tensile strain normal CDFs for individual bar sizes

4.4. Data Validation

As discussed previously, the configuration of the custom testing setup in which forces were recorded using a 200 kip load cell not in-line with the test specimen (Fig. 3.4) produced erroneous test results for the No. 11 through No. 18 bars for three of the parameters of interest. The parameters affected were the *Expected Yield Strength*, *Expected Tensile Strength*, and the *Ultimate Tensile Strain*. This section describes the problem that was discovered, how it was resolved, and what impact this had on the data.

The initial configuration of the load cell away from the bar served as a way to indirectly measure bar forces in excess of 200 kips using a single 200 kip load cell. In theory, the force at the load cell should be exactly one third of the force on the bar assuming each of the four identical jacks receives the same pressure from the hydraulic pump. In actuality, the three jacks loading the bar did not receive the same pressure as the single jack with the load cell. As a result, the force applied to the load cell did not correspond to exactly one third of the force experienced by the test specimen.

A relationship between the force applied to the load cell and the force experienced by the test specimen was obtained through the use of a second 200 kip load cell placed directly in-line with the test specimen (Fig. 4.17). Preliminary tests of a No. 9 bar, a No. 11 bar, and a No. 14 bar

using this modified test setup revealed a consistent five to six percent difference in the forces recorded by the two load cells after about 50 kips regardless of bar size. The tests also revealed that the off-bar load cell tended to register the maximum force 30-50 seconds after the on-bar load cell. The ultimate tensile strains associated with this 30-50 second delay differed by about 6.5% with the higher strain values corresponding to the delayed max force. This phenomenon arises from the fact that the Optotrak strain data is paired with the load cell data by matching record counts, as described in section 3.6.

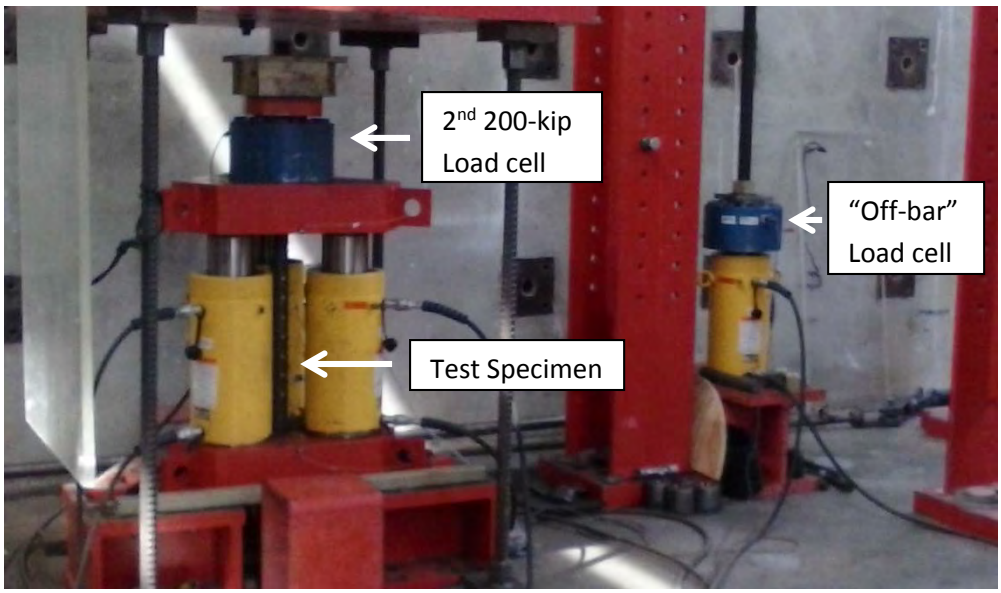

Figure 4.17. Modified test setup with one 200-kip load cell in-line with the test specimen and another 200-kip load cell on a separate jack connected to the same hydraulic source

An additional, more thorough series of tests on nine No. 11 bars and nine No. 14 bars was used to confirm the trend observed in the three tests just described. One test specimen was taken from each heat of each mill (18 total specimens) and tested in the modified test setup that included both 200 kip load cells, one in-line with the bar and one separate from the bar. These tests confirmed that the percent error between the two load cells followed a consistent trend regardless of bar size. The results of these tests are presented in Figure 4.18. Note that the tests could only be conducted up to a force of 230 kips before risking permanent damage to the load cell in-line with the bar. This upper limit allowed testing of the No. 11 bars fully to ultimate but required the No. 14 bar tests to be stopped during the strain hardening region.

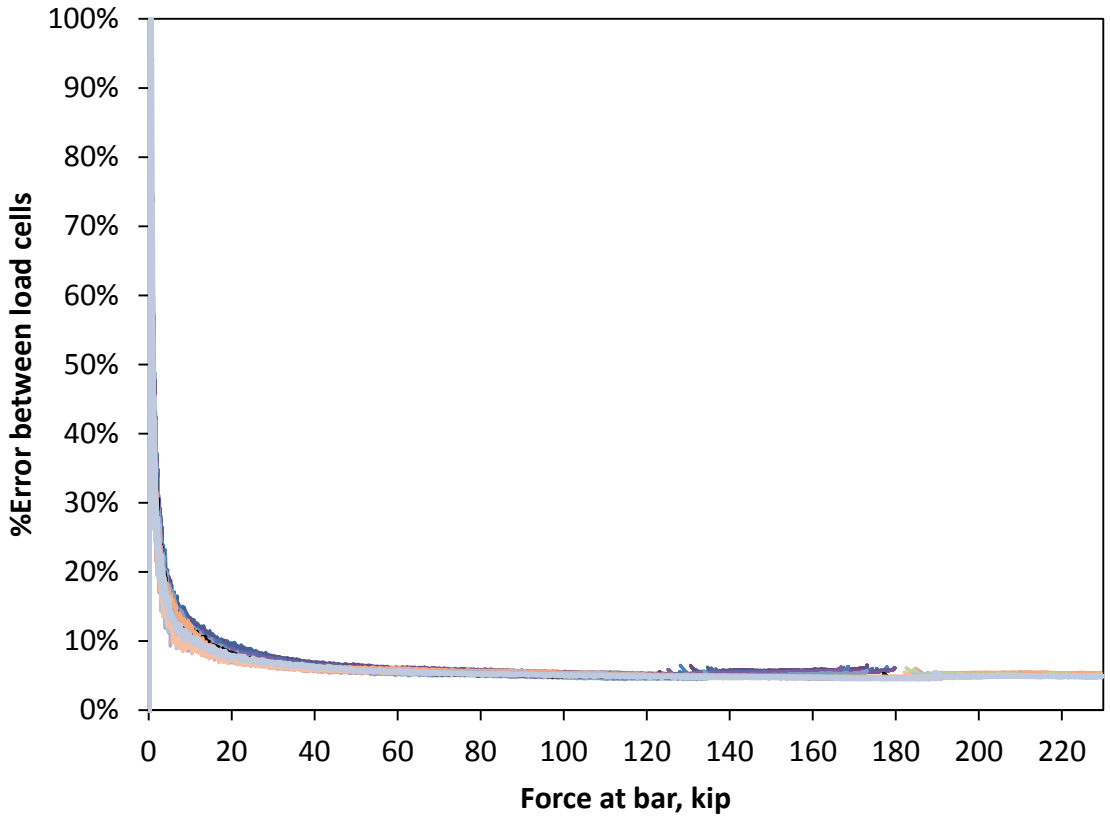

Figure 4.18. Relationship between the on-bar load cell and the off-bar load cell for 9 No. 11 and 9 No. 14 bar tests

Table 4.1 presents a summary of the average percent errors for the three affected parameters. Based on these values, the following reductions were applied to the No. 11, 14, and 18 bar data originally collected using the off-bar load cell: a 5% reduction in the expected yield strength values, a 6% reduction in the expected tensile strength values, and a 6.5% reduction in the expected ultimate tensile strain values.

Table 4.1. Results from the additional 9 No. 11 and 9 No. 14 bar tests

	f_{ye}	$f_{ye\ off\text{-}bar}$	%Error	f_{ue}	$f_{ue\ off\text{-}bar}$	%Error	ε_{su}	$\varepsilon_{su\ off\text{-}bar}$	%Error
Average	83.2	87.5	**5.07%**	110.9	117.8	**6.27%**	0.0999	0.1064	**6.54%**
St. Dev.	2.5	2.6	0.3%	2.9	3.1	0.2%	0.0031	0.0050	3.1%

4.5. Final Stress-Strain Data

The following sections highlight the effect of the changes to the No. 11 through No. 18 bar test results for the affected parameters: f_{ye}, f_{ue}, and ε_{su}. The format of the sections follows that of section 4.3 except that the values used now represent the final, adjusted numbers. Additionally, the graphs are updated to reflect the adjustments.

4.5.1. Expected Yield Strength, f_{ye}

The normal and empirical CDF curves for the expected yield strength considering all bar sizes and including the five percent reduction to the No. 11 through No. 18 bars are presented in Figure 4.19. The mean value of the empirical data is 85.0 ksi. The standard deviation and coefficient of variation are 3.0 ksi and 3.6% respectively. Also included in the graph are the ASTM minimum and maximum allowable yield strengths of 80 ksi and 98 ksi respectively. Because this parameter is determined based on load cell readings as opposed to Optotrak readings, there is only one normal and one empirical distribution.

Figure 4.20 illustrates the breakdown of the adjusted, expected yield strength data according to bar size. It is readily evident from the figure that the adjustment to the No. 11, 14, and 18 bars resulted in several values falling below the ASTM minimum allowable yield strength of 80 ksi. This is discussed in more detail in section 4.6.7. The mean values ranged from 80.7 ksi to 88.0 ksi with the No. 18 bars having the lowest mean value and the No. 4 bars having the highest. The general trend from the empirical CDF is that there is a decrease in median yield strength with increasing bar size. Figure 4.21 presents the normal distributions for the expected yield strength data considering the large bar adjustments.

The A706 Grade 60 section of the SDC currently provides a specified minimum yield strength and an expected yield strength. The specified minimum yield strength corresponds to the ASTM minimum allowable yield strength. The specified minimum yield strength for A706 Grade 80 rebar is 80 ksi. The recommended expected yield strength for A706 Grade 80 is defined as the mean value of the empirical data or 85.0 ksi. A complete summary of all recommended values is presented in section 5.2.

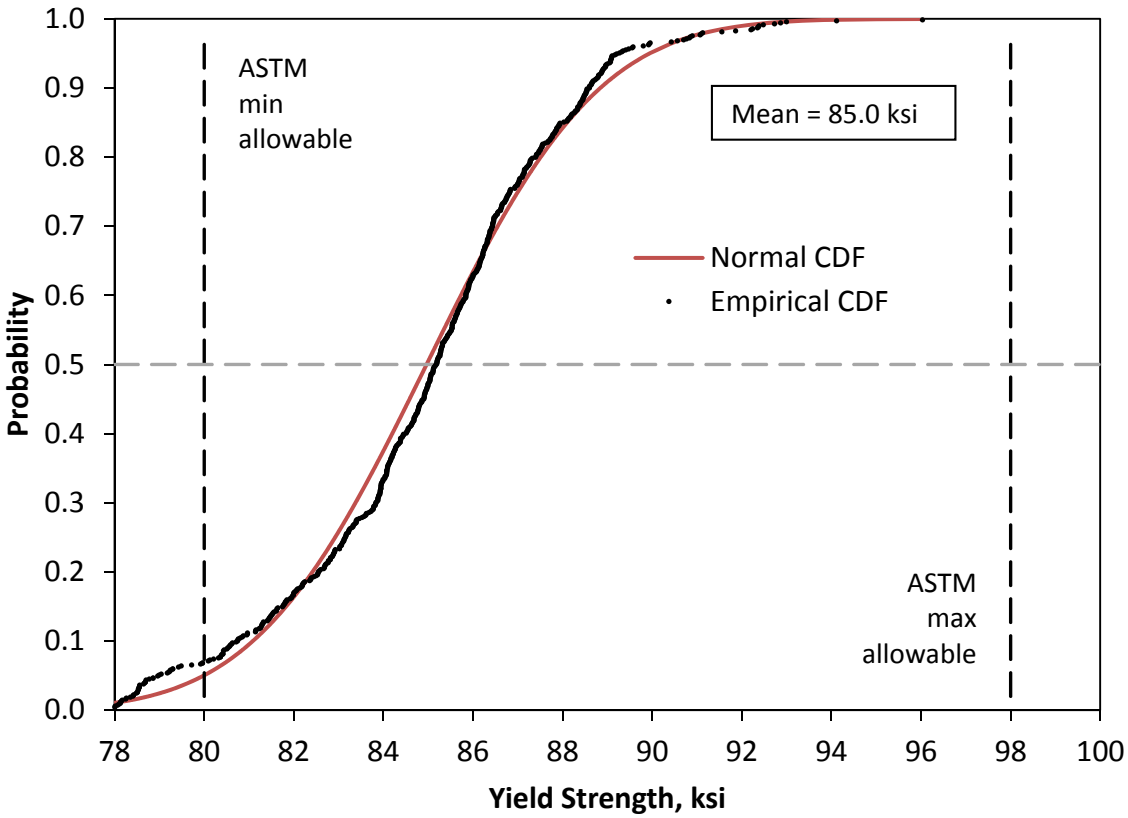

Figure 4.19. Yield strength normal and empirical CDFs of all bar sizes including adjusted No. 11-18 bar data

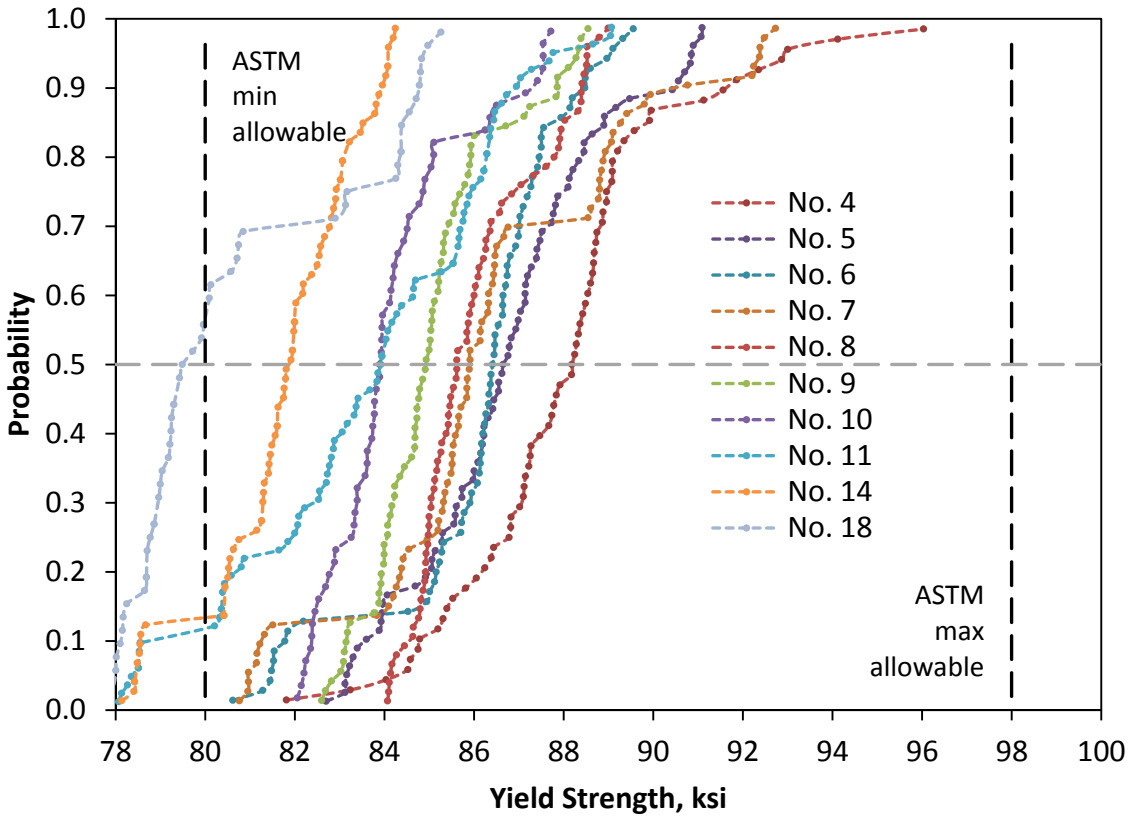

Figure 4.20. Yield strength empirical CDFs for individual bar sizes including adjusted No. 11-18 bar data

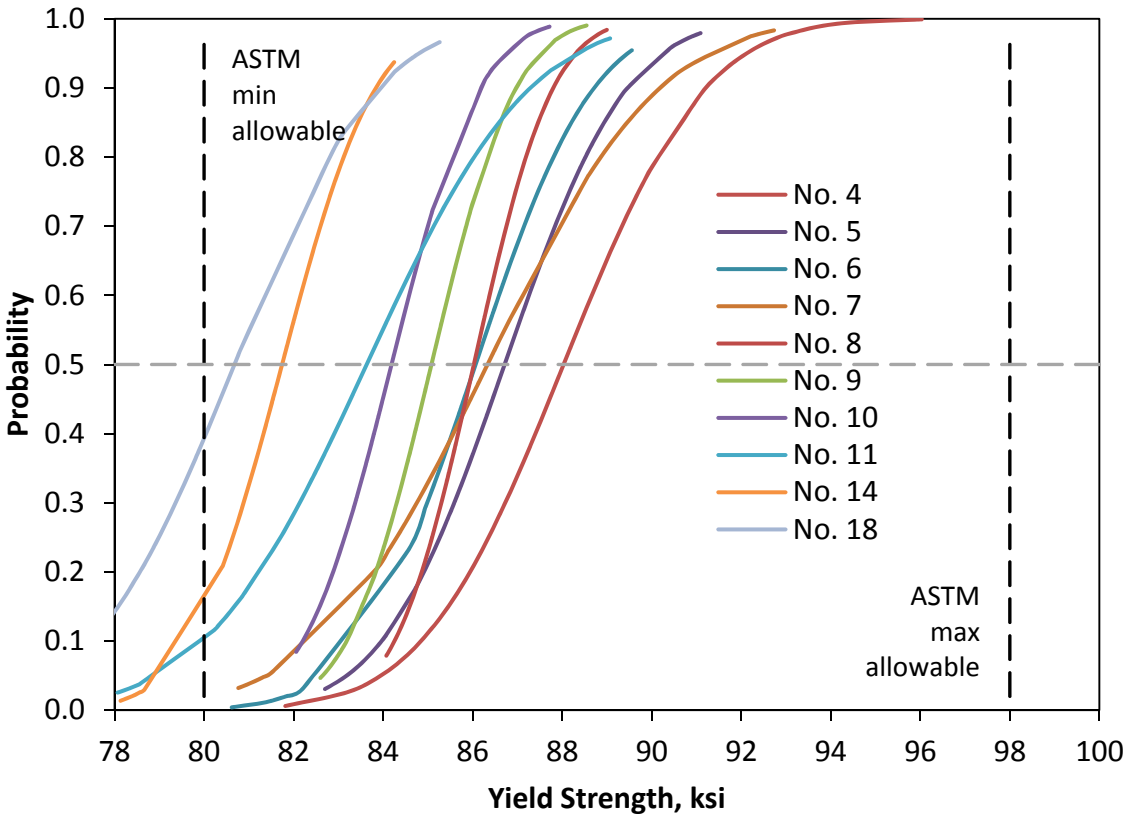

Figure 4.21. Yield strength normal CDFs for individual bar sizes including adjusted No. 11-18 bar data

4.5.2. Expected Tensile Strength, f_{ue}

The normal and empirical CDF curves for the expected tensile strength considering all bar sizes and including the six percent reduction to the No. 11 through No. 18 bars are presented in Figure 4.22. The mean value of the empirical data is 112.5 ksi. The standard deviation and coefficient of variation are 3.6 ksi and 3.2% respectively. The value corresponding to the 95th percentile of the empirical data is 118.9 ksi. Also included in the graph is the ASTM minimum allowable tensile strength of 100 ksi. Because this parameter is determined based on load cell readings as opposed to Optotrak readings, there is only one normal and one empirical distribution.

Figure 4.23 illustrates the breakdown of the adjusted, expected tensile strength data according to bar size. The mean values ranged from 107.6 ksi to 114.6 ksi with the No. 18 bars having the lowest mean value and the No. 10 bars having the highest. There is no indication that the tensile strength was influenced by bar size; however, the No. 11, 14, and 18 bars did have the three lowest mean tensile strengths. Figure 4.24 presents the normal distributions for the expected tensile strength data considering the large bar adjustments.

The A706 Grade 60 section of the SDC currently provides a specified minimum tensile strength and an expected tensile strength. The specified minimum tensile strength corresponds to the

ASTM minimum allowable tensile strength. The specified minimum tensile strength for A706 Grade 80 rebar is 100 ksi. The recommended expected tensile strength for A706 Grade 80 is defined as the mean value of the empirical data or 112.5 ksi. An additional parameter corresponding to the 95th percentile of the empirical data is provided with the recommended values. As this parameter represents an upper end of the empirical distribution, it may provide a reliable indication of the expected overstrength of the material. A complete summary of all recommended values is presented in section 5.2.

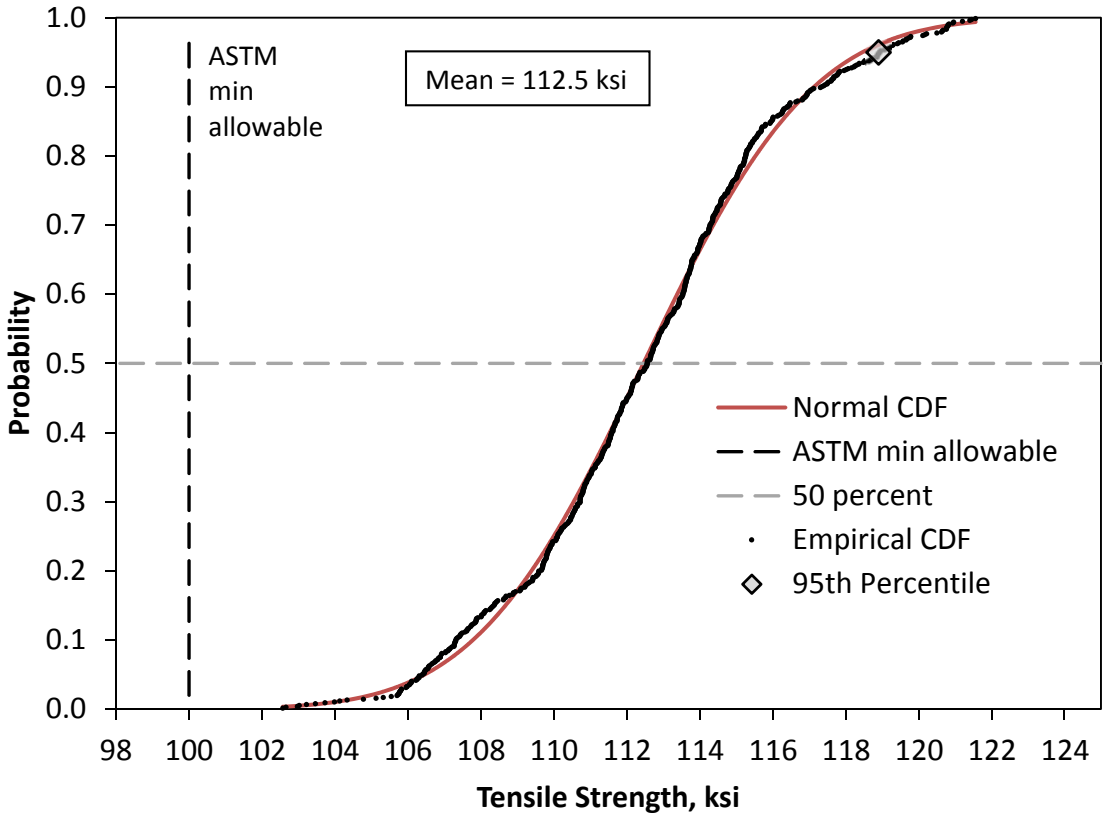

Figure 4.22. Tensile strength normal and empirical CDFs of all bar sizes including adjusted No. 11-18 bar data

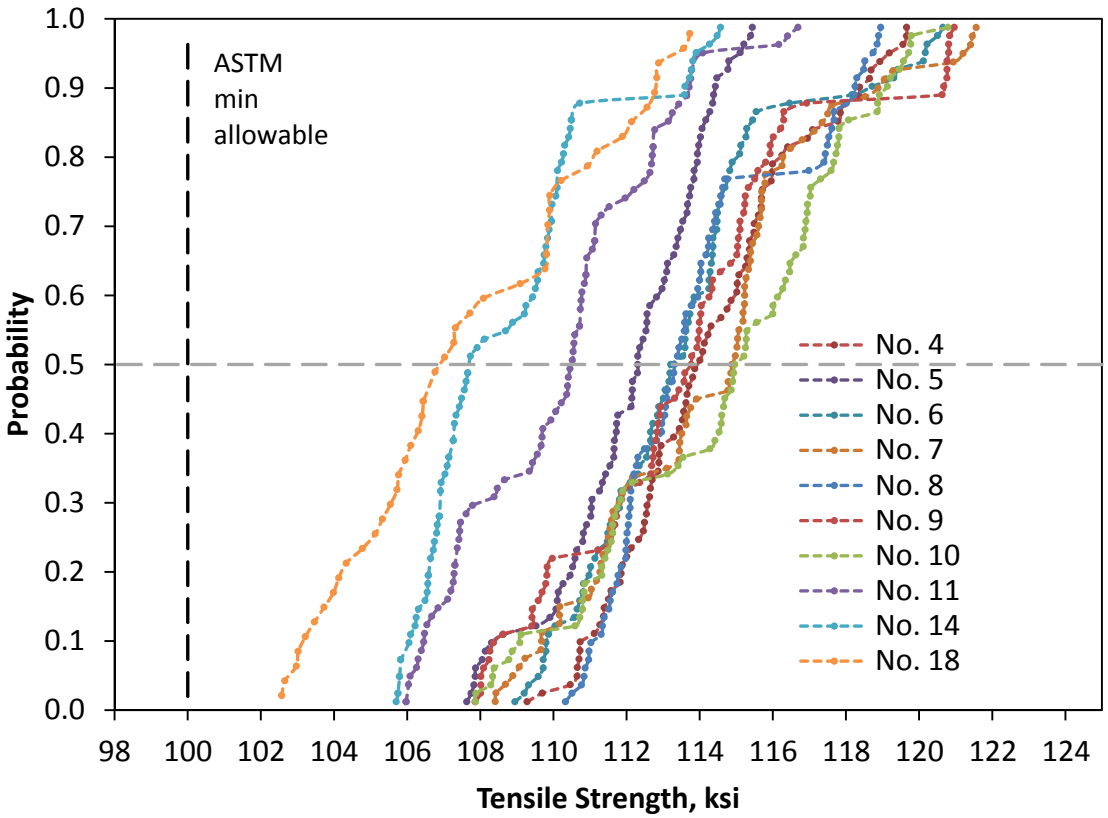

Figure 4.23. Tensile strength empirical CDFs for individual bar sizes including adjusted No. 11-18 bar data

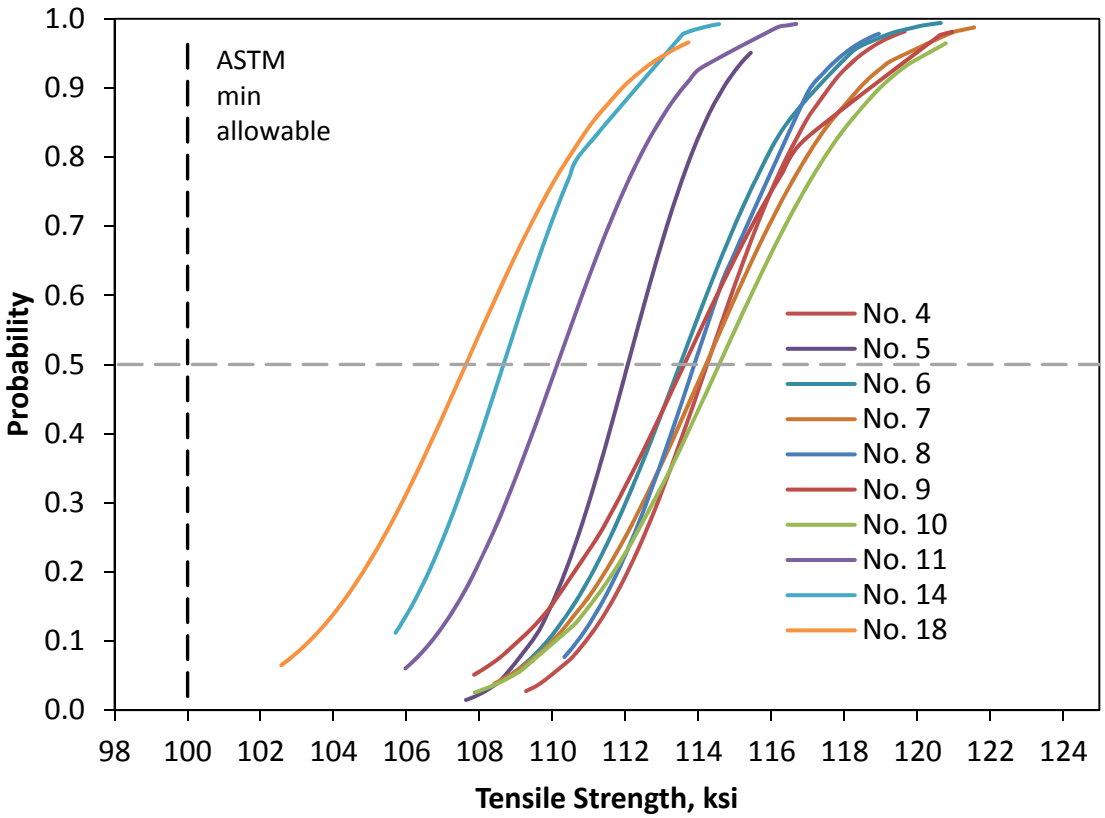

Figure 4.24. Tensile strength normal CDFs for individual bar sizes including adjusted No. 11-18 bar data

4.5.3. Ultimate Tensile Strain, ε_{su}

The normal and empirical CDF curves for the ultimate tensile strain considering all bar sizes and including the 6.5% reduction to the No. 11 through No. 18 bars are presented in Figure 4.25. The mean value of the mean empirical data is 0.0954 in/in. The corresponding standard deviation and coefficient of variation are 0.0055 and 5.8% respectively. The value corresponding to the 5th percentile of the empirical data is 0.0845 in/in.

Figure 4.26 illustrates the breakdown of the adjusted ultimate tensile strain data according to the mean CDFs for each bar size. The mean values ranged from 0.0922 to 0.0971 with the No. 4 bars having the lowest mean value and the No. 7 bars having the highest. There is no indication that the ultimate tensile strain was influenced by bar size. Figure 4.27 presents the normal distributions for the ultimate tensile strain data considering the large bar adjustments.

The A706 Grade 60 section of the SDC currently provides an ultimate tensile strain and a reduced ultimate tensile strain. For each of these parameters, one value is provided for No. 10 bars and smaller and another value is provided for No. 11 bars and larger. The reduced ultimate tensile strain represents a percentage reduction in the ultimate tensile strain to safeguard against fracture. The recommended ultimate tensile strain for A706 Grade 80 is defined as the mean

value of the mean empirical data or 0.0954. An additional parameter corresponding to the 5th percentile of the empirical data is provided with the recommended values as an alternative to the reduced ultimate tensile strain parameter. A complete summary of all recommended values is presented in section 5.2.

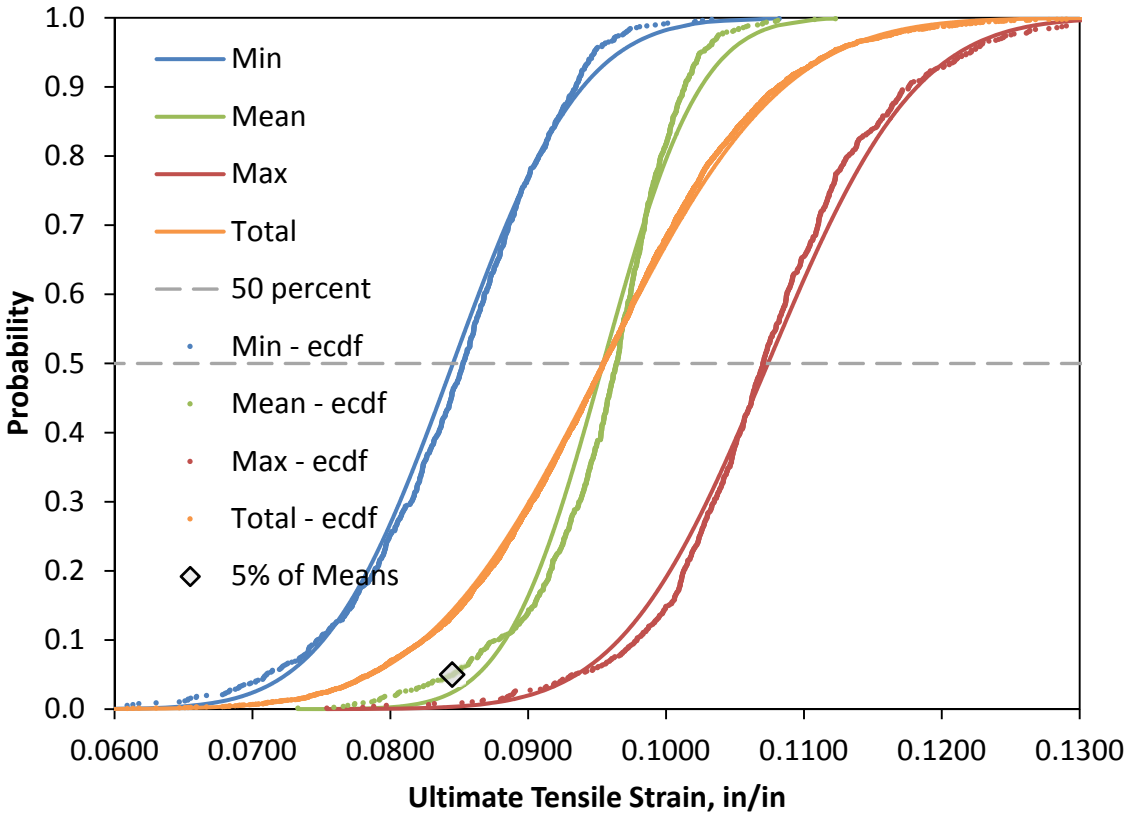

Figure 4.25. Ultimate tensile strain normal and empirical CDFs of all bar sizes including adjusted No. 11-18 bar data

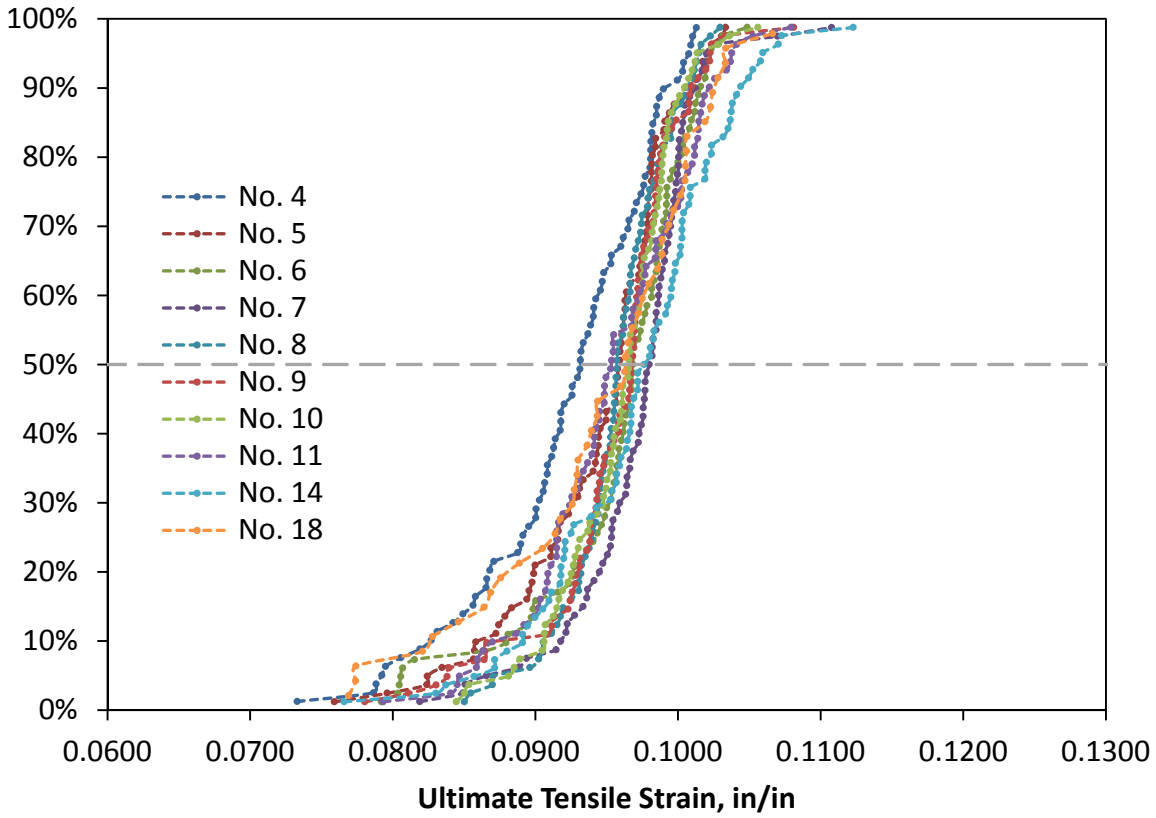

Figure 4.26. Ultimate tensile strain empirical CDFs for individual bar sizes including adjusted No. 11-18 bar data

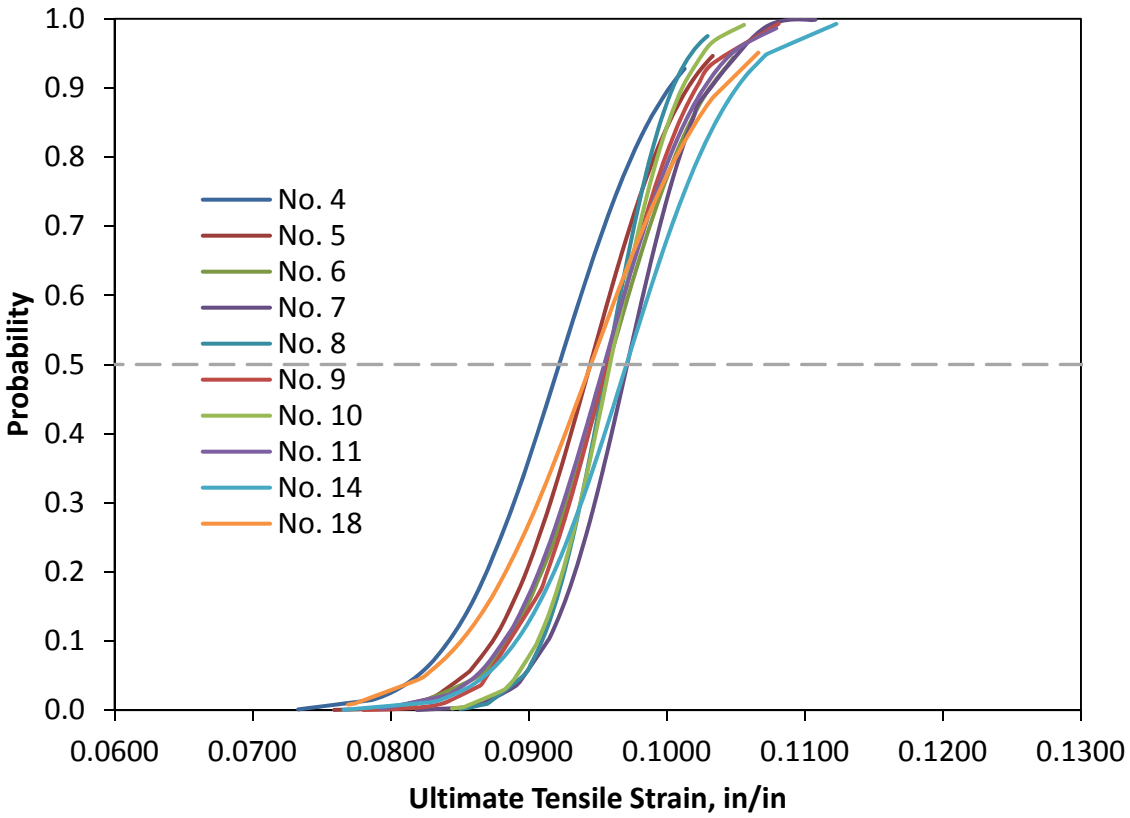

Figure 4.27. Ultimate tensile strain normal CDFs for individual bar sizes including adjusted No. 11-18 bar data

4.6. Post-Processing

In addition to providing the expected values of stress and strain for the five key parameters, as described in the previous section, the dataset that was generated from the relatively large number of A706 Grade 80 tensile tests can be taken advantage of for other types of analysis as well. The purpose of this section is to highlight some of the uses of the stress-strain data that resulted from the experimental program both in regards to the dataset itself and to tensile testing in general. While only a small number of topics are addressed, it is anticipated that the potential of the dataset will be adequately showcased so as to foster further research and analysis.

4.6.1. Variability in Strain over Bar Length

One of the unique traits of the Optotrak is the ability to track multiple markers simultaneously. Because this permits multiple gage lengths to be established on a single specimen, it is possible to assess the distribution of strain over the entire instrumented region of the specimen at each reading of the data. This poses an advantage over traditional methods of capturing bar strains such as with strain gages and extensometers which, while reliable, are limited to a single gage length.

An unanticipated consequence of using this type of instrumentation was the realization that the strains varied over the length of the test specimens at a given instant in time and that the variability between gage lengths seemingly increased with increasing strain. It is perhaps not surprising that the strains should vary over the length of the bar as it is neither a homogeneous material or of a continuous cross-section (as a result of the longitudinal and transverse ribs). Additionally, some degree of variability in the different gage lengths can be attributed to the precision of the instrumentation. Table 4.2 summarizes the average variation between the six 2" gage lengths for the yield strain, onset of strain hardening, and ultimate tensile strain considering all tests.

Table 4.2 and Figure 4.28 both indicate that the highest variability in the strains was at the yield point while the lowest was shortly thereafter at the onset of strain hardening. This trend for the variability to be high towards the beginning of the tests, lowest near the middle, and high again near the end may be the result of low variability in the strains while they are small and the precision of the Optotrak is lower coupled with an increased variability in the strains when they are large and the precision of the Optotrak is higher. This would imply that the higher variability at the yield point is more a result of instrumentation than actual variation in the strains. In any case, the point to be emphasized is not so much that the strains are not uniform over the length of the test specimen at a given instant in time, but that the strains will typically be measured at only one location on the bar at a given instant in time. Such knowledge may be useful in directing future tensile testing efforts.

Table 4.2. Average variabilities in the six strain values recorded for each parameter from each test

Parameter	Average coefficient of variation
ε_{ye}	9.57%
ε_{sh}	6.74%
ε_{su}	9.10%

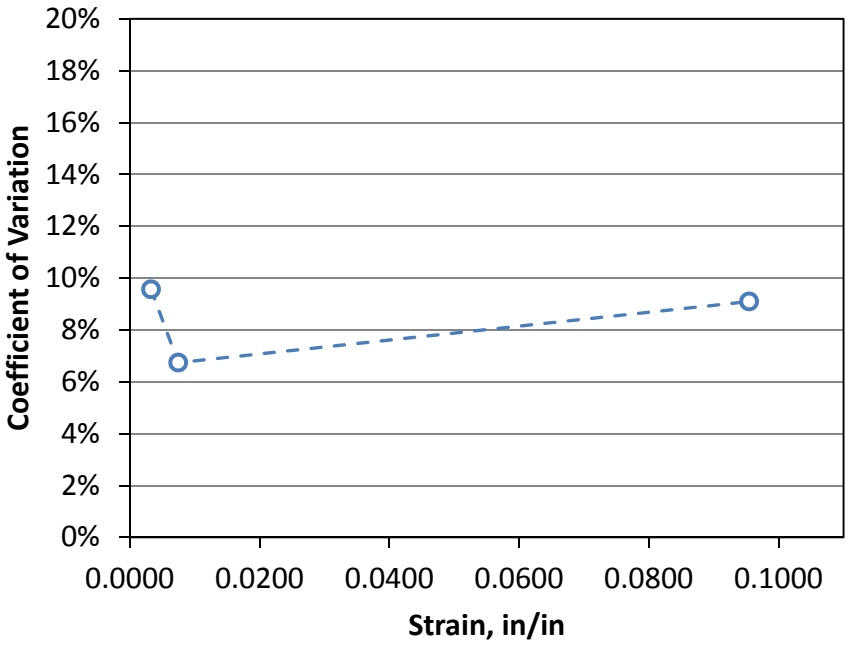

Figure 4.28. Change in variation between gage lengths with increasing strain

4.6.2. Shape of the Strain Hardening Curve

One of the expressed objectives of the current project was to assess the shape of the stress-strain curve for A706 Grade 80 rebar, in particular, the transition from elastic to inelastic behavior and the curvature of the strain hardening region. Identification of the stress and strain values at yielding and the onset of strain hardening necessarily resolves the first of these issues; however, the shape of the strain hardening region is not as readily obtainable.

While not as critical as the expected values of stress and strain at yield and ultimate and the strain at the onset of strain hardening, the shape of the strain hardening curve is important in modeling applications such as moment curvature analysis. As such, it becomes important to assess the ability of existing rebar models, formulated for a different grade of steel, to accurately describe this region.

This section offers a largely qualitative assessment of the shape of the strain hardening portion of the curve. Two existing monotonic rebar models, the King Model (King et al. 1986) and the Raynor Model (Raynor et al. 2002), are evaluated by first defining them in terms of the recommended A706 Grade 80 stress-strain parameter values presented in section 5.2 and then overlaying the results on a plot containing all of the experimental stress-strain curves. An additional comparison is made by overlaying an A706 Grade 60 curve on the same plot to visually compare the shape of the respective stain hardening regions. The remainder of this section discusses the results of these efforts.

Figure 4.29 provides a plot of all stress-strain curves generated during the testing phase of this research project overlaid one on top of another. The plot was generated using the as-measured No. 4 through No. 10 bar tests and the adjusted No. 11 through No. 18 bars tests. All curves have been plotted to their ultimate tensile strains. The relationship between the on-bar load cell and the off-bar load cell described in section 4.4. was used to adjust the entire range of stress-strain values for each of the No. 11 through No. 18 bar test results in order to plot the curves seen in the figure. Clearly illustrated by the figure is the variability across the different tests and the consistency in the shape of the strain hardening region.

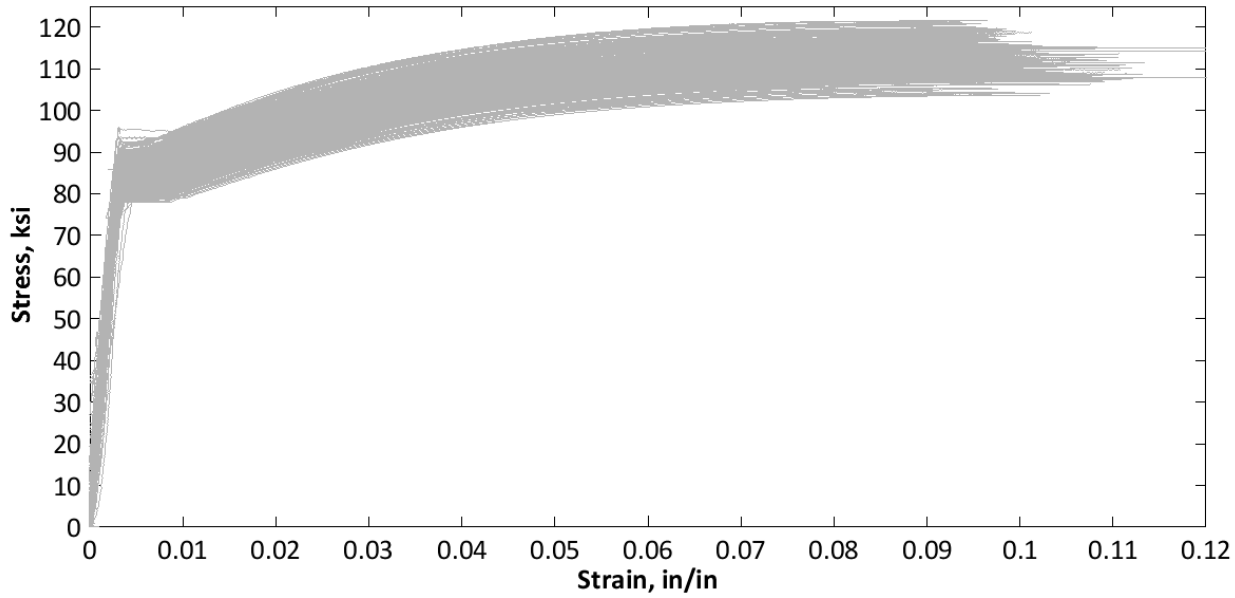

Figure 4.29. A706 Grade 80 stress strain curves for all tests

Figure 4.30 provides a visual demonstration of the King model's (King et al., 1986) ability to represent the strain hardening portions of the A706 Grade 80 stress-strain curves. The parameters required to define the model and the values used are also provided in the figure. It is clear that the model overestimates the curvature of the initial portion of the strain hardening curve.

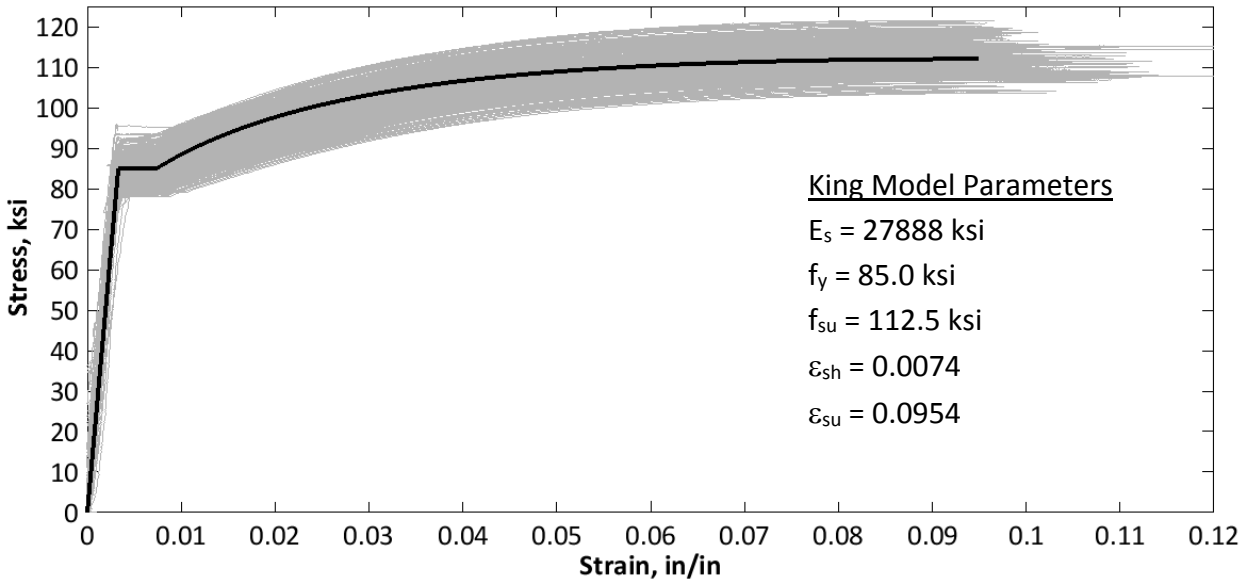

Figure 4.30. Overlay of King Model on all stress-strain curves using recommended parameter values (King et al., 1986)

Figure 4.31 provides a visual demonstration of the Raynor model's (Raynor et al., 2002) ability to represent the strain hardening portions of the A706 Grade 80 stress-strain curves. The parameters required to define the model and the values used are also provided in Figure 4.31. Distinct from the King model is the Raynor model's ability to define the slope of the yield plateau as well as adjust the curvature of the strain hardening region. A slope of zero for the yield plateau and a strain hardening exponent of 3 were used in the model shown in the figure. It is clear that the Raynor model, when defined with the given parameters, can reliably capture the shape of the A706 Grade 80 stress-strain curve.

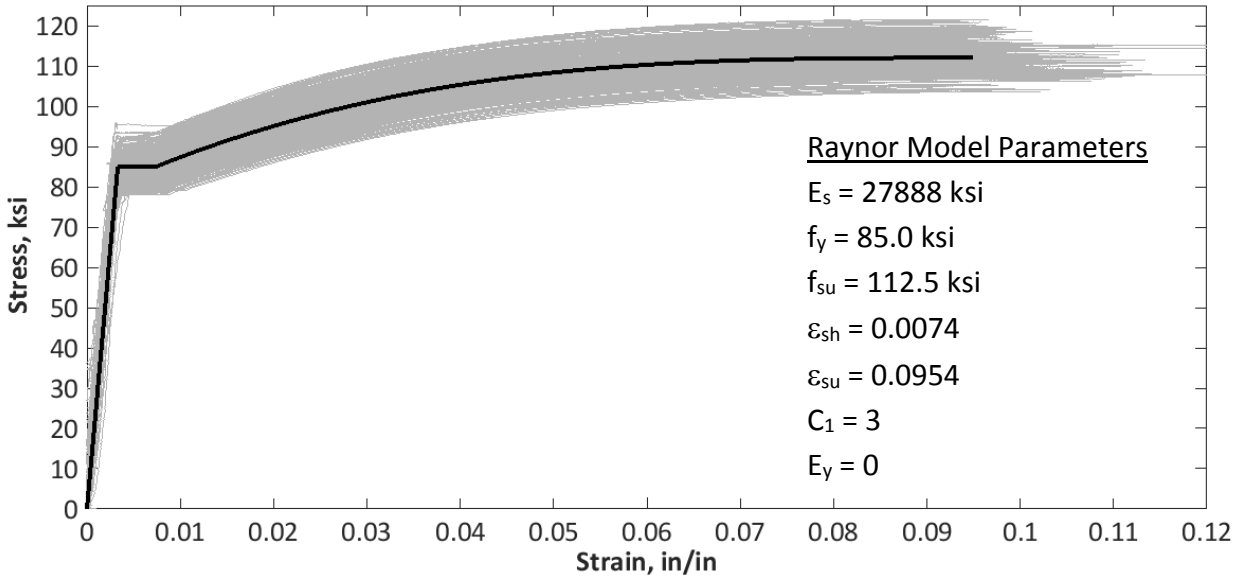

Figure 4.31. Overlay of Raynor Model on all stress-strain curves using recommended parameter values (Raynor et al., 2002)

Figure 4.32 provides a visual comparison between the shape of an A706 Grade 60 stress-strain curve and the A706 Grade 80 stress-strain curves. As indicated in the figure, the shape of the strain hardening region is essentially the same for both grades of steel. This lends support to the notion that existing monotonic stress-strain models commonly used in the analysis of reinforced concrete sections using A706 Grade 60 rebar can be reliably used to perform the same tasks using A706 Grade 80 rebar.

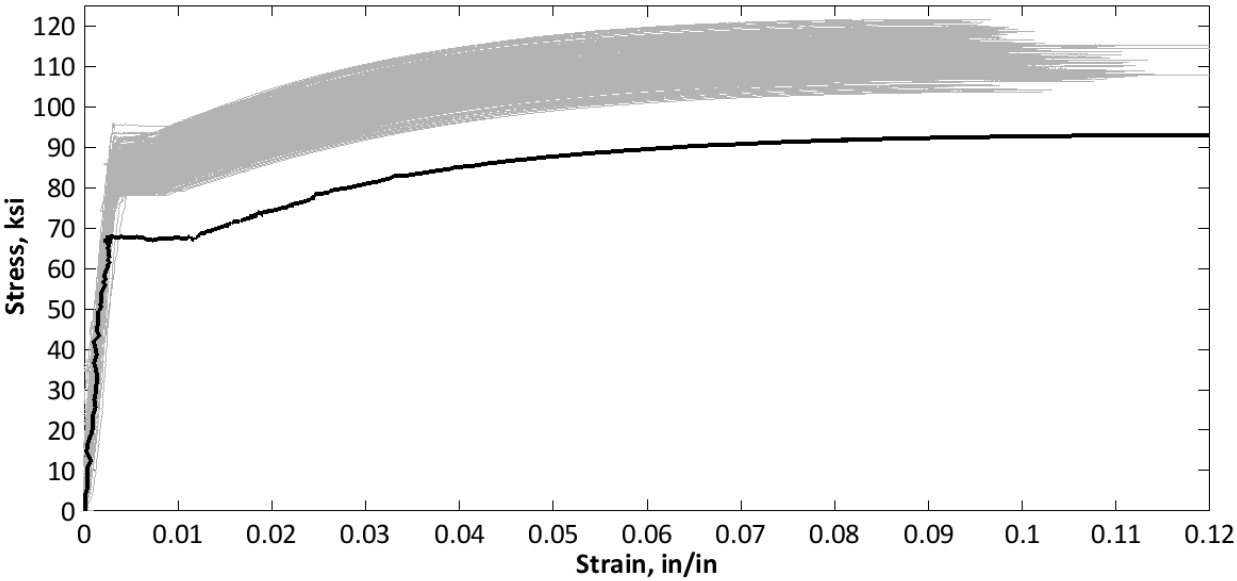

Figure 4.32. Overlay of an A706 Grade 60 curve on all stress-strain curves

4.6.3. Parameter Interactions

The current industry practice is for producing mills to provide with their steel shipments a certified test report indicating the mechanical and chemical properties of the steel being provided. Three of these properties that are readily available are the yield strength, the tensile strength, and the percent elongation at fracture; however, without the associated strains, these values alone are insufficient to fully characterize the stress-strain profile of the steel they represent. Should it be possible to establish a reliable correlation between the parameters provided by mills and the associated but unknown strain parameters, for example, percent elongation at fracture and ultimate tensile strain, then such a relationship could later be used to relate project-specific mill cert values to expected stress-strain performance.

This section summarizes the relationships between a few of the parameters of interest obtained from the A706 Grade 80 rebar tested over the course of this research. Specifically, the interaction between the expected yield strength and the onset of strain hardening and the interaction between the ultimate tensile strain and percent elongation at fracture are considered. The relationships are presented qualitatively in the form of scatter plots with some accompanying discussion. No correlations were established for either of the comparisons as will be discussed below.

4.6.3.1. f_{ye} vs ε_{sh}

The graph containing all of the A706 Grade 80 experimental stress-strain curves presented in Figure 4.29 seems to indicate an increased likelihood for the onset of strain hardening to occur at higher strains as the yield strength of the material decreases. Figure 4.33, however, reveals that this is not the case and that no distinguishable trend exists between the yield strength and the onset of strain hardening. Therefore, mill-specified values of yield strength cannot be used as an indicator of the onset of strain hardening for this type and grade of steel.

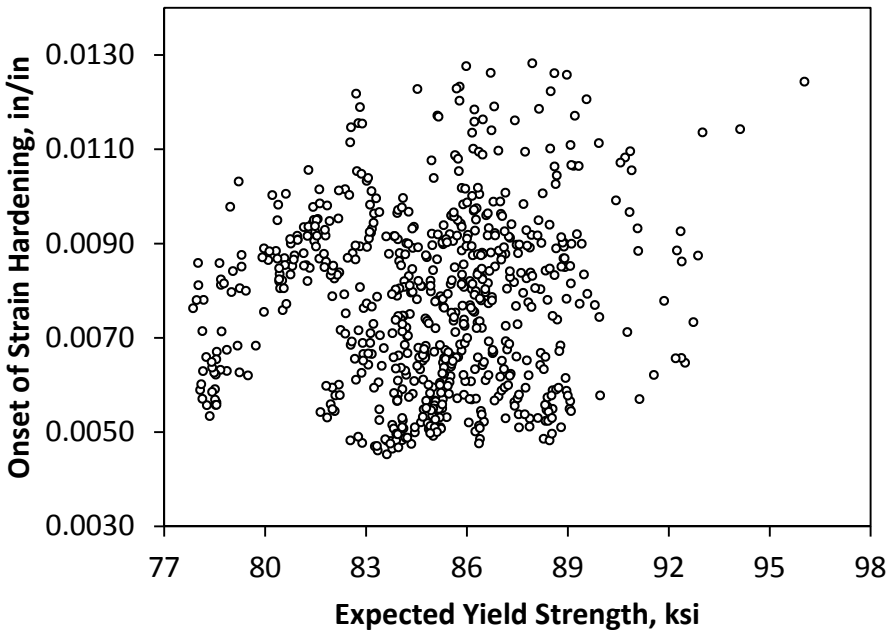

Figure 4.33. Interaction between expected yield strength and onset of strain hardening

4.6.3.2. percent elongation vs ε_{su}

The percent elongation at fracture and the ultimate tensile strain are both meant to serve as measures of ductility. While the ultimate tensile strain, sometimes referred to as the strain at max stress, is generally required in the calibration of reinforcing steel models, oftentimes the only material-specific parameter related to ductility is the percent elongation at fracture provided by the mill supplying the steel. The ability to confidently define a correlation between these two parameters would be of great value to a designer or analyst attempting to use project-specific material properties to define reinforcing steel models where other data was lacking.

Figure 4.34 presents a comparison between the A706 Grade 80 ultimate tensile strain values acquired by the current project and Optotrak-based percent elongation at fracture values. The figure indicates a slight correlation between the two parameters; however, no effort to quantify this correlation has been made for reasons discussed next.

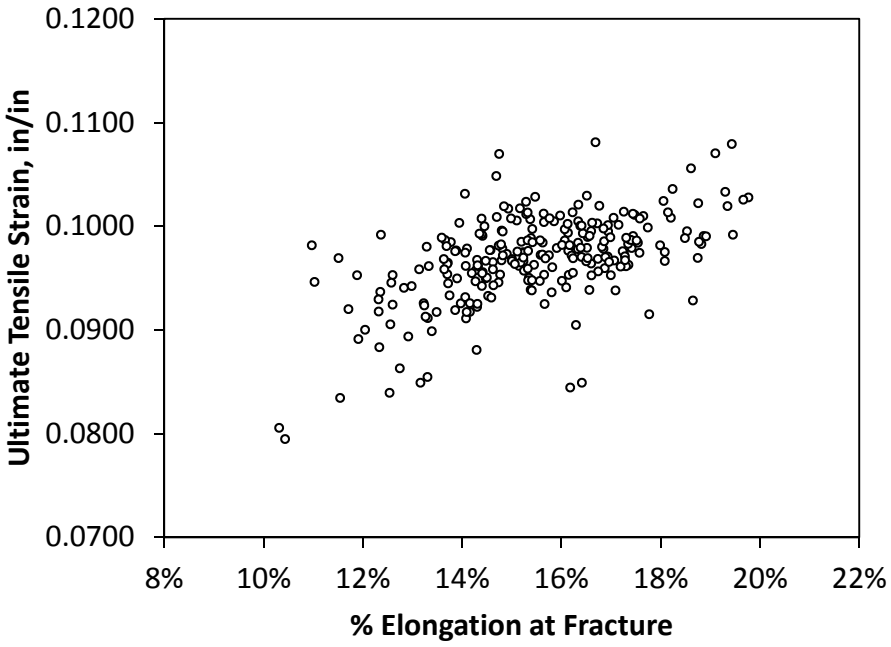

Figure 4.34. Interaction between Optotrak-based percent elongation at fracture and ultimate tensile strain

The percent elongation at fracture values used in Figure 4.34 have been based on Optotrak strain measurements in which the final reading from the markers just before bar fracture is used to calculate the percent elongation at fracture. Recall from section 3.5 that not all of the tests were taken fully to fracture of the bar; therefore, only a portion of the dataset is available to make this comparison. All of the data points in Figure 4.34 represent fractured bars. A limited number of additional percent elongation at fracture values were obtained using the conventional method of measuring a predefined 8" gage length prior to the test and then re-measuring the same gage length after the test in the event that fracture occurred within the gage length. A comparison of these hand measurements to the Optotrak-based values reveals that, on average, there is a 14 percent-difference in the percent elongation measurements. To clarify, this translates into Optotrak-based percent elongation at fracture values that are, on average, 1.8 percentage points higher than their corresponding hand measured values. An attempt to explain this behavior is provided in the next paragraph.

Prior to the onset of necking, a tensile test specimen is in a state of combined plastic and elastic strain. As necking commences (a concentration of plastic deformation) the non-necked regions of the bar can be observed to relax, essentially recovering some of the existing elastic strains. Upon fracture of the test specimen, any remaining elastic strains are recovered and the combined length of the two fractured ends represents the total plastic elongation. The traditional hand measurement approach to determining percent elongation at fracture by fitting the fractured ends together and re-measuring the elongated gage length necessarily captures the plastic strain in the bar. The Optotrak-based method of determining the percent elongation at fracture by taking the

last recording of strain before fracture necessarily captures the plastic strain in addition to any remaining elastic strains. For this reason, it can be expected that the Optotrak-based approach would predict a higher percent elongation at fracture value than the traditional approach, hence the hesitancy to define a quantitative relationship between the percent elongation at fracture values provided in the mill certificates and those obtained using the Optotrak system.

4.6.4. Analysis of Variabilities

As stated in section 3.4, each test specimen was given a unique identification number indicating its mill, heat, and 20' bar of origin. Not only does this allow the data to be filtered on the basis of one or more common variables (ex: tensile strengths of all No. 6 bar tests from Mill 2 Heat 3), but it also permits the data to be interpreted in terms of those common variables (ex: standard deviation for all No. 6 bar tests from Mill 2 Heat 3). An advantage of this is the increased ability to identify trends in the dataset and to detect and/or explain anomalies.

This section specifically addresses the degree of variability associated with each of the five key parameters in terms of three variables: producing mills, heats within a mill, and twenty-foot bars within a heat. The coefficient of variation (CV) is used as the primary indicator of variability. The following eight topics are addressed: variability between the three mills, average variability within a mill, average variability between heats from a common mill, average variability between heats from a common mill by bar size, average variability within a heat, average variability within a heat by bar size, average variability between three 20' bars from a common heat, and average variability within a 20' bar (between three specimens from a common 20' bar).

4.6.4.1. Mills

Table 4.3 provides the average experimental values corresponding to each of the three mills and the five key parameters. Included at the bottom of the table are the standard deviation and coefficient of variation (CV) of the mill averages for each of the five key parameters. In words, these describe the variability *between* the three mills. The low coefficient of variation values imply that specimens tested from any of the three mills generally behaved in the same way.

Table 4.3. Mill averages and variability between mills

Avg	f_{ye}	ε_{ye}	ε_{sh}	f_{ue}	ε_{su}
Mill 1	84.99	0.0032	0.0078	111.16	0.0965
Mill 2	85.42	0.0034	0.0069	113.29	0.0934
Mill 3	84.54	0.0032	0.0077	112.84	0.0965
St. Dev	0.44	0.0001	0.0005	1.12	0.0018
CV	0.51%	3.00%	6.93%	1.00%	1.89%

Table 4.4 provides the coefficients of variation of the experimental data corresponding to each of the three mills and the five key parameters. At the bottom of the table are the averages of the mill coefficients of variation for each of the five key parameters. In words, these describe the average

variability *within* each mill. The high coefficient of variation values imply that even within a single mill, specimens tended to exhibit a wide range of responses, particularly in the length of the yield plateau as indicated by the onset of strain hardening parameter. This general trend can be attributed to the fact that multiple heats were represented for each mill as described in the next section.

Table 4.4. Mill coefficients of variation and average CV across the mills

CV	f_{ye}	ε_{ye}	ε_{sh}	f_{ue}	ε_{su}
Mill 1	3.14%	7.74%	20.23%	2.28%	4.98%
Mill 2	3.67%	10.37%	24.67%	3.17%	6.73%
Mill 3	3.82%	7.87%	30.20%	3.74%	4.93%
Averages	3.54%	8.66%	25.03%	3.06%	5.55%

4.6.4.2. Heats

A similar approach to that just described for mills can be used to determine the variability between and within heats. Note that it would not make sense to compare all 25 heats with one another directly as they are associated with different producing mills. As such, the variability "between" heats is defined as the average variability between heats from a common mill. The average variability within a heat, however, is defined the same as for the mills: average of the coefficients of variation associated with each heat.

Two tables of heats analogous to Tables 4.3 and 4.4 for mills could be presented but would be too large to comfortably fit into the body of the report. Nonetheless, Tables 4.7 and 4.8 summarize what would have been the bottom lines of these tables. The values in Table 4.7 illustrate that even within a single mill the variability between different heats can be somewhat high. Compared to the average variability within a mill, the average variability within a heat is noticeably lower (Table 4.8). It should be noted that it is difficult to make broad, substantive claims about variation between heats as different heats contained different bar sizes (refer Appendix A). Section 4.6.4.4 addresses this issue by defining the variability within and between heats in terms of individual bar sizes.

4.6.4.3. Twenty-foot Bars

Table 4.7 summarizes the average variability between twenty-foot bars from a common heat in terms of the coefficient of variation. Table 4.8 summarizes the average variability within a single twenty-foot bar. The coefficients of variation presented in these two tables for the twenty-foot bars were defined in the same way as just described for the heats. At this level of detail, the coefficients of variation for the yield strength, tensile strength, and onset of strain hardening are lower than in any of the other methods of comparison.

4.6.4.4. Heats by Bar Size

The primary purpose of this section is to expand on the observations presented in section 4.6.4.2 by evaluating the variability between and within heats in terms of individual bar sizes as this offers a more practical interpretation of the data. Table 4.5 summarizes the variability between heats from a common mill for each bar size. The values in the table are obtained by finding the coefficient of variation of the heat averages within a mill (ex: M1H1, M1H2, M1H3 – 9 tests in each) for a given bar size and then taking the average coefficient of variation across the three mills for that bar size. This represents the case in which a shipment of steel from a single manufacturer includes multiples heats for a given bar size, and the variability between those heats is of interest.

Table 4.6 summarizes the average variability with a single heat for each bar size. The values in this table where obtained by determining the coefficient of variation for each combination of mill, heat, and bar size (ex: M1H1 No. 4 bars – 9 tests in each) and averaging across all the heats for that bar size (9 heats for each bar size). This represents the case in which a shipment of steel includes bars from only one heat, and the variability within that heat and for a given bar size is of interest.

Table 4.5. Coefficients of variation of averages – variability "between" (heats from a common mill for each bar size)

CV	f_{ye}	ε_{ye}	ε_{sh}	f_{ue}	ε_{su}
No. 4	1.64%	3.62%	10.59%	1.60%	3.20%
No. 5	2.39%	2.40%	11.59%	1.62%	1.79%
No. 6	1.54%	5.36%	21.10%	2.29%	3.41%
No. 7	2.99%	5.08%	6.06%	1.49%	1.79%
No. 8	1.30%	3.63%	11.22%	1.33%	0.87%
No. 9	0.94%	5.66%	13.66%	1.86%	3.11%
No. 10	1.74%	4.45%	9.75%	1.57%	1.75%
No. 11	3.35%	5.07%	22.79%	2.09%	1.57%
No. 14	1.70%	5.17%	18.32%	2.09%	2.62%
No. 18	4.00%	7.42%	14.50%	3.44%	2.00%

Table 4.6. Averages of coefficients of variation – variability "within" (a heat for a given bar size)

AVG CV	f_{ye}	ε_{ye}	ε_{sh}	f_{ue}	ε_{su}
No. 4	1.46%	5.50%	12.36%	1.28%	5.72%
No. 5	1.11%	4.69%	12.02%	0.86%	5.37%
No. 6	1.06%	5.02%	10.82%	1.11%	4.49%
No. 7	1.03%	6.87%	8.91%	0.62%	3.95%
No. 8	0.60%	5.25%	7.34%	0.45%	3.71%
No. 9	0.58%	6.28%	8.44%	0.58%	3.82%
No. 10	0.68%	5.15%	6.93%	0.78%	3.81%
No. 11	1.26%	5.57%	8.53%	0.86%	5.57%
No. 14	0.66%	6.44%	9.02%	0.66%	5.87%
No. 18	1.19%	6.23%	11.89%	1.31%	6.43%

Table 4.7. Coefficients of variation of averages – variability "between"

CV	f_{ye}	ε_{ye}	ε_{sh}	f_{ue}	ε_{su}
Mills	0.51%	3.00%	6.93%	1.00%	1.89%
Heats	3.34%	5.44%	20.51%	2.82%	2.25%
20' Bars	1.77%	5.50%	14.77%	1.75%	3.83%

Table 4.8. Averages of coefficients of variation – variability "within"

AVG CV	f_{ye}	ε_{ye}	ε_{sh}	f_{ue}	ε_{su}
Mills	3.54%	8.66%	25.03%	3.06%	5.55%
Heats	1.72%	7.08%	14.79%	1.74%	5.18%
20' Bars	0.34%	4.40%	3.56%	0.25%	3.82%

4.6.4.5. Summary of Variabilities

Table 4.8 summarizes the results discussed in the preceding sections on the basis of variability within each of the three categories. While it is possible to make a comparison between categories such as between mills, between heats, and between twenty-foot bars, the meaning of such numbers begins to lose significance even at the heat comparison level. The more intuitive comparison is the variability within these categories. As such, Table 4.8 presents the average coefficients of variation for each category and for each of the five parameters. The results follow what would be expected in that there is more variability between tests within a heat than tests within a single twenty-foot bar and more variability between tests within a mill than tests within a heat. Past studies of reinforcing steel mechanical properties have indicated similar results (Allen, 1972). The high variability in the length of the yield plateau likely results from the fact

that this parameter is sensitive to a number of factors related to the manufacturing process (grain refinement due to rolling, cooling, etc.) as well as chemical composition (Lim, 1991; Pussegoda, 1978). As such, high variability in this parameter is not unexpected.

4.6.5. Comparison with Mill and CRSI Data

As described in Chapter 2, there seems to be a trend for steel mill rebar-test results to differ from research laboratory tests of the same batch of steel. This section presents a comparison of the tensile test results acquired through the current project with the corresponding certificate values from the three mills providing steel that supports this trend. Additional mill-derived data taken from the CRSI mill database is included in the comparison. The parameters available for comparison are the yield strength, the tensile strength, percent elongation at fracture, and tensile-to-yield ratio.

Figure 4.35 presents the empirical CDF curves from the three datasets for the yield strength parameter. The experimental data includes the 5% adjustment to the No. 11, 14, and 18 bar data as described in section 4.4. The mill certificate values provided with the steel used in the current project lie along the empirical CDF curve derived from the CRSI mill database which is composed of mill test results submitted to CRSI. As illustrated in the figure, the yield strength results from the current experimental program are consistently lower than the mill-based values. There is an approximate 2.2% difference in the means. Table 4.9 summarizes the mean values for each of the four parameters.

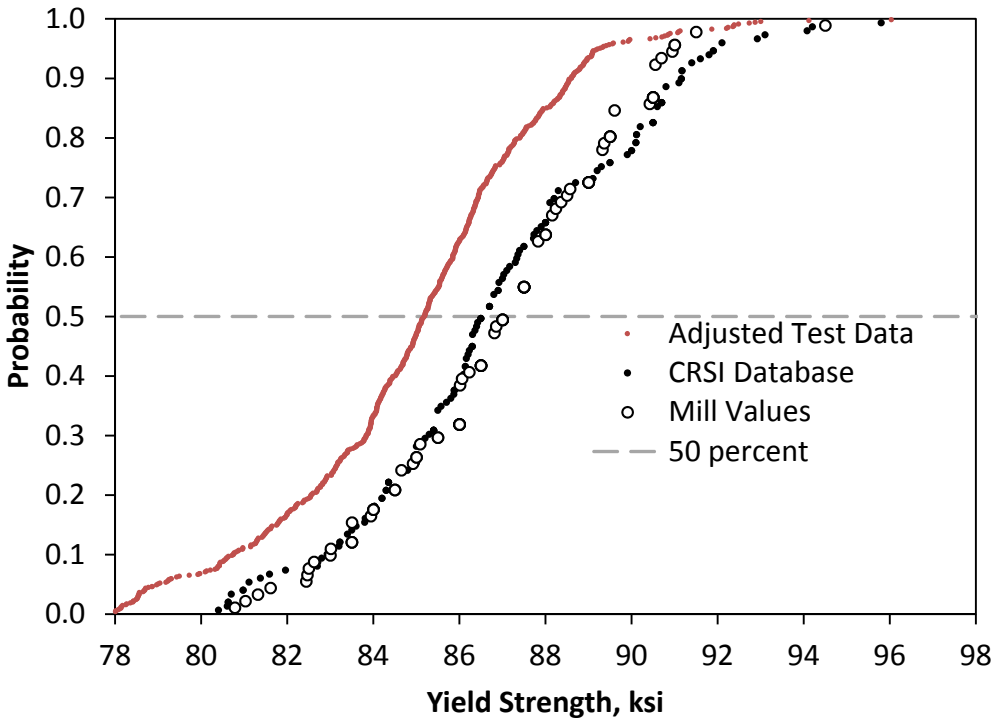

Figure 4.35. Empirical CDFs comparing project data (including 5% adjustment to No. 11-18 bars), CRSI, and mill certificate Yield Strength data

Figure 4.36 presents the empirical CDF curves from the three datasets for the tensile strength parameter. The experimental data includes the 6% adjustment to the No. 11, 14, and 18 bar data as described in section 4.4. As with the yield strength graphs, the mill cert values related to the current project tend to follow along the CRSI mill database values. There is an approximate 1.8% difference in the mean tensile strengths with the mill values being higher than the experimental results.

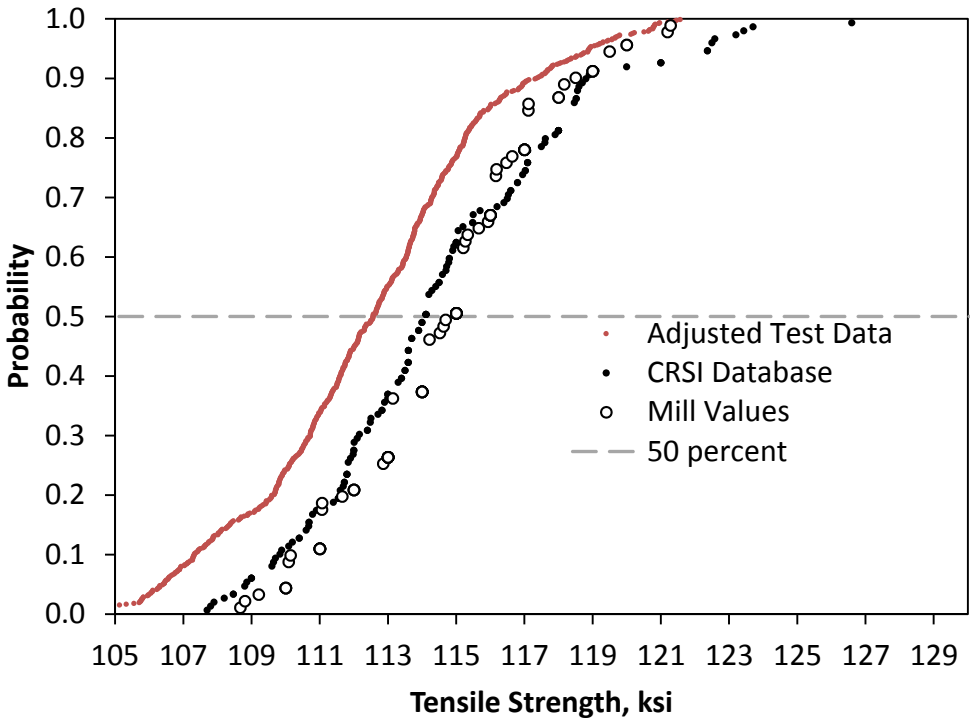

Figure 4.36. Empirical CDFs comparing project data (including 6% adjustment to No. 11-18 bars), CRSI, and mill certificate Tensile Strength data

Figure 4.37 presents the empirical CDF curves from the three datasets for the percent elongation at fracture. The CRSI mill data base values essentially coincide with the mill certificate values; however, unlike with the previous two parameters, the experimental program data lies consistently higher than the mill-based values. A possible reason for this trend was discussed in section 4.6.3.2. There is an approximate 8.6% difference in the means.

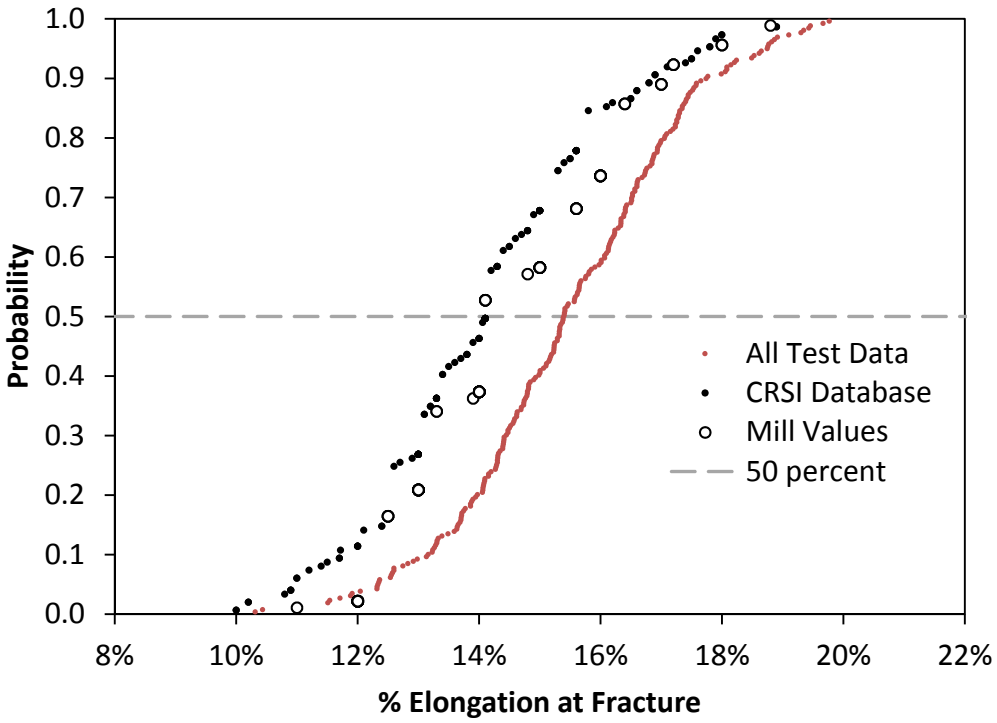

Figure 4.37. Empirical CDFs comparing project data, CRSI, and mill certificate Percent Elongation at Fracture data

Figure 4.38 presents the empirical CDF curves from the three datasets for the tensile-to-yield ratio. The experimental data includes the 5% adjustment to the No. 11, 14, and 18 bar yield strengths and the 6% adjustment to the No. 11, 14, and 18 bar tensile strengths as described in section 4.4. In this case, all three datasets follow the same trend with the mill certificate values closely aligning with the experimental results. These results indicate that, while the mill-acquired yield and tensile strength values are higher than what was found experimentally, the ratio between the two is equivalent in both cases. There is an approximate 0.2% difference in the means.

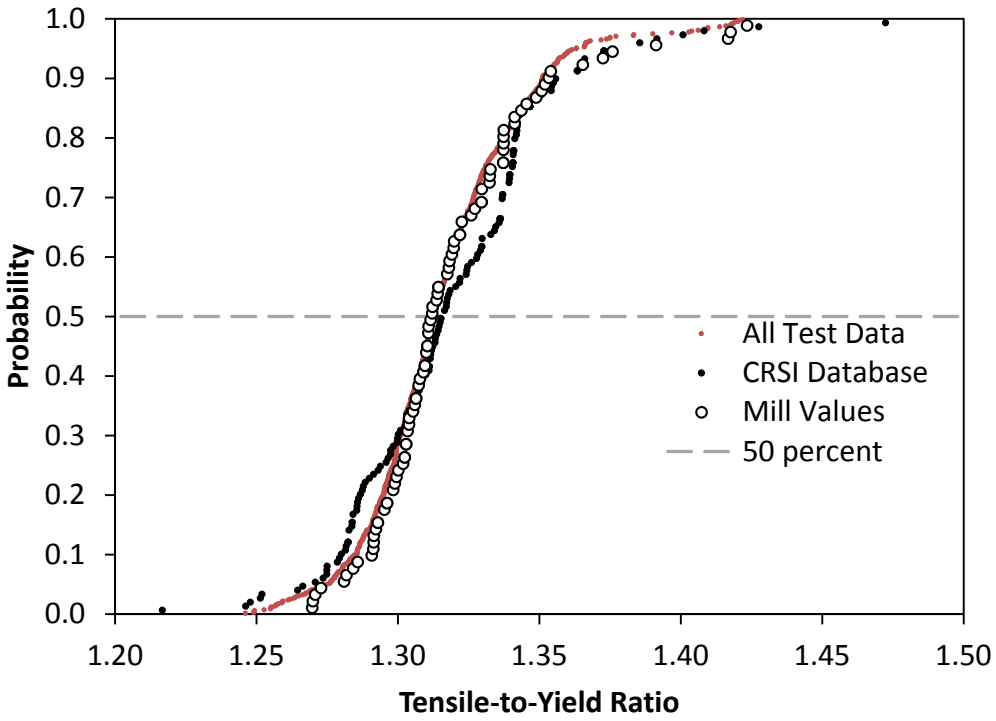

Figure 4.38. Empirical CDFs comparing All Data with adjusted No. 11-18, CRSI, and Mill cert Tensile-to-Yield Ratio data

Table 4.9. Percent difference between experimental and mill-based data

Averages	Experimental Data	Combined Mill & CRSI Data	%Difference
f_{ye} [ksi]	85.0	86.9	2.20%
f_{ue} [ksi]	112.5	114.5	1.78%
%elong	15.5%	14.2%	8.62%
f_{ue}/f_{ye}	1.32	1.32	0.20%

4.6.6. Graphical Comparison with Literature Data

Section 2.4 specifically focused on the availability of A706 Grade 80 stress-strain curves in the literature and what insight these curves offered in terms of the transition from elastic to inelastic behavior (nature of the yield plateau) and the shape of the strain hardening region. Several of these stress-strain curves, which were taken from one of three reports (WJE, 2013; GCR, 2014; and Trejo et al., 2014), have been reproduced below superimposed over the entire set of A706 Grade 80 stress-strain curves obtained during the experimental phase of this project.

The results indicate that the project data is consistent with currently available literature data with respect to the shape of the stress-strain curve. Figure 4.39 highlights the consistency in the length of the yield plateau and the initial slope of the strain hardening region. Figure 4.40 highlights the consistency in the shape of the strain hardening curve and the ultimate tensile strain. Note that

the project data curves have been plotted to ε_u in Figures 4.40 and 4.41. Figure 4.41 illustrates a consistency in length of the yield plateau and shape of the strain hardening curve but a difference in the ultimate tensile strains.

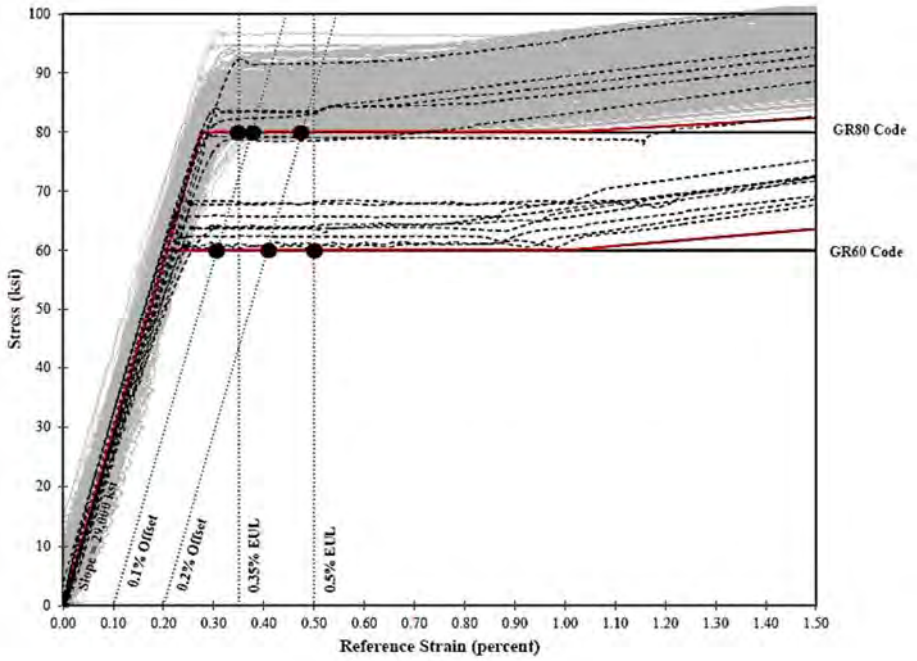

Figure 4.39. WJE (2013) stress-strain curves superimposed over project data

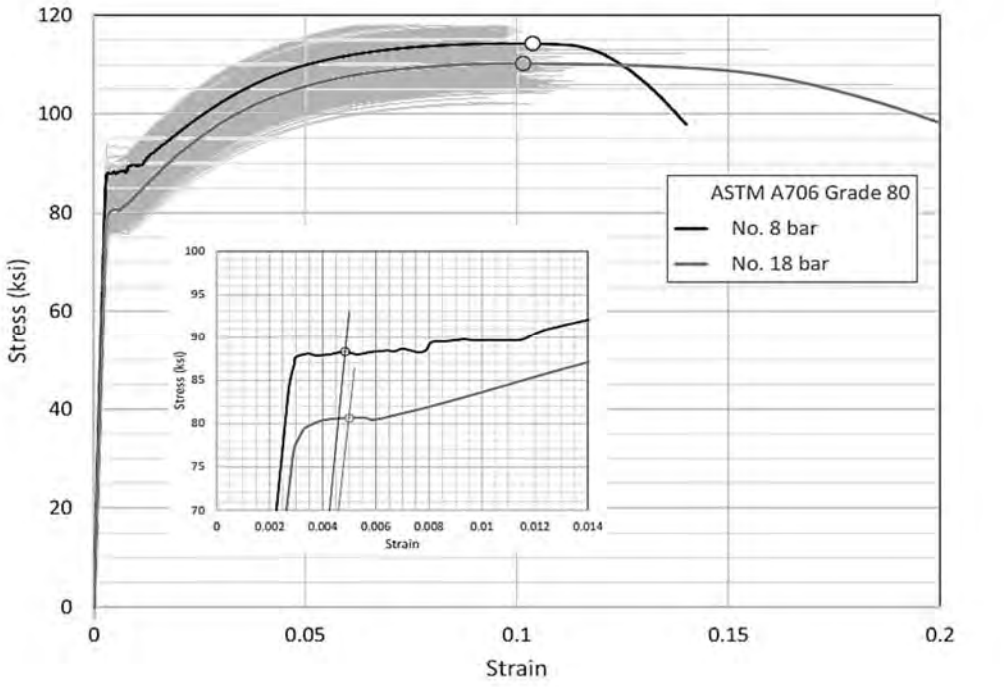

Figure 4.40. GCR (2014) stress-strain curves superimposed over project data (plotted up to ε_u)

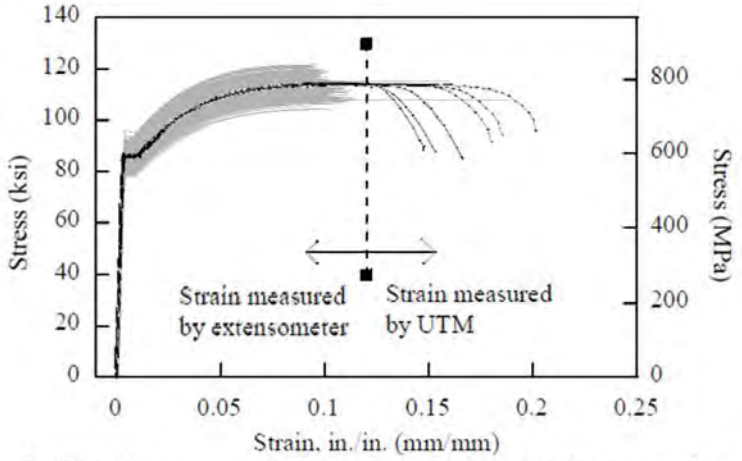

Figure 4.41. Trejo et al. (2014) stress-strain curves superimposed over project data (plotted up to ε_u)

4.6.7. Yield Strengths falling below 80 ksi

As stated in section 4.5.1, adjustment of the No. 11, 14, and 18 bar test results revealed that several of the specimens had yield strengths falling below the ASTM lower limit of 80 ksi. The additional tests of nine No. 11 bars and nine No. 14 bars described in section 4.4 confirmed that this was an accurate assessment and not a by-product of the adjustment factor. While no definitive explanation is offered as to why this behavior revealed itself exclusively in the No. 11, 14, and 18 bar tests, the remainder of this section describes the extent of the phenomenon.

The number of No. 11 bar tests having yield strength below 80 ksi was limited to a single heat from Mill 1 (heat 5). In this specific case, there were no other bar sizes represented in this heat (see Appendix A); therefore, no comparison can be made to determine if the behavior was related to the bar size or the entire heat. Following the adjustment, all nine of the test specimens from this heat had yield strengths below 80 ksi with 78.1 ksi being the minimum and 78.6 ksi the maximum.

Similar to the No. 11 bars, the number of No. 14 bar tests having yield strength below 80 ksi was also limited to a single heat, this time from Mill 3 (heat 7). However, unlike the previous case, there were additional bar sizes represented in this heat. The average yield strength of Mill 3 Heat 7, which was comprised of No. 10-No. 18 bars (Appendix A), was 80.35 ksi. Table 4.10 summarizes the averages by bar size. From the table, it is clear that between the No. 10 and No. 14 bars there is a decrease in average yield strength with increase in bar size. This pattern did not hold for the No. 18 bars. The minimum No. 14 bar yield strength was 78.1 ksi and the maximum was 78.7 ksi.

Table 4.10. Mill 3 Heat 7 mean yield strengths by bar size

Mill 3 Heat 7	**No. 10**	**No. 11**	**No. 14**	**No. 18**
Averages	83.8	80.5	78.5	79.0

Four heats of No. 18 bars contained tests having yield strength below 80 ksi. These included two heats from Mill 3 (heats 6 and 7) and two heats from Mill 2 (heats 1 and 7). While at least one specimen was tested from each of the three Mill 1 heats containing No. 18 bars, it is uncertain whether additional testing would have resulted in any specimens yielding below 80 ksi. Recall that only a subset of the Mill 1 No. 18 bars could be tested because of the "bamboo-style" transverse ribs on the bars which caused the wedge grips to crack and fracture within one to three tests. All No. 18 specimens tested from Mill 2 Heat 1 and Mill 3 Heat 7 had yield strengths below 80 ksi. Each of these heats contained additional bar sizes (Appendix A). Mill 2 Heat 7 had seven out of nine specimens falling below the yield limit, and Mill 3 Heat 6 had three out of nine specimens falling below the yield limit. Mill 2 Heat 7 did not contain any additional bar sizes. Mill 3 Heat 6 did contain additional bar sizes.

5. CHAPTER 5 – RECOMMENDATIONS AND FUTURE WORK

5.1. Chapter Summary

Included in this chapter is a table compiling the recommended values for the following five parameters based on experimental testing conducted as part of the current research effort: expected yield strength, expected yield strain, onset of strain hardening, expected tensile strength, and ultimate tensile strain. Following this is a brief section highlighting summary statistics (mean, standard deviation, and coefficient of variation) associated with each of the parameters. The remainder of the chapter discusses future research that could be conducted in light of the newly developed dataset on A706 Grade 80 reinforcing steel mechanical properties.

5.2. Recommendations

Table 5.1 summarizes the A706 Grade 80 stress-strain recommendations. Included in the table are both the specified and the expected material properties. Specified values are taken from the ASTM A706/A706M specification (ASTM A706/A706M, 2013). Expected values are based on the experimental results presented in sections 4.3 and 4.5. Two additional parameters, the 95th percentile tensile strength and the 5th percentile ultimate tensile strain, offer an indication of the spread of the data.

Table 5.1. Recommendations for A706 Grade 80 monotonic stress-strain parameters

Parameter	Notation	Value	Units
Modulus of elasticity	E_s	29000	ksi
Specified minimum yield strength	f_y	80	ksi
Expected yield strength	$f_{ye\ (mean)}$	85	ksi
Nominal yield strain	ε_y	0.0028	
Expected yield strain	$\varepsilon_{ye\ (mean)}$	0.0033	
Specified minimum tensile strength	f_u	100	ksi
Expected tensile strength	$f_{ue\ (mean)}$	112	ksi
95th percentile tensile strength	$f_{ue\ (95\%)}$	119	ksi
Ultimate tensile strain	$\varepsilon_{su\ (mean)}$	0.0954	
5th percentile ultimate tensile strain	$\varepsilon_{su\ (5\%)}$	0.0845	
Onset of strain hardening	$\varepsilon_{sh\ (mean)}$	0.0074	

5.3. Recommendation Summary Statistics

Table 5.2 provides a more detailed assessment of the parameters presented in Table 5.1 by including the standard deviation and coefficient of variation for each in addition to their mean values. Based on the coefficients of variation, force-based parameters had the least variability

when compared with the strain-based parameters. The high coefficient of variation for the onset of strain hardening data is attributable to the variation in yield plateau lengths observed throughout the testing phase of the project.

Table 5.2. Summary statistics on recommendations

Parameter	Notation	Mean	St. Dev.	CV
Modulus of elasticity	E_s			
Specified minimum yield strength	f_y	--	--	--
Expected yield strength	$f_{ye\ (mean)}$	85	3.03	3.56%
Nominal yield strain	ε_y	--	--	--
Expected yield strain	$\varepsilon_{ye\ (mean)}$	0.0033	0.0003	9.03%
Specified minimum tensile strength	f_u	--	--	--
Expected tensile strength	$f_{ue\ (mean)}$	112	3.65	3.24%
95th percentile tensile strength	$f_{ue\ (95\%)}$	--	--	--
Ultimate tensile strain	$\varepsilon_{su\ (mean)}$	0.0954	0.0055	5.8%
5th percentile ultimate tensile strain	$\varepsilon_{su\ (5\%)}$	--	--	--
Onset of strain hardening	$\varepsilon_{sh\ (mean)}$	0.0074	0.0019	26.17%

5.4. Future Tensile Testing

A similar analysis as that presented in section 4.6.4 can be used to determine the extent to which reducing the breadth of testing performed in this project would have influenced the final recommended values for the five key parameters. Should it be the case that sampling only 1 specimen per bar or just 1 specimen per heat resulted in nearly identical mean values for each stress-strain parameter and with similar variability, then future tensile testing programs could be designed around this knowledge to acquire comparably reliable results from fewer total tests.

5.4.1. Effect of Testing 1 Specimen per Bar

Testing only 1 specimen per twenty-foot bar would have decreased the total possible number of tests from 810 to 270. Table 5.3 summarizes the impact of such a testing program on the final recommended values. In order to generate the results presented in Table 5.3, a separate dataset containing only the first test specimen from each of the three twenty-foot bars sampled for every heat, bar size, and mill (ID: "x x x 1") was compiled and analyzed the same as the full dataset.

It is clearly evident from Table 5.3 that there was little difference in the final outcome between the two approaches. In particular, the yield and tensile strengths differed by less than 0.1 percent between the two datasets. While the strains tended to differ by a larger amount, this was still limited to a percent difference of less than 0.2 percent. The 95th percentile tensile strengths differed by less than 0.01 percent. The 5th percentile ultimate tensile strains differed by the largest margin of about 0.5 percent with the reduced dataset predicting a lower value. From these results, it is clear that reducing the dataset by a factor of 3 had little impact on the final mean values that would have gone into the final recommendations.

Table 5.3. Impact on recommendations considering only 1 specimen per 20' bar

	All Tests	1/Bar	% Diff.
E_s	27888	27871	0.06%
f_{ye}	85.0	84.9	0.07%
ε_{ye}	0.0033	0.0033	0.19%
ε_{sh}	0.0074	0.0074	0.14%
f_{ue}	112.5	112.4	0.01%
ε_{su}	0.0954	0.0956	0.14%
$f_{ue\ (95\%)}$	118.9	118.9	0.00%
$\varepsilon_{su\ (5\%)}$	0.0845	0.0840	0.54%

5.4.2. Effect of Testing 1 Specimen per Bar per Heat

Testing only 1 specimen per heat would have decreased the total possible number of tests from 810 to 90. Table 5.4 summarizes the impact of such a testing program on the final recommended values. In order to generate the results presented in Table 5.4, a separate dataset containing only the first test specimen from the first of the three twenty-foot bars sampled for every heat, bar size, and mill (ID: "x x x 1 1") was compiled and analyzed the same as the full dataset.

As with the case of testing 1 specimen per twenty-foot bar, there was little difference in the final outcome between the two approaches; however, the percent differences did increase as the size of the dataset was reduced. The yield and tensile strengths differed the least between the two datasets – again, less than 0.1 percent each. Excluding the yield strain parameter, the expected onset of strain hardening strains and the ultimate tensile strains differed between the two datasets by less than 1 percent. The 95th percentile tensile strengths differed by less than 0.1 percent. The 5th percentile ultimate tensile strains differed by less than 0.01 percent with the reduced dataset now predicting a slightly higher value. Reducing the dataset by a factor of 9 had some impact on the final mean values that would have gone into the final recommendations; however, the largest percent difference between any two parameters was still below 1.5 percent. It should be noted that these percentages are extremely small and, for several of the parameters, no observable difference between the two datasets is even distinguishable at the provided number of decimal places.

Table 5.4. Impact on recommendations considering only 1 specimen per 20' bar and 1 20' bar per heat

	All Tests	1/Bar/Heat	% Diff.
E_s	27888	27970	0.29%
f_{ye}	85.0	84.9	0.03%
ε_{ye}	0.0033	0.0033	1.26%
ε_{sh}	0.0074	0.0074	0.49%
f_{ue}	112.5	112.5	0.06%
ε_{su}	0.0954	0.0961	0.67%
$f_{ue\ (95\%)}$	118.9	119.0	0.09%
$\varepsilon_{su\ (5\%)}$	0.0845	0.0845	0.01%

5.5. Future Research

Based on the results of this research program, it is the opinion of the authors that A706 Grade 80 steel may be used for capacity protected members without any further study. Such members should be designed using specified material properties, of which only the yield strength is important. Although some reinforcing bars have yield strength values just below 80 ksi, use of a flexural strength reduction factor in design of capacity protected members is more than sufficient to account for this.

The situation is rather different for members forming plastic hinges. While a comprehensive and exhaustive program is not likely needed, a set of focused experiments and analysis should be conducted prior to using A706 Grade 80 reinforcement for members forming plastic hinges. Of particular interest should be (1) Theoretical plastic hinge length and spread of plasticity; and (2) Strain limits for non-linear performance limit states.

Recent research has resulted in a better understanding of both of these items for members constructed from A706 Grade 60 steel. A series of 30 large scale columns were tested under both reversed cyclic loading and real earthquake time histories (Goodnight et al., 2015). Variables in the tests included aspect ratio, axial load ratio, longitudinal steel ratio, and transverse steel ratio. A key aspect of the work involved the use of a non-contact 3D position measurement system to monitor strains in the reinforcement. Examples of the instrumentation system (Fig. 5.1) and some of the data obtained as a consequence of that work (Fig. 5.2) are shown below.

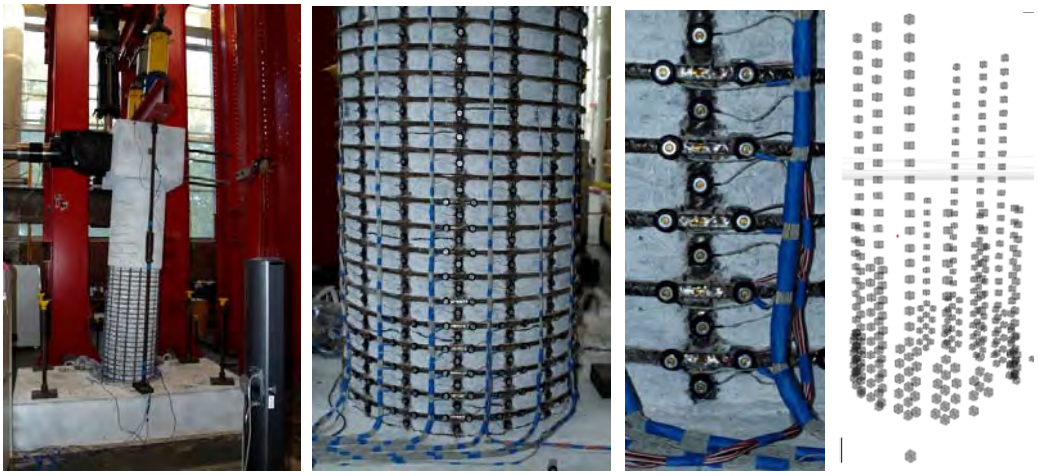

Figure 5.1. Sample past column test with Optotrak sensors

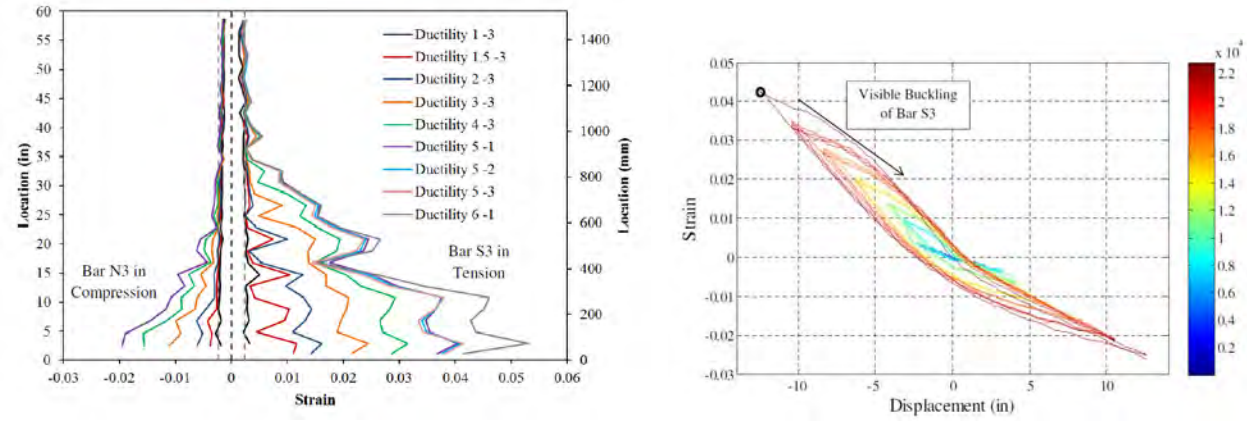

Figure 5.2. Sample strain profiles and strain histories from Optotrak data

The outcome of the research led to a better understanding of the distribution of inelastic curvature along a member, which led to revised plastic hinge length equations suitable for relating material levels strains to member displacements. Shown in Eqs. 1 – 3 are the plastic hinge length models – Eq. 2 applies for tensile strain limits while Eq. 3 applies for compression strain limits. In addition, reinforcing bar strain limits at the onset of spiral yielding (Eq. 4 – compressive strain) and just prior to the onset of bar buckling (Eq. 5 – tensile strain) were developed as shown in the equations below.

$$k = 0.2\left(\frac{f_u}{f_y} - 1\right) \leq 0.08 \qquad \text{Eq. 1}$$

$$Lpr_t = 2kL_c + 0.75D \qquad \text{Eq. 2}$$

$$Lpr_c = 2kL_c \qquad \text{Eq. 3}$$

$$\varepsilon c_{yield}^{sprial} = 0.009 - 0.3\frac{A_{st}}{A_g} + 3.9\frac{f_{yhe}}{E_s} \qquad \text{Eq. 4}$$

$$\varepsilon s_{buckling}^{bar} = 0.03 + 700\rho_s \frac{f_{yhe}}{E_s} - 0.1\frac{P}{f_{ce}^{'} A_g} \quad \text{Eq. 5}$$

It is worth noting that all of these expressions imply that reinforcing bar yield and ultimate stress are important. Given the large database of tests that have been conducted using modern non-contact optical instrumentation systems on members constructed with A706 Grade 60, a set of column tests on columns constructed from A706 Grade 80 steel would allow for a direct comparison of key design variables. With regards to the plastic hinge length, existing models imply a correlation to reinforcing bar yield and ultimate stress. With regards to strain limit states, the research conducted as part of this program identified a reduced level of strain at maximum stress. This reduction may be significant in terms of its effect on ductility capacity. Modern detailed sections fail by bar rupture under tension, usually after the onset of local buckling, although in well confined sections with lower levels of longitudinal steel, rupture without local buckling may occur. In either scenario, these limit states are defined on the basis of tensile strain limits (reinforcing bars will only buckle if first placed into tension, assuming adequate levels of transverse steel reinforcement). It is not clear how the reduced strain at maximum stress may impact cyclic tensile capacity and local buckling. Furthermore, the increased strength of the reinforcement may compensate by providing a slightly higher degree of resistance against bar buckling.

The same series of tests could be performance to evaluate plastic hinge length and strain limit states, and should consider columns of different transverse steel levels (between 0.7 and 1.3% of volumetric ratio), longitudinal steel ratio (from 1% to 3%), aspect ratio (from 4 to 9) and axial load ratio (from 5% to 15%). The recommendations previously identified for grade 60 based columns could be evaluated with a focused set of tests to determine if additional research would be required. Tests should be instrumented such that strain and curvature histories and profiles can be obtained at high resolution as shown previously for grade 60 steel. **A total of 12 large scale tests should be sufficient** to provide a point of comparison against columns tested previously using A706 Grade 60 steel (Goodnight et al., 2015). Based on the outcome of those tests and suitability of existing models, further studies could be explored.

6. CHAPTER 6 – DEPLOYMENT AND IMPLEMENTATION

6.1. Chapter Summary

The current version of the Caltrans Seismic Design Criteria (Caltrans, 2013) makes provisions for the use of A706 Grade 60 steel in both capacity protected members and members designed to perform inelastically by specifying nominal and expected material properties. The implementation of the A706 Grade 80 reinforcing steel properties identified by the present research program into the SDC would ideally follow a similar format.

Presented in this chapter is a revised portion of the SDC version 1.7 chapter 3.2 "Material Properties for Concrete Components" that includes a new section titled "Reinforcing Steel A706/A706M (Grade 80/Grade 550)," in which the recommendations presented in Chapter 5 have been included. Minor changes to the wording and headings of surrounding sections were made to accommodate the proposed A706 Grade 80 section. In addition to the provided material properties, a new, A706 Grade 80 stress-strain curve based on Figure 4.31 is proposed to parallel the existing grade 60 curve.

6.2. Implementation of Recommendation into the SDC

Contained in this section is a reproduction of the Caltrans SDC version 1.7 sections 3.2.1 through 3.2.4. The new A706 Grade 80 section occupies section 3.2.4 directly after the A706 Grade 60 section. The remaining sections in the chapter have been shifted to headings 3.2.5 through 3.2.8. While the new grade 80 section mirrors the existing grade 60 section as closely as possible, several distinctions exist. There is no longer a distinction between bar sizes for the onset of strain hardening and ultimate tensile strain parameters as the research finding indicated limited variability between bar sizes for these parameters. The reduced ultimate tensile strain values have been replaced with the 5^{th} percentile ultimate tensile strain value. It is anticipated that this new parameter would serve the same purpose of acting as a type of strain limit for use in modeling applications to decrease the probability of fracture of the reinforcement but that it would now include a more direct tie to the supporting data. Along these same lines, the 95^{th} percentile tensile strength is incorporated as a new parameter since it offers a reliable indication of the expected overstrength of the material. The final major addition is a new stress-strain curve for A706 Grade 80 rebar to complement the existing stress-strain curve which now only applies to the grade 60 reinforcing steel properties (moved to section 3.2.3). As is, the new curve (Figure 3.2.4-1) is a direct adaptation from Figure 4.31 which illustrates the Raynor model (Raynor et al., 2002) characterized by the grade 80 recommended values plotted over the experimental stress-strain curves. The curve is plotted to the ultimate tensile strain, however, the location of the 5^{th} percentile ultimate strain is specifically marked. What follows is simply meant to serve as an example of how the A706 Grade 80 expected material properties could be incorporated into the SDC. The final decision on how to best implement the test data is, of course, left to Caltrans.

3.2 Material Properties for Concrete Components

3.2.1 Expected Versus Nominal Material Properties

The capacity of concrete components to resist all seismic demands except shear, shall be based on most probable (expected) material properties to provide a more realistic estimate for design strength. An expected concrete compressive strength, f'_{ce} recognizes the typically conservative nature of concrete batch design, and the expected strength gain with age. The yield stress f_y for ASTM A706 Grade 60 steel can range between 60 ksi and 78 ksi. Likewise, the yield stress f_y for ASTM A706 Grade 80 steel can range between 80 ksi and 98 ksi. An expected reinforcement yield stress, f_{ye} is a "characteristic" strength and better represents the actual strength than the specified minimums of 60 ksi and 80 ksi. The possibility that the yield stress may be less than f_{ye} in ductile components will result in a reduced ratio of actual plastic moment strength to design strength, thus conservatively impacting capacity protected components. The possibility that the yield stress may be less than f_{ye} in essentially elastic components is accounted for in the overstrength magnifier specified in Section 4.3.1. Expected material properties shall only be used to assess capacity for earthquake loads.

Seismic shear capacity shall be conservatively based on the nominal material strengths (i.e., f_y, f'_c), not the expected material strengths.

For all seismic-related calculations involving capacity of ductile, non-ductile and capacity protected members, the resistance factor, ϕ shall be taken as 0.90 for shear and 1.0 for bending.

3.2.2 Nonlinear Reinforcing Steel Models for Ductile Reinforced Concrete Members

Reinforcing steel shall be modeled with a stress-strain relationship that exhibits an initial linear elastic portion, a yield plateau, and a strain hardening range in which the stress increases with strain. The yield point should be defined by the expected yield stress of the steel, f_{ye}. The length of the yield plateau shall be a function of the steel strength and bar size (grade 60 only). The strain-hardening curve can be modeled as a parabola or other non-linear relationship and should terminate at the ultimate tensile strain, ε_{su}. The ultimate strain should be set at the point where the stress begins to drop with increased strain as the bar approaches fracture.

3.2.3 Reinforcing Steel A706/A706M (Grade 60/Grade 400)

For A706/A706M Grade 60/Grade 400 reinforcing steel, the following properties based on a limited number of monotonic pull tests conducted by Material Engineering and Testing Services (METS) may be used. The designer may use actual test data if available. It is Caltrans' practice to reduce the ultimate strain by up to thirty-three percent to decrease the probability of fracture of the reinforcement. The commonly used grade 60 steel model is shown in Figure 3.2.3-1 [4].

Modulus of elasticity	E_s = 29,000 ksi	(200,000 MPa)
Specified minimum yield strength	f_y = 60 ksi	(420 MPa)
Expected yield strength	f_{ye} = 68 ksi	(475 MPa)
Specified minimum tensile strength	f_u = 80 ksi	(550 MPa)
Expected tensile strength	f_{ue} = 95 ksi	(655 MPa)
Nominal yield strain	$\varepsilon_y = 0.0021$	
Expected yield strain	$\varepsilon_{ye} = 0.0023$	

Ultimate tensile strain

$$\varepsilon_{su} = \begin{cases} 0.120 & 10\ (Metric\ \#32)\text{bars and smaller} \\ 0.090 & 11\ (Metric\ \#36)\text{bars and larger} \end{cases}$$

Reduced ultimate tensile strain

$$\varepsilon_{su}^{R} = \begin{cases} 0.090 & 10\ (Metric\ \#32)\text{bars and smaller} \\ 0.060 & 11\ (Metric\ \#36)\text{bars and larger} \end{cases}$$

Onset of strain hardening

$$\varepsilon_{sh} = \begin{cases} 0.0150 & 8\ (Metric\ \#25)\text{bars} \\ 0.0125 & 9\ (Metric\ \#29)\text{bars} \\ 0.0115 & 10, 11\ (\text{Metric}\#32, \#36)\text{bars} \\ 0.0075 & 14\ (Metric\ \#43)\ \text{bars} \\ 0.0050 & 18\ (Metric\ \#57)\text{bars} \end{cases}$$

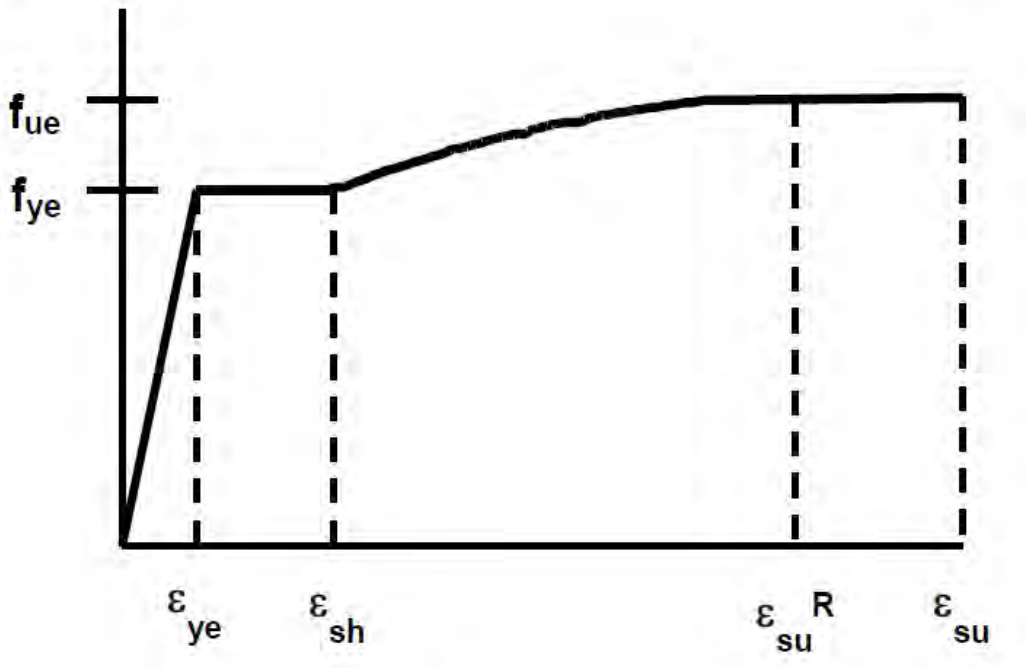

Figure 3.2.3-1 Steel Stress-Strain Model (grade 60)

3.2.4 Reinforcing Steel A706/A706M (Grade 80/Grade 550)

For A706/A706M Grade 80/Grade 550 reinforcing steel, the following properties based on a number of monotonic pull tests obtained through a Caltrans-funded research grant (Overby et al., 2015) may be used. The designer may use actual test data if available. A grade 80 steel model is shown in Figure 3.2.4-1.

Modulus of elasticity	E_s = 29,000 ksi	(200,000 MPa)
Specified minimum yield strength	f_y = 80 ksi	(550 MPa)
Expected yield strength	f_{ye} = 85 ksi	(585 MPa)
Specified minimum tensile strength	f_u = 100 ksi	(690 MPa)
Expected tensile strength	f_{ue} = 112 ksi	(775 MPa)
95th percentile tensile strength	$f_{ue\ (95\%)}$ = 119 ksi	(820 MPa)
Nominal yield strain	ε_y = 0.0028	
Expected yield strain	ε_{ye} = 0.0033	
Ultimate tensile strain	ε_{su} = 0.095	

5th percentile ultimate tensile strain $\varepsilon_{su\,(5\%)} = 0.084$

Onset of strain hardening $\varepsilon_{sh} = 0.0074$

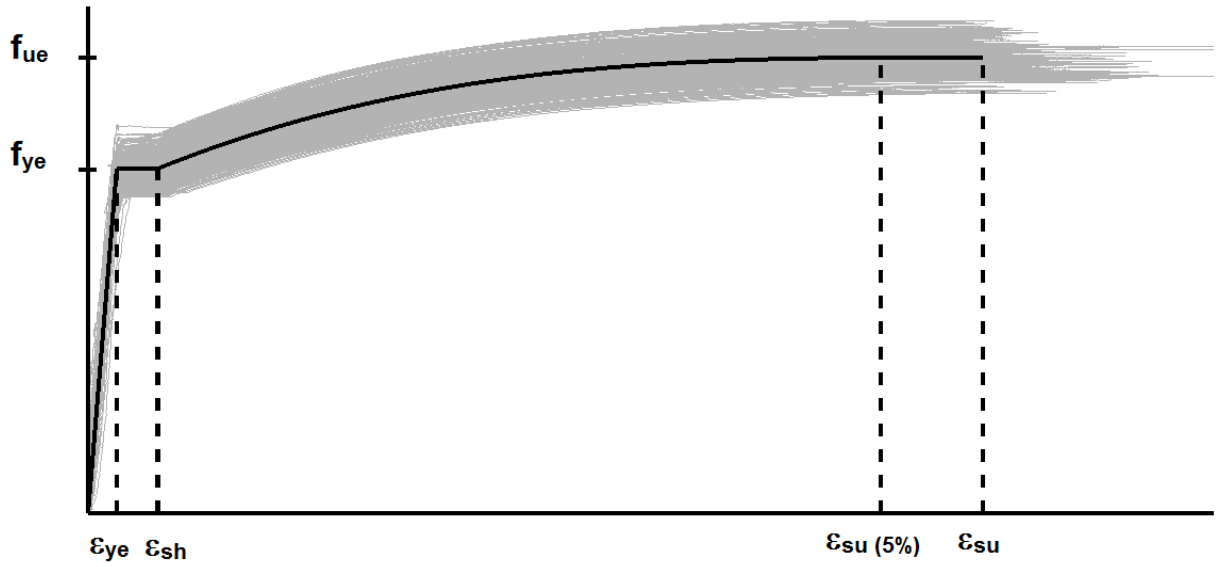

Figure 3.2.4-1 Steel Stress-Strain Model (grade 80)

3.2.5 Nonlinear Prestressing Steel Model

3.2.6 Nonlinear Concrete Models for Ductile Reinforced Concrete Members

3.2.7 Normal Weight Portland Cement Concrete Properties

3.2.8 Other Material Properties

7. REFERENCES

ACI Committee 318, "Building Code Requirements for Structural Concrete (ACI 318-14) and Commentary," American Concrete Institute, Farmington Hills, MI.

Allen, D. E. 1972. "Statistical Study of the Mechanical Properties of Reinforcing Bars," Building Research Note No. 85, Division of Building Research, National Research Council, Ottawa, Canada, April, 8 pp.

ASTM A370 (2009), "Standard Test Methods and Definitions for Mechanical Testing of Steel Products," American Society for Testing and Materials, West Conshohocken, PA, 47 pp.

ASTM A370-13, "Standard Test Methods and Definitions for Mechanical Testing of Steel Products," ASTM International, West Conshohocken, PA, 2013, 48 pp.

ASTM A706/A706M-13, "Standard Specification for Low-Alloy Steel Deformed and Plain Bars for Concrete Reinforcement," ASTM International, West Conshohocken, PA, 2013, 7 pp.

CALTRANS. 2013. *CALTRANS SEISMIC DESIGN CRITERIA*. Version 1.7. CALTRANS.

CRSI, 2013, data from an unpublished database of the Concrete Reinforcing Steel Institute.

Goodnight, J.C, Kowalsky, M.J., and Nau, J.M. (2015). The effects of load history and design variables on Performance Limit States of Circular Bridge Columns. Vol. 1-3. Final report to Alaska Department of Transportation and Public Facilities. January. 1258 pp.

Gustafson, D.P. 2010. "Raising the Grade." *Concrete International* V. 32, No. 4, April 2010, pp. 59-62.

King, D. J., M. Priestley, and R. Park. *Computer Programs for Concrete Column Design*. Research Report 86/12, Department of Civil Engineering, University of Canterbury, New Zealand, May 1986.

Lim, W. T., "Statistical Analysis of Reinforcing Steel Properties," Master's Thesis, University of Canterbury, Christchurch, New Zealand, June 1991, 151 pp.

Mirza, S. A. and J. MacGregor. 1979. "Variability of Mechanical Properties of Reinforcing Bars." *Journal of the Structural Division, ASCE* V. 105, May, pp. 921-937.

NEES, "NEES Project Warehouse," 2009, http://nees.org/warehouse/project/904. (last accessed Aug. 21, 2015)

NIST, 2014, *Use of High-Strength Reinforcement in Earthquake-Resistant Concrete Structures*, NIST GCR 14-917-30 Report, prepared by the NEHRP Consultants Joint Venture, a partnership of the Applied Technology Council and the Consortium of Universities for Research in

Earthquake Engineering, for the National Institute of Standards and Technology, Gaithersburg, Maryland.

Nowak. A. S., and M. Szerszen. 2003. “Calibration of Design Code for Building (ACI318): Part 1-Statistical Models for Resistance.” *ACI Structural Journal* V. 100, May-June, pp. 377-382.

Overby, D. T., M. Kowalsky, and R. Seracino. 2015. “A706 Grade 80 Reinforcement for Seismic Applications.” Caltrans-funded Research Project. August 2015.

Pussegoda, L.N., "Strain Age Embrittlement in Reinforcing Steels", Ph.D. Thesis, 1978, Dept. of Mechanical Eng., University of Canterbury, New Zealand.

Rautenberg, J. M., “Drift Capacity of Concrete Columns Reinforced with High-Strength Steel,” PhD dissertation, Purdue University, West Lafayette, IN, May 2011, 263 pp.

Rautenberg, J.M., S. Pujol, H. Tavallali, and A. Lepage. 2013. “Drift Capacity of Concrete Columns Reinforced with High-Strength Steel.” *ACI Structural Journal* V. 110, No. 2, March-April 2013, pp. 307-317.

Raynor, D. J., D. Lehman, and J. Stanton. 2002. “Bond Slip Response of Reinforced Bars Grouted in Ducts.” *ACI Structural Journal* V. 99, No. 5, 2002.

Trejo, D., A.R. Barbosa, and T. Link. 2014. “Seismic Performance of Circular Reinforced Concrete Bridge Columns Constructed with Grade 80 Reinforcement.” Research Project SRS 500-610, March 2014.

Barbosa, A.R., T. Link, and D. Trejo. 2015. "Seismic Performance of High-Strength Steel RC Bridge Columns." J. Bridge Eng., 10.1061/(ASCE)BE.1943-5592.0000769 , 04015044.

Wiss, Janney, Elstner and Associates, Inc. (WJE) (2013). “Determination of Yield Strength for Nonprestressed Steel Reinforcement,” WJE Project No. 2013.4171, Dec. 31.

8. APPENDIX A – Summary of Bar Sizes by Heat and Mill

8.1. Mill 1

Heat 1	Heat 2	Heat 3	Heat 4	Heat 5	Heat 6	Heat 7	Heat 8	Heat 9
No. 4	No. 4	No. 4	No. 18	No. 11	No. 11	No. 11	No. 18	No. 18
No. 5	No. 5	No. 5						
No. 6	No. 6	No. 6						
No. 7	No. 7	No. 7						
No. 8	No. 8	No. 8						
No. 9	No. 9	No. 9						
No. 10	No. 10	No. 10						
No. 14	No. 14	No. 14						

8.2. Mill 2

Heat 1	Heat 2	Heat 3	Heat 4	Heat 5	Heat 6	Heat 7
No. 4	No. 6	No. 5	No. 4	No. 7	No. 4	No. 18
No. 5	No. 7	No. 6	No. 8	No. 9	No. 5	
No. 6	No. 9	No. 8	No. 9	No. 10	No. 7	
No. 8	No. 10				No. 10	
No. 11	No. 11				No. 11	
No. 14	No. 14				No. 14	
No. 18	No. 18					

8.3. Mill 3

Heat 1	Heat 2	Heat 3	Heat 4	Heat 5	Heat 6	Heat 7	Heat 8	Heat 9
No. 5	No. 5	No. 4	No. 4	No. 4	No. 10	No. 10	No. 10	No. 5
No. 6	No. 6	No. 8	No. 8	No. 8	No. 11	No. 11	No. 11	No. 6
No. 7	No. 7	No. 9	No. 9	No. 9	No. 14	No. 14	No. 14	No. 7
					No. 18	No. 18	No. 18	

9. APPENDIX B – Determination of Stress-Strain Parameters

9.1. Modulus of elasticity

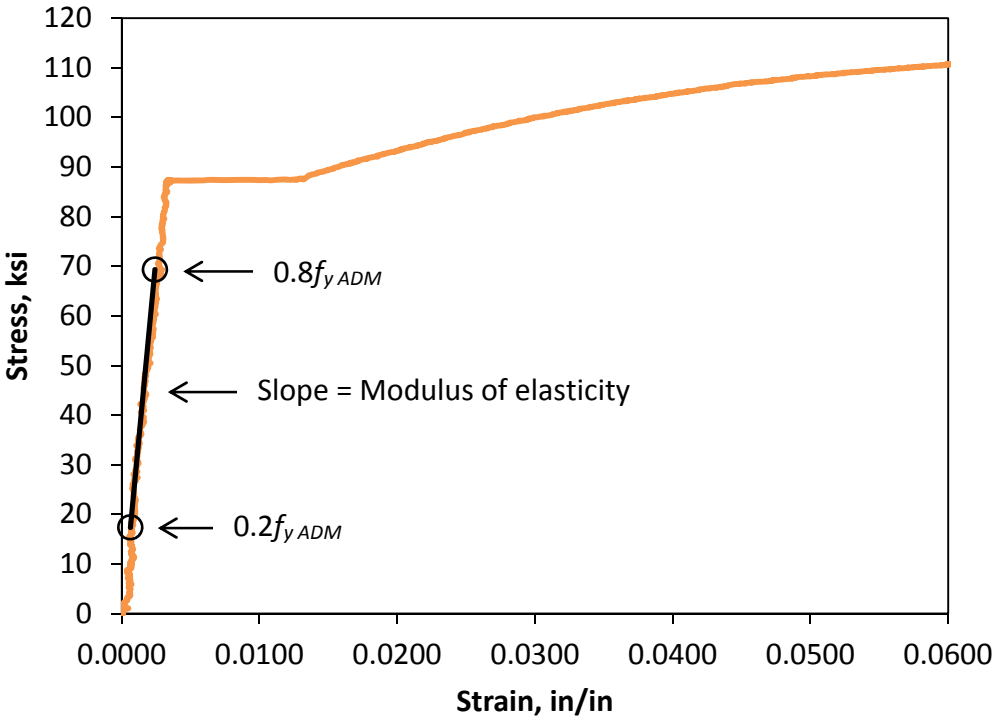

9.2. Yield Strength

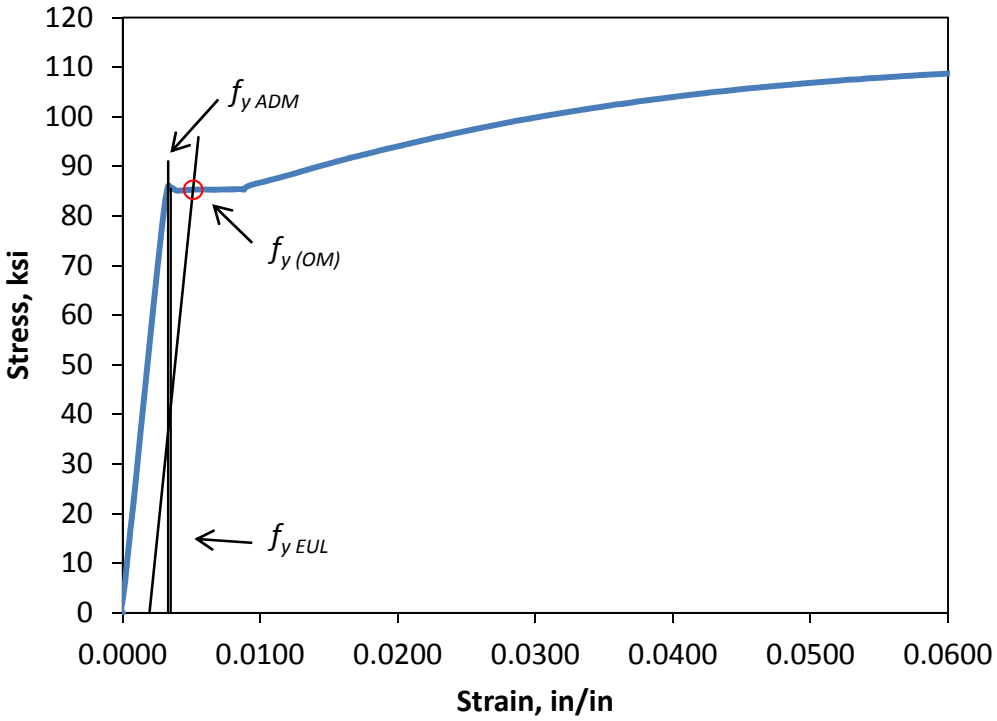

9.3. Onset of Strain Hardening

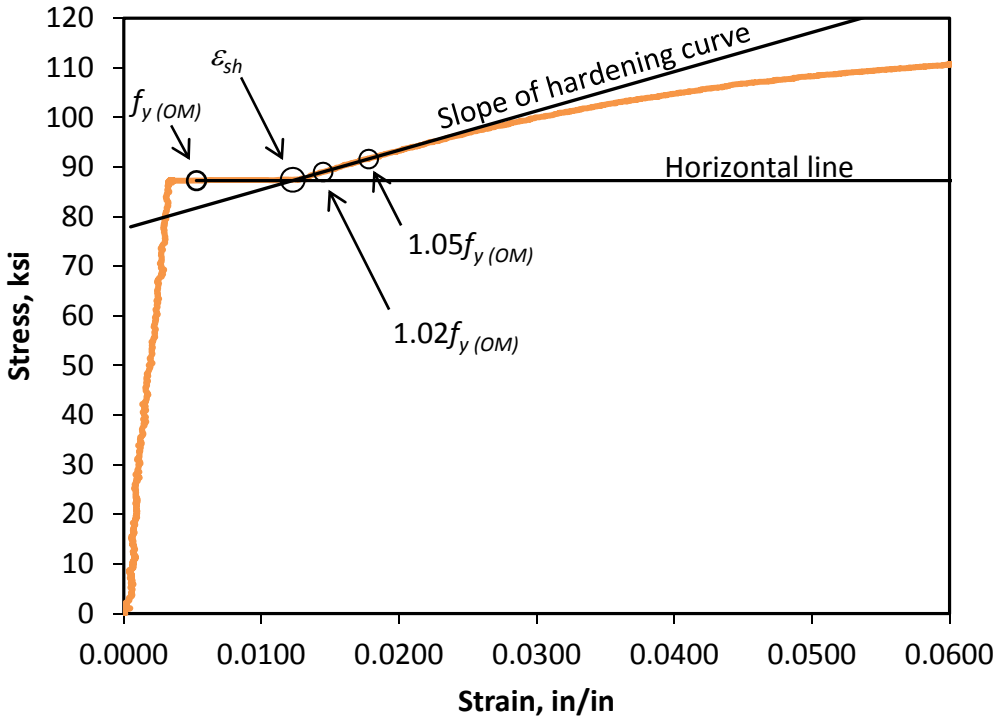

10. APPENDIX C – Summary of Yield Behaviors

Percent of Total	well-defined yield plateau	knee but no drop in stress	completely roundhouse
All Tests	87.6%	9.6%	2.8%
Mill 1 tests	100%	--	--
Mill 2 tests	75.9%	15.9%	8.1%
Mill 3 tests	87.8%	12.2%	--

11. APPENDIX D – 2” VS 8” GAGE LENGTH COMPARISON

11.1. Yield Strain

ε_y	Mean		St. Dev.		CV	
	2-inch	8-inch	2-inch	8-inch	2-inch	8-inch
No. 4	0.0034	0.0034	0.0003	0.0003	8.9%	8.8%
No. 5	0.0032	0.0032	0.0002	0.0002	5.8%	6.0%
No. 6	0.0031	0.0031	0.0002	0.0003	7.9%	8.6%
No. 7	0.0033	0.0033	0.0004	0.0005	12.6%	14.1%
No. 8	0.0032	0.0032	0.0002	0.0002	6.6%	6.6%
No. 9	0.0031	0.0031	0.0003	0.0003	8.9%	8.9%
No. 10	0.0031	0.0031	0.0002	0.0002	7.6%	7.4%
No. 11	0.0034	0.0033	0.0003	0.0003	8.6%	8.4%
No. 14	0.0034	0.0033	0.0003	0.0003	7.4%	7.5%
No. 18	0.0033	0.0033	0.0003	0.0003	8.0%	8.0%
Total	**0.0033**	**0.0032**	**0.0003**	**0.0003**	**9.0%**	**9.5%**

11.2. Onset of Strain Hardening

ε_{sh}	Mean		St. Dev.		CV	
	2-inch	8-inch	2-inch	8-inch	2-inch	8-inch
No. 4	0.0072	0.0072	0.0020	0.0020	27.7%	27.8%
No. 5	0.0084	0.0085	0.0015	0.0015	18.3%	18.2%
No. 6	0.0085	0.0085	0.0025	0.0025	28.9%	29.4%
No. 7	0.0078	0.0078	0.0012	0.0013	16.0%	16.1%
No. 8	0.0069	0.0068	0.0017	0.0017	24.9%	25.0%
No. 9	0.0065	0.0066	0.0015	0.0015	23.3%	23.0%
No. 10	0.0056	0.0055	0.0012	0.0012	22.0%	21.9%
No. 11	0.0084	0.0084	0.0023	0.0023	27.2%	27.3%
No. 14	0.0076	0.0075	0.0014	0.0014	18.5%	18.9%
No. 18	0.0076	0.0076	0.0014	0.0014	18.3%	19.0%
Total	**0.0074**	**0.0074**	**0.0019**	**0.0020**	**26.2%**	**26.3%**

11.3. Ultimate Tensile Strain

ε_u	Mean		St. Dev.		CV	
	2-inch	8-inch	2-inch	8-inch	2-inch	8-inch
No. 4	0.0922	0.0922	0.0062	0.0067	6.8%	7.3%
No. 5	0.0945	0.0945	0.0055	0.0058	5.8%	6.2%
No. 6	0.0958	0.0959	0.0057	0.0059	6.0%	6.2%
No. 7	0.0971	0.0973	0.0045	0.0047	4.6%	4.8%
No. 8	0.0957	0.0960	0.0037	0.0036	3.9%	3.8%
No. 9	0.0956	0.0956	0.0051	0.0054	5.3%	5.6%
No. 10	0.0959	0.0961	0.0041	0.0040	4.3%	4.2%
No. 11	0.0955	0.0954	0.0056	0.0060	5.9%	6.3%
No. 14	0.0971	0.0966	0.0062	0.0066	6.4%	6.8%
No. 18	0.0945	0.0946	0.0073	0.0069	7.8%	7.3%
Total	**0.0954**	**0.0955**	**0.0055**	**0.0057**	**5.8%**	**6.0%**

12. APPENDIX E – Comparison of Yield Strength Determination Methods

Means	$f_{y\,ADM}$	$f_{y\,OM}$	Percent Difference
No. 4	88	87	0.84%
No. 5	87	86	0.63%
No. 6	86	86	0.14%
No. 7	86	86	0.19%
No. 8	86	86	0.04%
No. 9	85	85	0.48%
No. 10	84	86	1.56%
No. 11	84	84	0.23%
No. 14	82	82	0.75%
No. 18	81	81	0.62%
Total	85.0	85.1	0.20%

13. APPENDIX F – Test Photos

No. 4 Bars

No. 5 Bars – necked and untested

No. 6 Bars

No. 7 Bar

No. 8 Bar

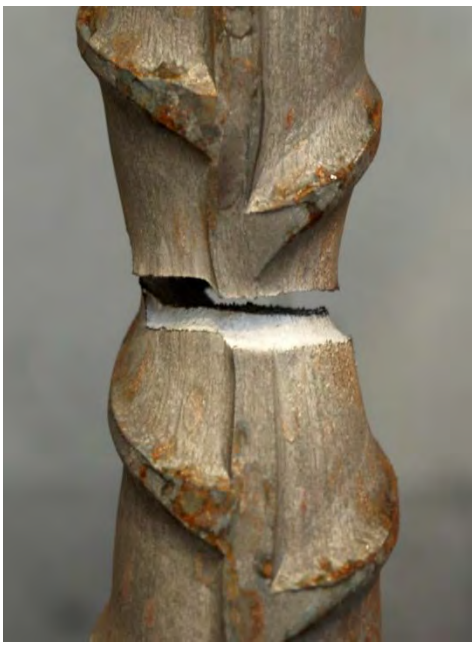

No. 9 Bar

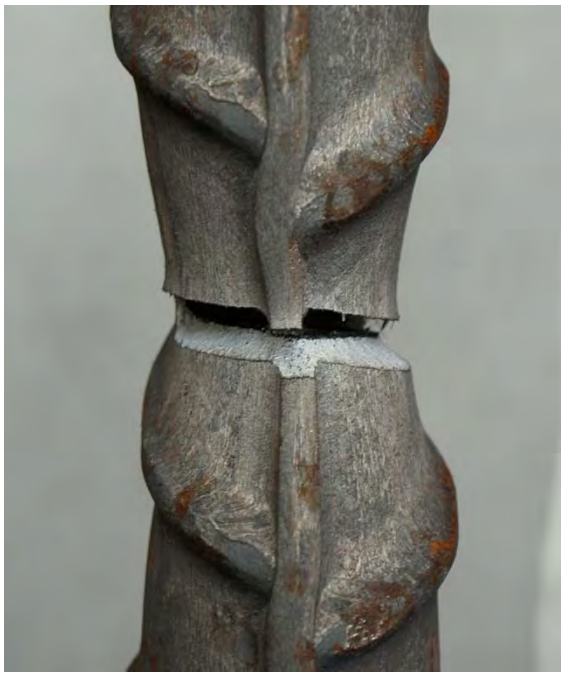

No. 10 Bar

No. 11 Bar

No. 14 Bar – mill stamp digitally removed for confidentiality

No. 18 Bar – brittle failure at grips early into necking